A Study of the Development Potential in Tsim Sha Tsui East Using 3D Spatial Analysis Technologies

(Final Report)

By Prof. Geoffrey Shen

Co-investigators:

Dr Orianna Guo, Dr Stanley Yeung, Dr Ivy Wong & Dr Charles Wong

Department of Building and Real Estate

Department of Land Surveying and Geo-Informatics

June 2017

A Study of the Development Potential in Tsim Sha Tsui East Using 3D Spatial Analysis Technologies

(Executive Summary)

The Green Deck proposed by The Hong Kong Polytechnic University (PolyU) will not only provide people with a green open space but also promote sustainable development of Tsim Sha Tsui East (TSTE) area. As a result of the proposed Green Deck, more tourists, participants in conferences and other activities, and local residents will visit this area. Since many of them will choose to stay in nearby hotels, TSTE will become their first choice. The carrying capacity of TSTE and its development potential is, therefore, the focus of this study.

This study investigates the environmental impacts of minor relaxation of maximum Plot Ratio /Building Height (PR/BH) restrictions in TSTE using 3D spatial technologies. The two specific research objectives are: (1) To establish and verify 3D models of TSTE into several different PR/BH scenarios by collecting and integrating 3D spatial data; and (2) to compare these PR/BH scenarios in terms of their impact on urban skylines, mountain ridgelines, wind ventilation, air temperature, and transportation. The 3D spatial analysis technologies were applied to provide scientific evidence to support decision making for sustainable urban development in the area.

Through comparison among different scenarios, it is noted that there is no significant change in urban skylines and mountain ridgeline, wind ventilation, air temperature, and transportation after the minor relaxation. For the solar exposure, there is no obvious change in sunlight hours, the radiation energy on the west facing facades was increased but the intensity of radiation on west-facing facades was decreased after the minor relaxation. The findings show that the minor PR/BH relaxation in TSTE leads to a potential increase in GFA from 842,585m^2 to 1,051,078m^2, with a net increase of 208,493m^2. It concluded that there is a potential to have minor PR/BH relaxation on buildings in TSTE to increase the living and working spaces to meet the increased population flow whilst minimizing its environmental impact.

Table of Contents

The Hong Kong Polytechnic University Research Team

Prof. Geoffrey Q.P. Shen (PI)

········Chair Professor, Department of Building and Real Estate

Dr. Stanley C.W. Yeung (Co-PI)

········Associate Professor, Department of Building and Real Estate

Dr. Ivy S.W. Wong (Co-PI)

········Assistant Professor, Department of Building and Real Estate

Dr. Charles M.S. Wong (Co-PI)

········Assistant Professor, Department of Land Surveying and Geo-Informatics

Dr. Orianna J. Guo (Co-PI)

········Scientific Officer, Department of Building and Real Estate

Dr. Jerry Z. Qin

········Postdoctoral Fellow, Department of Building and Real Estate

Dr. Sawaid Abbas

········Research Associate, Department of Building and Real Estate

Dr. Helen W. Zheng

········Postdoctoral Fellow, Department of Building and Real Estate

Ms. Coco Kwok

········PhD Student, Department of Land Surveying and Geo-Informatics

Mr. Y.D. Zhu

········Student Helper, Department of Building and Real Estate

Acknowledgements

The research team wishes to acknowledge The Hong Kong Polytechnic University's financial support for this project. The research team also greatly appreciates the assistance of Dr. Jason NI Meng-cheng from the Department of Architecture and Civil Engineering of City University of Hong Kong in the traffic impact analysis.

List of Figures

List of Tables

1. INTRODUCTION

1.1 Research Background

To achieve sustainable development in Hong Kong, especially for the heavily-loaded Cross Harbour Tunnel district, The Hong Kong Polytechnic University (PolyU) has proposed an innovative solution that involves constructing a Green Deck (HKPU, 2015) over the Cross Harbour Tunnel plaza to enhance its immediate and neighbouring environments. The proposed 43,000m^2 deck will accommodate a wide variety of recreational, cultural and sports facilities while solving existing problems in the area. It will not only provide people with a green open space to unwind from the hustle and bustle of city life, but also help to promote the sustainable development of Tsim Sha Tsui (TST) especially Tsim Sha Tsui East (TSTE) and Hung Hom. As a result of the proposed Green Deck and the convention and exhibition centre, more tourists, participants in conferences and other activities, and local residents will visit this area. Since most of them will choose to stay in nearby hotels, TSTE will undoubtedly become the first choice for them. TSTE is therefore the focus area of this study (see Figure 1-1) with the current carrying capacity of the existing buildings in TSTE and the development potential of TSTE being rigorously examined.

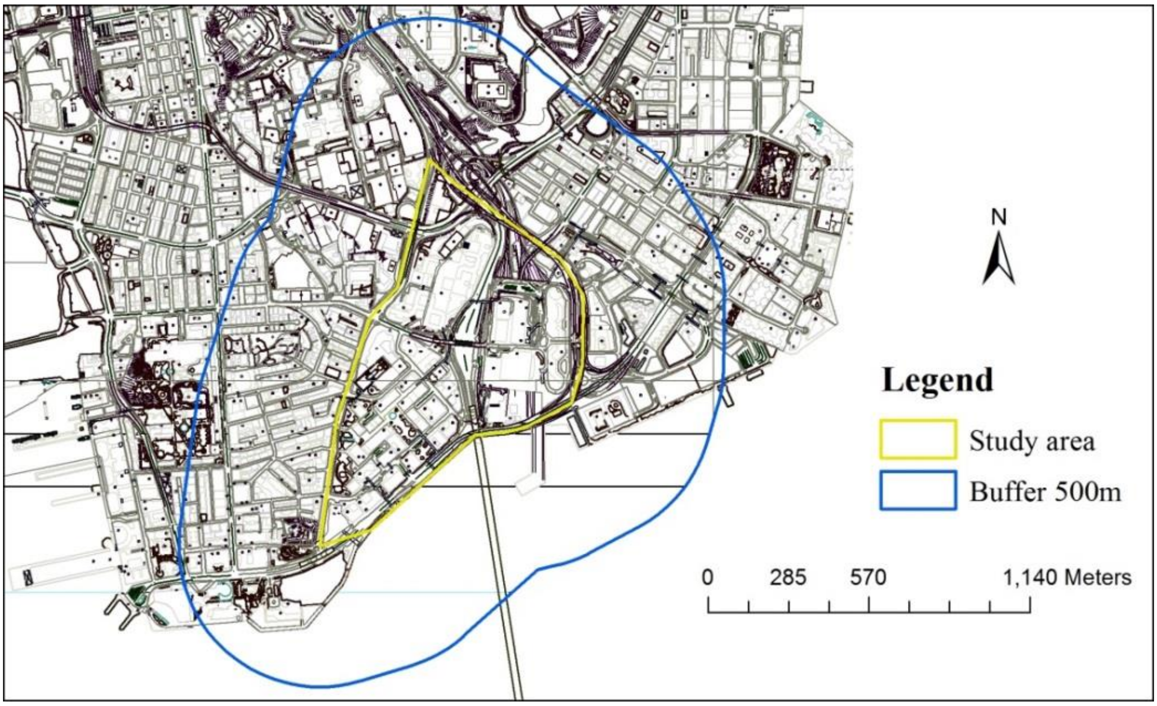

Figure 1-1. Study area

Development potential in Hong Kong is mainly controlled by Lease Conditions, Outline Zoning Plans (OZPs) and Building (Planning) Regulations (BPR), all of which inevitably impose restrictions on the plot ratio (PR) and building height (BH) of individual land zones. Hong Kong has been struggling to develop every single piece of land in urban areas to its maximum potential and so the development of the Green Deck project will bring unprecedented opportunities to TSTE. To meet the increased high passenger flow, it is necessary to ensure enough living and working spaces in TSTE. TSTE currently has the carrying capacity for 842,585.105m^2 of gross floor area (GFA) for buildings. In this regard, elevating the development potential of this area through minor relaxation of the maximum PR/BH restrictions is a viable option for increasing living and working spaces within a short timeframe. However, increasing the development potential will bring a higher development intensity, which must be considered and controlled in order to maintain development sustainability. The extent to which this relaxation will be acceptable to the public is rigorously analysed in this study.

Development intensity is generally explored through an Environmental Impact Assessment (EIA) as it is subject to the public's tolerance to changes in the environment. Although previous studies have integrated GIS for assessing air ventilation and visual permeability etc., they have mainly focused on the use of 2D GIS. Since the spatial distribution of land units in the real world is three-dimensional, 3D GIS can help us to look into the real world in true perspective and make better-informed decisions. Therefore, this research is devoted to the investigation of the development potential of existing businesses in TSTE through 3D modelling and spatial analyses.

1.2 Research Objectives

This study investigates the environmental impacts of minor relaxation of maximum PR/BH restrictions in TSTE, such as the visual impact on urban skylines and mountain ridgelines, the impact on solar exposure, the effect on wind ventilation, the effect on air temperature, and the influence on transportation from a sustainability perspective. The study will use 3D spatial analysis technology so as to provide scientific evidence to support decision making for the sustainable urban development of Hong Kong.

The specific objectives of this research are as follows:

1) To establish and verify 3D models of TSTE into several different PR/BH scenarios by collecting and integrating 3D spatial data (3D building/infrastructure and terrain models).

2) To compare these different PR/BH scenarios in terms of urban skyline, mountain ridgeline, wind ventilation, air temperature, and transportation.

It is expected that this study would provide scientific evidence inform decision makers for the sustainable development of TSTE to support the development of the proposed Green Deck in Hung Hom. The approach used in this study could be in other similar urban development projects.

2. LITERATURE REVIEW

It is apparent from the literature that the development potential of urban areas is one of the most important research topics in urban planning. Most relevant studies are dedicated to providing scientific findings to support and to guide the proper consideration of land use, building and facility renewal/development, culture, and heritage preservation for improving social benefit without damaging the environment. In this regard, some scholars have focused on the use of fundamental data (e.g. spatial characteristics, financial data, political documents, environmental data and socio-economic data) to explore the impact of urban development on the environment and to analyse the development feasibility of a city or urban area. This study adopts the same focus and has a few relevant studies.

One such study by Terzi and Bölen (2012) focused on the feasibility of urban development strategies (i.e. market-led development, conservative-led development and fiscal incentives-led development) for dealing with urban sprawl while preserving the environment in Istanbul. Three other studies (Stevens et al., 2007; Tayyebi et al., 2011; He et al., 2016) are dedicated to the modelling of urban expansion. All four studies made use of 2D spatial analysis technology to deal with the potential of urban sprawl rather than 3D spatial analysis technology (3DSAT). The latter technology was developed from the former by adding a vertical dimension to the original two horizontal dimensions in spatial analysis. Three dimensions enable representation and visualization of real world space better than two dimensions, and many urban development studies are conducted using 3DSAT. The viability of using 3DSAT to study urban development was touched upon by Ranzinger and Gleixner (1997), Pullar and Tidey (2001), Zhang et al. (2004), Mak et al. (2005), Thill et al. (2011), Leszek (2015), and Guo et al. (2017), all of whom achieved effective results that help with making decisions in urban planning. In particular, the impact on the environment of building PR/BH relaxation in the Kai Tak area in Hong Kong was analysed by Guo et al. (2017) whose study is similar to this TSTE project although the TSTE project is different from the Kai Tak study in terms of its commercial land zones and popularity with tourists. The success of the Kai Tak study gives a great insight into the application of 3DSAT for assessing the development potential of TSTE. The increased application of 3DSAT for urban development has resulted in the following proposed tools based on 3DSAT: a GIS tool for urban climate evaluation (Li et al., 2004) and for community engagement in urban planning (Foth et al., 2009); a method for investigating the wall effect caused by high-rise buildings (Wong et al., 2011); a platform for assisting decision making in urban development projects (Isaacs et al., 2011); an integrated approach for assessing residential development (Xu and Coors, 2012); and a framework for assessing development potential of Liuzhou city in China (Xia et al., 2015). Although the latter tool is similar to the one used for this study, there are obvious differences in respect of urban situation, socio-economic conditions, and the scale of study area. Hong Kong is a high-density city with many skyscrapers around the centre area and so the development of its urban areas involves different environmental issues. Even though TSTE is a relatively small-scale urban area, it is nevertheless important that the proposed development be implemented as soon as possible in order to help maintain Hong Kong as one of world's leading financial centres.

The development of Green Deck project and its influence can also be addressed in terms of transportation. In the past, the relationship between "built environment" and people's travel behaviour has been explored and confirmed (Ni and Loo, 2012). To express the built environment, one way is to adopt the 3Ds (Density, Diversity, and Design) first advanced by Cervero and Kockelman (1997). In previous literatures, specific variables were linked to the 3Ds. For example, population density, employment density and household density are related to "Density"; Land-use diversity, shopping square feet and number of pedestrian bridges are related to "Diversity"; Sidewalk width, proportion of blocks and street density are related to "Design". In addition to the definition of the built environment, there are many research studies exploring the relationship between the built environment and vehicle use. A study of mode choice in Montgomery County, Maryland (Cervero, 2002) revealed that development intensities and mixtures of land use significantly influence decisions to drive-alone, share a ride, or patronize transit, while the influences of urban design tend to be more modest. A disaggregate cross-sectional study used primary data on the cycling behaviour of 608 randomly sampled respondents in urbanized King County, Washington (Moudon, et al., 2005) to show that both perceived and objective environmental conditions contribute to the likelihood of cycling. Proximity to walking trails and the presence of agglomerations of offices, clinics/hospitals, and fast food restaurants, measured objectively, are significant environmental variables. Previously researched correlates of cycling, such as the presence of bicycle lanes, traffic speed and volume, slope, block size, and the presence of parks, are found insignificant when objectively measured. In another study about the effect of transit-oriented development (TOD) using the heavy rail systems in New York City and Hong Kong as case studies (Loo et al., 2010), the results showed that a combination of variables in different dimensions, including land use, station characteristics, socio-economic and demographic characteristics and inter-modal competition were important in accounting for the variability of rail transit ridership. Station characteristics appeared to be the most important dimension in affecting average weekday railway patronage. Interestingly, the results showed that car ownership is both significant and positively associated with railway patronage, which suggests that higher car ownership may be associated with more pick-ups, drop-offs and park-and-ride activities to the transit stations for the longer transit trip legs.

3. RESEARCH METHODOLOGY

3.1 Framework of this Study

The framework of this study is shown in Figure 3-1 below. It can be seen from the framework that this study is implemented in two major parts: 1) Data collection and 3D modelling and, 2) 3D spatial analyses. In particular, the 3D spatial analyses include visual impacts (on urban skyline and mountain ridgeline), effects on solar exposure, on wind ventilation and on air temperature. All analyses are conducted by using 3D spatial analysis technology, which is better than 2D spatial analysis technology because it is more representative of the real physical world.

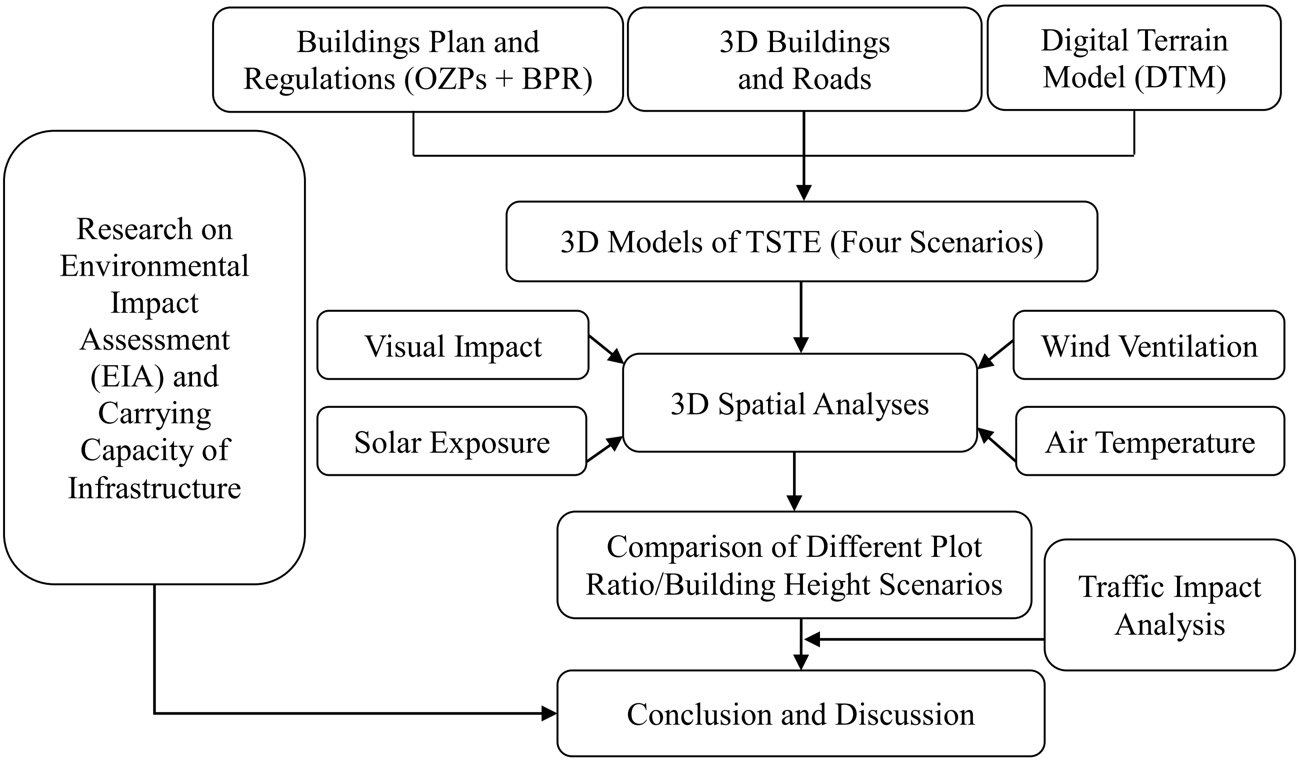

Figure 3-1. Framework of this study

3.2 Data Collection and 3D Modelling

As shown in Figure 3-2, the 3D spatial data to be collected, such as 3D buildings, roads, and the Digital Terrain Model (DTM) are available from the Lands Department (2016). However, as some of the available data is not up to date, the data does not always identically match the current situation. For example, the data for some parts of the Royal Garden Hotel and the New World Centre do not match the actual current situation. Such 3D buildings are developed based on the current situation.

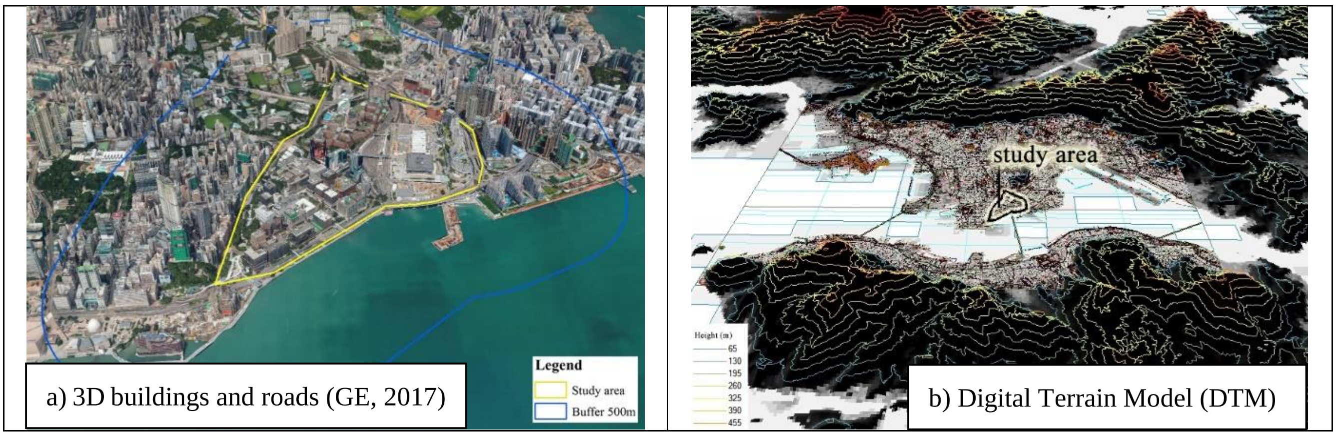

Figure 3-2. 3D Spatial data in/around the study area

Table 3-1. Buildings plan

No.	Buildings	Site class	Zone	Site area (m^2)	PR (total)	GFA (m^2)	SC (%)	BH (m)	OZPs (Max)		BPR (Max)	
									PR	BH (m)	PR	SC (%)
1	Kowloon Shangri-La			4000.000	11.599	46383.644	74.079	47.10				
2	InterContinental Grand Stanford			2479.000	10.540	26128.660	75.000	47.00		80.0		
3	New World Millennium		C	2850.000	11.832	33718.948	74.253	47.96	12			
4	The Royal Garden			2219.600	14.993	33278.630	74.960	62.60		95.0		
5	Regal Kowloon Hotel			2560.000	12.401	31746.004	74.767	49.00				
6	Hotel ICON		G/IC	4000.000	8.991	35964.050	64.960	107.00	-	111.5		
7	TST Centre			3979.500	12.000	47753.070	71.867	49.00		80		
8	Peninsula Centre	C		4400.000	11.999	52797.950	75.000	47.10		95		
9	Energy Plaza			1500.000	12.000	17999.945	74.890	47.02				
10	Wing On Plaza			2899.920	11.967	34703.923	68.802	49.00		80		
11	Mirror Tower		C	1550.000	11.990	18585.491	71.048	44.00		95		
12	Inter-Continental Plaza			1380.000	11.993	16550.158	74.739	49.00			15	65
13	Empire Centre			2600.000	11.744	30533.856	74.990	47.45		80		
14	Houston Centre			3199.732	11.940	38203.503	67.103	49.00				
15	Hilton Towers			2150.000	11.974	19311.737	38.080	45.25	12			
16	New East Ocean Centre	A	C(5)	3116.000	10.996	34265.340	59.860	61.58				
17	Harbour Crystal Centre			2350.000	11.996	28190.304	75.000	44.64		95		
18	Chinachem (Golden) Plaza		C	5067.000	11.986	60734.869	71.299	47.11				
19	South Seas Centre			3458.000	11.976	41413.253	75.000	47.03				
20	New Mandarin Plaza	C		4500.000	11.989	53954.740	75.000	45.70				
21	Concordia Plaza		C(4)	5535.000	11.999	66419.730	64.160	92.60		98.3		
22	East Ocean Centre		C	2900.000	11.999	34797.903	74.980	46.65		95		
23	Auto Plaza		C(3)	3149.000	12.432	39149.397	75.017	49.00				

Source: BD, 2017

The other non-spatial collected data relates to the updated approved building plan including Site Class, Zone, Site Area, PR, Gross Floor Area (GFA), Site Coverage (SC) and BH of the current 23 buildings in TSTE (Table 3-1) and it is available from the Buildings Department (BD, 2017). The data is considered in the relaxation of the maximum PR/BH restrictions and make appropriate determinations of designing and developing effective scenarios for 3D spatial analyses.

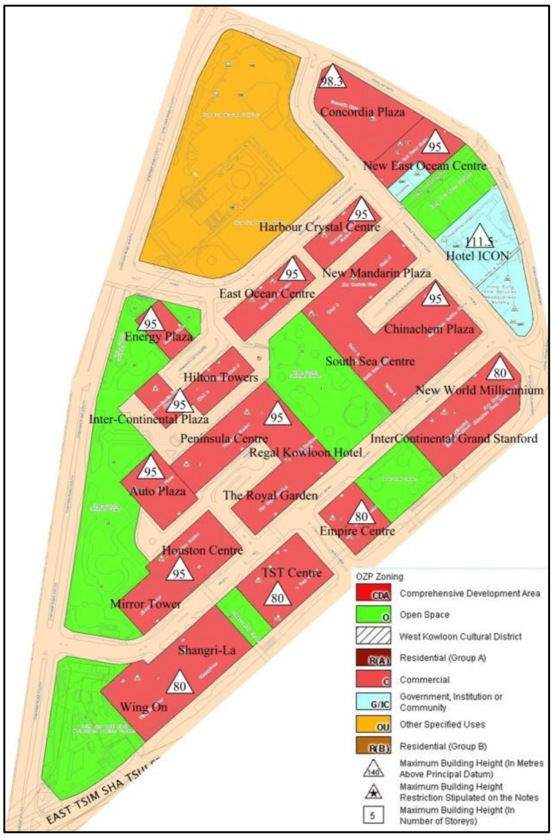

Figure 3-3. Map of OZPs for the TSTE (Source: Adapted from TPB, 2016)

The maximum PR/BH restrictions are shown in the Lease Conditions proposed by The Land Registry (LR, 2017), OZPs proposed by the Town Planning Board (TPB, 2016) and the BPR proposed by the Buildings Department (BD, 2012). Specifically, the OZPs is one of statutory plans prepared by the TPB under the Town Planning Ordinance and shows land zonings and major road systems for each planning scheme area. The OZPs (S/K1/28) is one of the most important regulations in the consideration of the PR/BH relaxation. From the map of OZPs shown in Figure 3-3, it can be clearly seen that four major types of zones - Commercial (C), Open Space (O), Government, Institution or Community (G/IC), and Other Specific Uses (OU) are in the study area. It is also found that the use of each zone is restricted by the maximum BH, which is highlighted by a triangular symbol, and by specific notes that describes the restrictions in detail, e.g. the approved maximum PR, the maximum GFA, and the requirement of supporting spaces for car parking and public passage.

The BPR is made under the Buildings Ordinance (BD, 2012), which statutorily governs the planning, design and construction of buildings. The BPR is another important regulation in the consideration of the PR/BH relaxation. The BPR regulates the sites of buildings. These regulations classify the sites of buildings into three classes - Classes A, B, and C with the following definitions (described in regulation 18A):

> "class A site means a site, not being a class B site or class C site, that abuts on one specified street not less than 4.5 m wide or on more than one such street; class B site means, a corner site that abuts on 2 specified streets neither of which is less than 4.5 m wide; class C site means, subject to paragraph (2), a corner site that abuts on 3 specified streets none of which is less than 4.5 m wide."

These regulations restrict the maximum PR/SC in terms of buildings' site and height (described in regulations 20 and 21). The detail of these regulations is shown in Table 3-2.

Table 3-2. Maximum PR/SC in relation to BH under BPR

Domestic/Non-Domestic Buildings						
Height of Building in Metres	**Percentage Site Coverage**			**Plot Ratio**		
	Class A Site	**Class B Site**	**Class C Site**	**Class A Site**	**Class B Site**	**Class C Site**
Not exceeding 15m	66.6/100	75/100	80/100	3.3/5	3.75/5	4.0/5
Over 15m but not exceeding 18m	60/97.5	67/97.5	72/97.5	3.6/5.8	4.0/5.8	4.3/5.8
Over 18m but not exceeding 21m	56/95	62/95	67/95	3.9/6.7	4.3/6.7	4.7/6.7
Over 21m but not exceeding 24m	52/92	58/92	63/92	4.2/7.4	4.6/7.4	5.0/7.4
Over 24m but not exceeding 27m	49/89	55/90	59/90	4.4/8.0	4.9/8.1	5.3/8.1
Over 27m but not exceeding 30m	46/85	52/87	55/88	4.6/8.5	5.2/8.7	5.5/8.8
Over 30m but not exceeding 36m	42/80	47.5/82.5	50/85	5.0/9.5	5.7/9.9	6.0/10.2
Over 36m but not exceeding 43m	39/75	44/77.5	47/80	5.4/10.5	6.1/10.8	6.5/11.2
Over 43m but not exceeding 49m	37/69	41/72.5	44/75	5.9/11.0	6.5/11.6	7.0/12.0
Over 49m but not exceeding 55m	35/64	39/67.5	42/70	6.3/11.5	7.0/12.1	7.5/12.6
Over 55m but not exceeding 61m	34/60	38/62.5	41/65	6.8/12.2	7.6/12.5	8.0/13.0
Over 61 m	33.33/60	37.5/62.5	40/65	8.0/15	9.0/15	10.0/15

Source: Adapted from BD, 2012

With careful consideration of the maximum PR/BH/SC restrictions, the relaxation of the maximum PR restrictions in OZPs is increased from 12 to 15 under the BPR, and the maximum BH restriction in The Lease Conditions is modified from the current BH (prevailing 51.5 meters) to the Max under OZPs (80 to 95 meters). With consideration for the foregoing, four hypothetical scenarios with different PR/BH of the 23 buildings in TSTE are developed (see Figure 3-4). Scenario 1 (S1) is the current situation, which follows the current PR/BH of the buildings; Scenario 2 (S2) is developed by increasing the PR to the max under BPR and by increasing the BH to the max under OZPs; Scenario 3 (S3) is developed by increasing the PR to the max under BPR with maintaining the current SC; and Scenario 4 (S4) is developed by rebuilding all the buildings to the maximum PR under BPR and the maximum BH under OZPs.

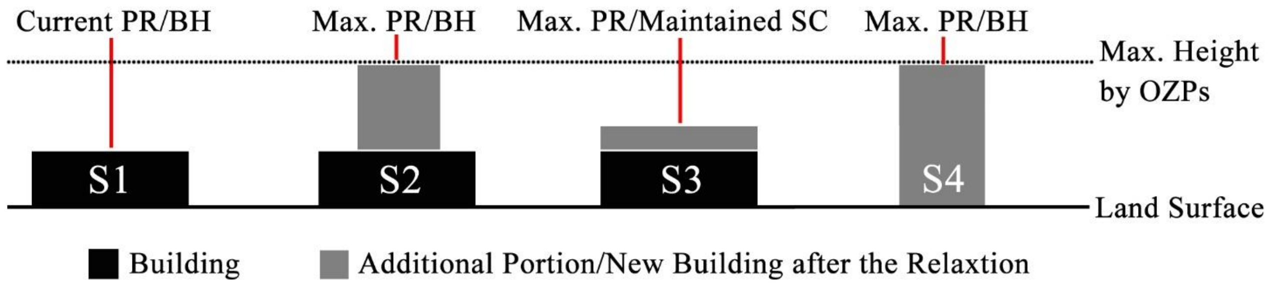

Figure 3-4. Four hypothetical scenarios

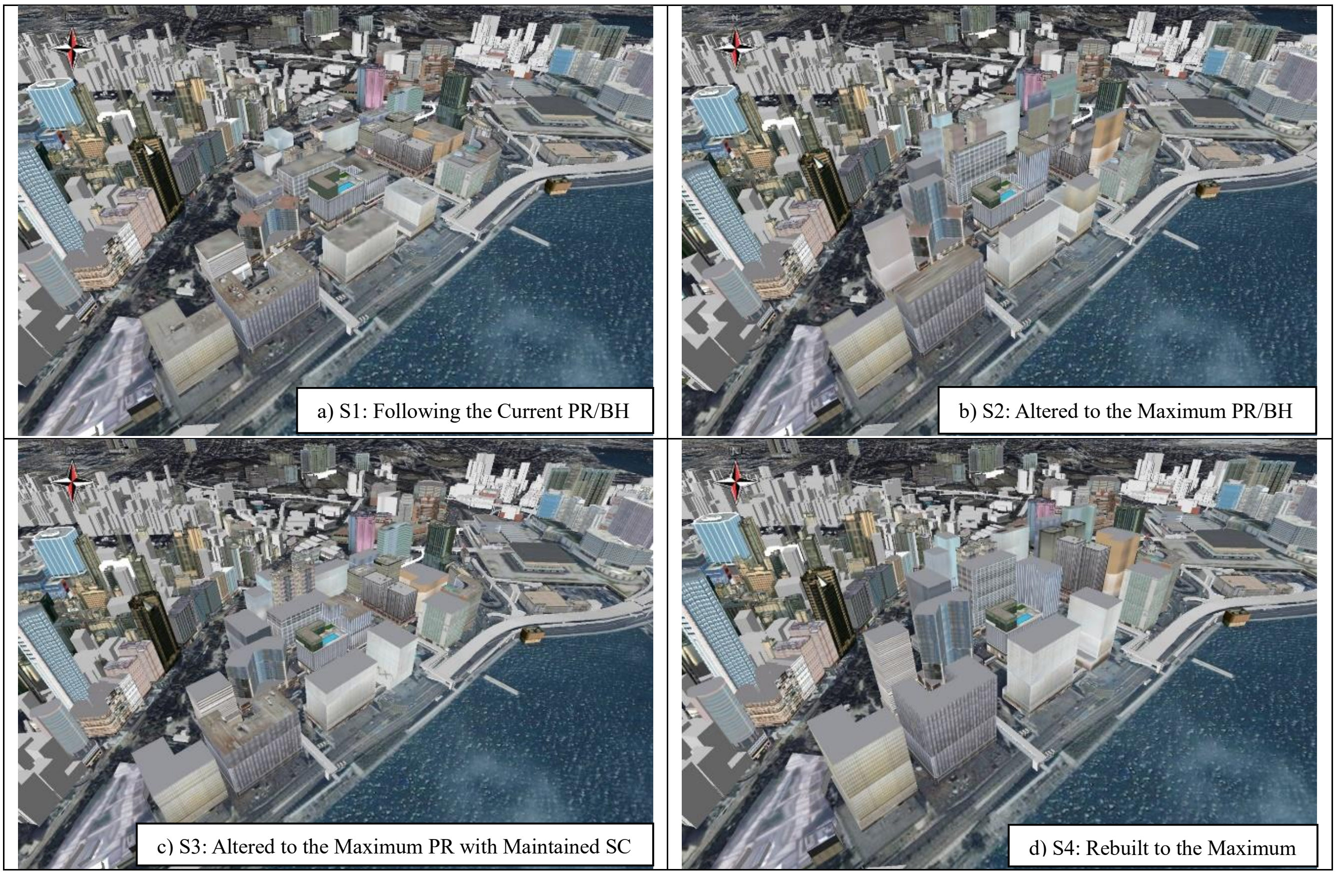

Figure 3-5. 3D buildings in the four scenarios

By following the four hypothetical scenarios, the 3D buildings are developed. The completed building models are shown in Figure 3-5 and the parameters of the developed building models are shown in Tables 3-3a, 3-3b and 3-3c.

Table 3-3a. Parameters for modelling the six hotels (No. 1 to 6) in TSTE

Buildings	Kowloon Shangri-La	InterContinental Grand Stanford	New World Millennium	The Royal Garden	Regal Kowloon Hotel	Hotel ICON
OZPs						
Max. SC	65%					
Max. PR	12			14.997	12	-
Max. BH (m)	80				95	111.5
BPR	Domestic/Non-domestic Buildings					
Max. SC (if >61m)	40%/65%					
Lease Conditions						
Original Max. BH (m)	51.50	51.00	-	51.80	51.41	51.50
Modified Max. BH (m)	-	-	-	Relaxed for sports and accommodation usages	-	111.50
Max. GFA (m^2)	-	-	34568.93	-	-	-
Max. PR/BH/SC	Complied with Buildings/Town Planning Ordinance		-	Complied with Buildings/Town Planning Ordinance		
Scenario 1 (current PR/BH)						
PR + Bonus	10.124+1.475	10.540	10.688+1.144	14.993	11.025+1.376	8.991
SC	74.079%	75.000%	74.253%	74.960%	74.767%	64.960%
GFA (m^2)	46383.644	26128.660	33718.948	33278.630	31746.004	35964.050
BH (m)	47.100	47.000	47.958	62.600	49.000	107.000
Scenario 2 (altered to the max. PR/BH)						
PR + Bonus	15+1.475	15	15+1.144	n/a	15+1.376	n/a
SC	74.079%	75.000%	74.253%	n/a	74.767%	n/a
GFA (m^2)	65900.000	37185.000	46010.400	n/a	41922.560	n/a
BH (m)	80.000			n/a	95.000	n/a
Scenario 3 (altered to the max. PR & maintained SC)						
PR + Bonus	15+1.475	15	15+1.144	n/a	15+1.376	n/a
SC	74.079%	75.000%	74.253%	n/a	74.767%	n/a
GFA (m^2)	65900.000	37185.000	46010.400	n/a	41922.560	n/a
BH (m)	66.484	63.413	64.393	n/a	67.155	n/a

Scenario 4 (rebuilt to the max. PR/BH)						
PR + Bonus	15+1.475	15	15+1.144	n/a	15+1.376	n/a
SC	55.867%	57.670%	54.952%	n/a	47.440%	n/a
GFA (m^2)	65900.000	37185.000	46010.400	n/a	41922.560	n/a
BH (m)	80.000			n/a	95.000	n/a

Table 3-4b. Parameters for modelling the additional ten buildings (No. 7 to 16) in TSTE

Buildings	TST Centre	Peninsula Centre	Energy Plaza	Wing On Plaza	Mirror Tower	Inter-Conti nental Plaza	Empire Centre	Houston Centre	Hilton Towers	New East Ocean Centre
OZPs										
Max. SC	65%									
Max. PR	12									
Max. BH (m)	80	95		80	95		80	95		
BPR	Domestic/Non-domestic Buildings									
Max. SC (if >61m)	40%/65%									33.33%/60%
Lease Conditions										
Original Max. BH (m)	51.8	51.5					51.816	51.5		51.82
Modified Max. BH (m)	-									61.58
Max. PR/BH/SC/GFA	Complied with Buildings/Town Planning Ordinance									
S1 (current PR/BH)										
PR	12.000	11.999	12.000	11.967	11.990	11.993	11.744	11.940	11.974	10.996
SC	71.867%	75.000%	74.890%	68.802%	71.048%	74.739%	74.990%	67.103%	38.080%	59.860%
GFA (m^2)	47753.070	52797.950	17999.945	34703.923	18585.491	16550.158	30533.856	38203.503	19311.737	34265.340
BH (m)	49.00	47.10	47.02	49.00	44.00	49.00	47.45	49.00	45.25	61.58
S2 (altered to the max. PR/BH)										
PR	15	15	15	15	15	15	15	15	15	15
SC	71.867%	75.000%	74.890%	68.802%	71.048%	74.739%	74.990%	67.103%	38.080%	59.860%
GFA (m^2)	59692.500	66000.000	22500.000	43498.800	23250.000	20700.000	39000.000	47995.980	32250.000	46740.000
BH (m)	80	95		80	95		80	95		

S3 (altered to the max. PR & maintained SC)										
PR	15									
SC	71.867%	75.000%	74.890%	68.802%	71.048%	74.739%	74.990%	67.103%	38.080%	59.860%
GFA (m^2)	59692.500	66000.000	22500.000	43498.800	23250.000	20700.000	39000.000	47995.980	32250.000	46740.000
BH (m)	63.61	60.54	60.96	64.43	57.30	63.61	62.17	63.91	91.38	84.45
S4 (rebuilt to the max. PR/ BH)										
PR	15									
SC	58.698%	49.580%	50.317%	57.142%	45.293%	52.231%	59.376%	47.079%	29.558%	53.302%
GFA (m^2)	59692.500	66000.000	22500.000	43498.800	23250.000	20700.000	39000.000	47995.980	32250.000	46740.000
BH (m)	80	95		80	95		80	95		

Table 3-5c. Parameters for modelling the additional seven buildings (No. 17 to 23) in TSTE

Buildings	Harbour Crystal Centre	Chinachem Plaza	South Seas Centre	New Mandarin Plaza	Concordia Plaza	East Ocean Centre	Auto Plaza
OZPs							
Max. SC	65%						
Max. PR	12						
Max. BH (m)	95				98.3	95	
BPR	Domestic/Non-domestic Buildings						
Max. SC (if >61m)	40%/65%						
Lease Conditions							
Max. BH (m)	51.5	51.82	51.5		-	51.5	
Max. PR/BH/SC/GFA	Complied with Buildings/Town Planning Ordinance						
S1 (current PR/BH)							
PR + Bonus	11.996	11.986	11.976	11.989	11.999	11.999	11.984+0.448
SC + Bonus	75.000%	71.299%	75.000%		64.160%	74.980%	72.093%+2.924%
GFA (m^2)	28190.304	60734.869	41413.253	53954.740	66419.730	34797.903	39149.397
BH (m)	44.64	47.11	47.03	45.70	92.60	46.65	49.00
S2 (altered to the max. PR/BH)							
PR + Bonus	15						15+0.448
SC + Bonus	75.000%	71.299%	75.000%		n/a	74.980%	72.093%+2.924%
GFA (m^2)	35250.000	76005.000	51870.000	67500.000	n/a	43500.000	48645.752
BH (m)	95				n/a	95	
S3 (altered to the max. PR & maintained SC)							
PR + Bonus	15						15+0.448
SC + Bonus	75.000%	71.299%	75.000%		n/a	74.980%	72.093%+2.924%
GFA (m^2)	35250.000	76005.000	51870.000	67500.000	n/a	43500.000	48645.752
BH (m)	57.42	60.38	61.63	58.78	n/a	59.10	63.07
S4 (rebuilt to the max. PR/ BH)							
PR + Bonus	15						15+0.448
SC + Bonus	47.197%	46.784%	51.336%	48.220%	n/a	47.545%	50.480%
GFA (m^2)	35250.000	76005.000	51870.000	67500.000	n/a	43500.000	48645.752
BH (m)	95				n/a	95	

3.3 Approach for Analysing Skyline

This section proposes an approach for comparative assessment of the impact on skyline. This approach is designed to identify the pattern of visible number/portion of objects for determining the skylines and to assess the view to mountain ridgeline. The visibility pattern within an assessment area is achieved based on viewshed analysis (Fisher, 1992; 1993; 1994; 1996). Viewshed analysis is used for providing visibility results (view from one or a set of designated vantage points) of a surface of land and all the objects on it. This analysis is operated by sightline-based identification between visible and invisible areas (see Figure 3-6) with a consideration of the uncertainty of the spatial data.

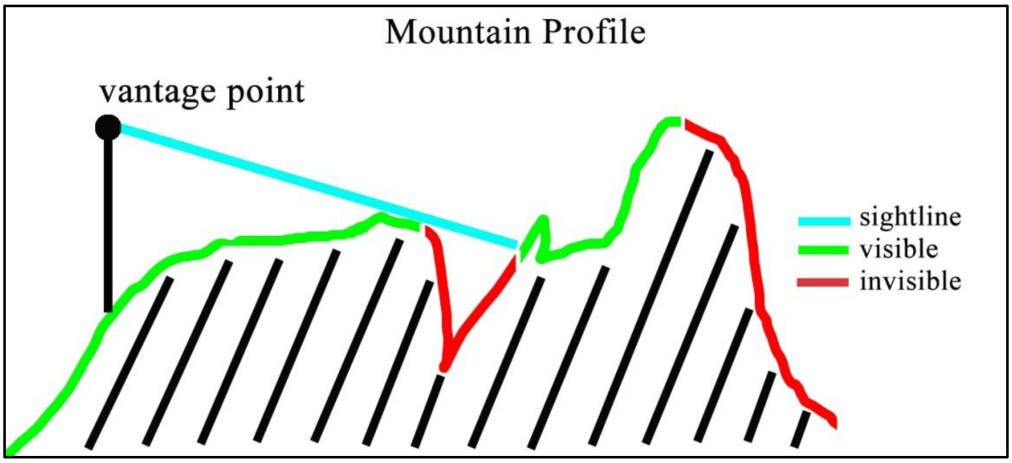

Figure 3-6. Sightline based approach for identifying the visible/invisible areas

The result of the operation shows a level of uncertainty in the visibility and a probable model is introduced to confront this uncertainty. One of the typical algorithms (Fisher, 1992) for calculating the 'probable viewshed' (viewshed generated by considering a probable model) is as follows:

$$\mathrm{p}(x_{ij}) = \frac{\sum_{k=1}^{n} x_{ijk}}{n} \tag{1}$$

Where $p(x_{ij})$ means the probability of a cell at row i and column j in a raster image (the Digital Surface Model (DSM)) being visible. The x_{ijk} means the value at the cell of the binary-coded viewshed in realization k. Such that the k takes values 1 to 'n'.

In the assessment of the skyline in TSTE, the approach is applied in the determination of skylines. A workflow of the determination is proposed (see Figure 3-7 and Table 3-4).

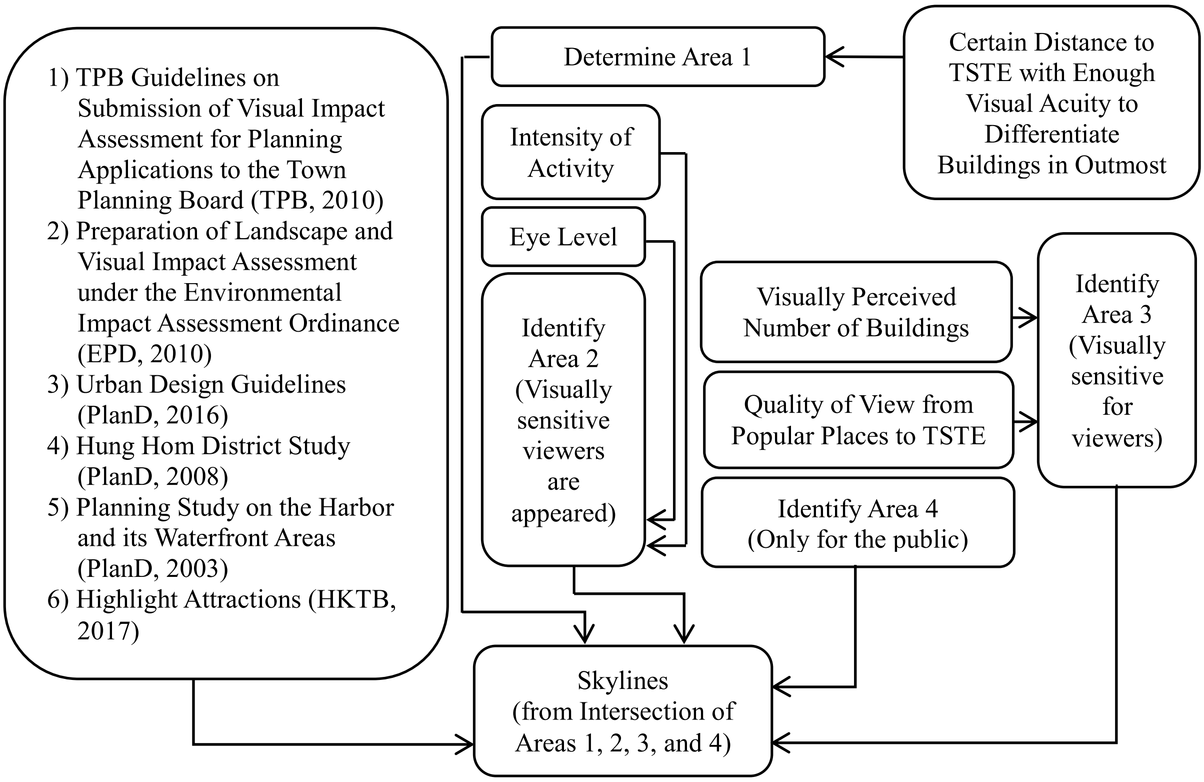

Figure 3-7. Workflow of determining TSTE skylines

Table 3-6. Specifications for determining TSTE skylines

<table>
<tr><th></th><th colspan="6">Indicator 1</th></tr>
<tr><td rowspan="2">Identifying area 1</td><td colspan="2">Visual acuity to the TSTE</td><td colspan="2">Indicated Area</td><td colspan="2">Reference</td></tr>
<tr><td colspan="2">1) Not clear enough to differentiate buildings in outmost
2) Clear enough to differentiate buildings in outmost</td><td colspan="2">1) n/a
2) Envelope (area) with buffer at the three times of the max. BH in TSTE</td><td colspan="2">Sample plan for key visual elements for VIA (Appendix C) in TPB PG-NO.41 (TPB, 2010) and (Hegemann and Peets, 1972)</td></tr>
<tr><th></th><th colspan="3">Indicator 2</th><th colspan="3">Indicator 3</th></tr>
<tr><td rowspan="2">Identifying area 2 where visually sensitive viewers are appeared</td><td>Intensity of Activity</td><td>Indicated Area</td><td>Reference</td><td>Eye Level (Vertical Position)</td><td>Indicated Area</td><td>Reference</td></tr>
<tr><td>1) Tense
2) Relax</td><td>1) n/a
2) Excluding those for business, e.g. office buildings</td><td>Viewing points (Paragraph 4.6) in TPB PG-NO.41 (TPB, 2010)</td><td>1) Out of eye level
2) In eye level</td><td>1) n/a
2) Ground/ road/ floor/ water surfaces</td><td>Viewing points (Paragraph 4.5) in TPB PG-NO.41 (TPB, 2010)</td></tr>
<tr><th></th><th colspan="3">Indicator 4</th><th colspan="3">Indicator 5</th></tr>
<tr><td rowspan="2">Identifying area 3 where are visually sensitive to TSTE</td><td>Visually perceived number of buildings</td><td>Indicated Area</td><td>References</td><td>Quality of view from popular places to TSTE</td><td>Indicated Area</td><td>References</td></tr>
<tr><td>1) 0
2) (0, 50%]
3) (50%, 100%]</td><td>1) n/a
2) n/a
3) With more than half of buildings being visible</td><td>a) Assessment area (Paragraph 4.3) in TPB PG-NO.41 (TPB, 2010)
b) Assessment area (Section 3.3c) in EIAO Guidance Note No. 8/2010 (EPD, 2010)</td><td>1) Low grade of visual perception value
2) High grade of visual perception value</td><td>1) n/a
2) Higher perception value of view among local popular places: Cultural Complex (PlanD, 2016), Victoria Harbour, Avenue of Stars (HKTB, 2017), Signal Hill Garden (PlanD, 2003), Hung Hom Bypass (PlanD, 2008)</td><td>a) Viewing points (Paragraphs 4.5, 4.6 and 4.7) in TPB PG-NO.41 (TPB, 2010)
b) Urban design guidelines in Chapter 11 of Hong Kong Planning Standards and Guidelines (PlanD, 2016)
c) Top 10 attractions (HKTB, 2017)
d) Sections 3.7 and 6.2.4 in Planning Study on the Harbor and its Waterfront Areas (PlanD, 2003)
e) Section 3.5.4 in Chapter 3 of Hung Hom District Study (PlanD, 2008)</td></tr>
<tr><th></th><th colspan="6">Indicator 6</th></tr>
<tr><td rowspan="2">Identifying area 4 where are only for the public</td><td colspan="2">Property of Space</td><td colspan="2">Indicated Area</td><td colspan="2">Reference</td></tr>
<tr><td colspan="2">1) Private space
2) Public space</td><td colspan="2">1) n/a
2) Pedestrian / vehicle / train / tram / shipping routes, Parks, public gardens, squares and playgrounds</td><td colspan="2">Viewing points (Paragraph 4.5) in TPB PG-NO.41(TPB, 2010)</td></tr>
<tr><td colspan="7">Skylines of TSTE viewed from intersection of areas 1, 2, 3, and 4</td></tr>
</table>

Area 1 is identified by considering visual acuity, which refers to the clearness of view for visually differentiating outmost buildings of TSTE. The distance of the area boundary to the focused buildings is not larger than three times of the building height (BH) (Hegemann and Peets, 1972) of the lowest building in outmost (along the area boundary).

Area 2 refers to where the sensitive viewers possibly appear. Sensitive viewers are people carriying out activies in a specific place for relaxation rather than engaging in business. Two indicators extracted from the sensitive viewers are the intensity of activity and the vertical position of the eye level, which is the position of eye achieved by the average height of the human above the accessible surface (TPB, 2010), e.g. ground/road/roof/water surfaces, subtracting 4.4 inches (distance from the nasal root depression between the eyes sellion to the top level of the head).

Area 3 refers to the places that are visually sensitive for TSTE. The view from such an area represents a relative high quality of TSTE image in vision. Two indicators of the quality are the visble number/portion of TSTE buildings (TPB, 2010; EPD, 2010) and the quality of view (PlanD, 2016; HKTB, 2017; PlanD, 2003; PlanD, 2008) to TSTE from popular places (e.g. Cultural Complex, and the other four popular vantage points, which are Victoria Harbour, Avenue of Stars, Signal Hill Garden and Hung Hom Bypass).

Area 4 refers to the places of concern based on spaces for public use only. Specifically, these areas are the routes for pedestrains, vehicles, trains, trams, shipping, and places such as parks, public gardens, squares, playgrounds, and harbours. Finally, the skylines are determined based on the intersection of Areas 1, 2, 3, and 4, which forms view corridors forward to the TSTE skylines.

3.4 Approach for Analysing Mountain Ridgeline

In the assessment of mountain ridgeline, the approach is to analyse the visibility of the ridgeline. This analysis measures to what extent the PR/BH relaxation affects the view to the mountain ridgeline. When a ridgeline is visible to humans, the sightline between the ridgeline and the human eyes must not be blocked by any other physical objects (e.g. buildings). The workflow of analysing ridgeline is shown in Figure 3-8 below.

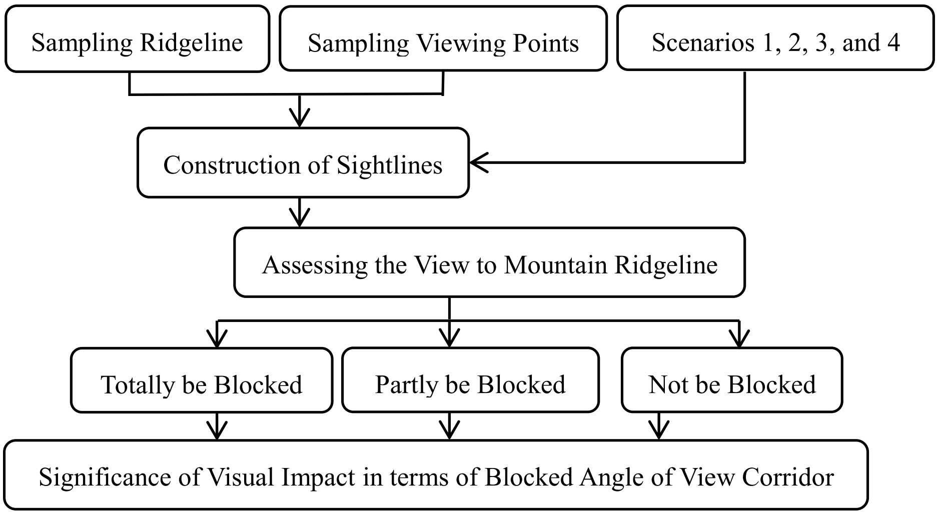

Figure 3-8. Workflow of ridgeline analysis

Based on the technical flow, the analysis firstly selects and samples the viewing points and the ridgeline for constructing the sightlines. The selection follows the recommendations (Figure 3-9) of the Urban Design Guidelines for Hong Kong (PlanD and RMUM Hong Kong Limited, 2002). Totally four strategic viewing points, which are defined by TPB (TPB, 2010), are proposed in this analysis:

1) Quarry Bay Park.
2) Hong Kong Convention and Exhibition Centre.
3) Sun Yat Sen Memorial Park.
4) Central Pier No.7.

It is proposed to preserve the ridgeline by protecting the "20% Building Free Zone" - a defined zone beneath the ridge and above the limit of roofline as shown in Figure 3-9c. The ridgeline therefore is sampled with 1° intervals (see Figure 3-10) of target points along this zone (i.e. the limit of roofline) running from Beacon Hill through Lion Rock and Tsz Wan Shan to Kowloon Peak when viewed from each of four strategic viewing points. Totally four sets of ridgelines are sampled, corresponding to the different views from the viewing points.

a) Strategic viewing points for ridgelines

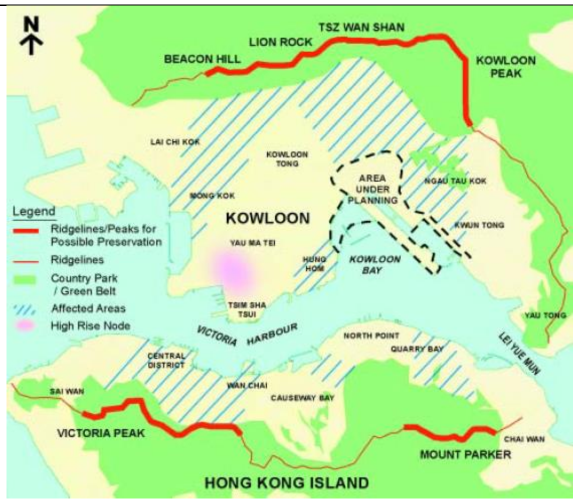

b) Ridgelines for preservation

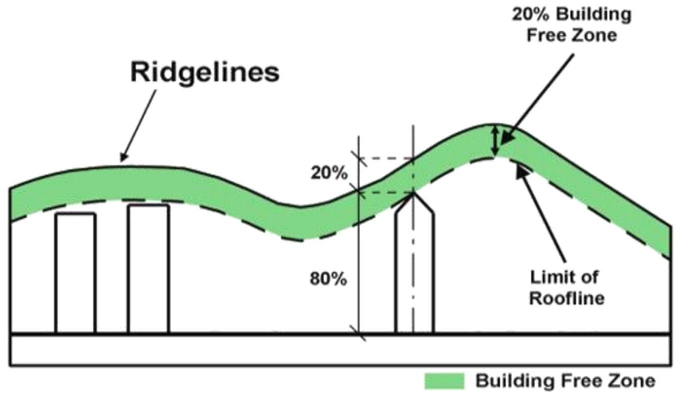

c) 20% building free zone

Figure 3-9. Strategic viewing points and ridgelines (Source: PlanD, 2010)

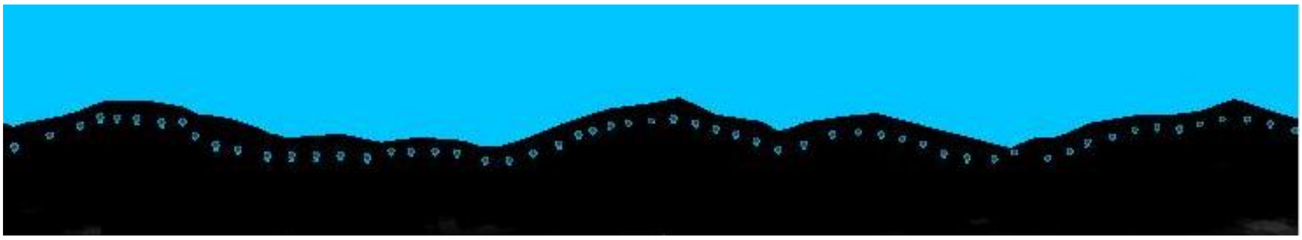

Figure 3-10. Sampling of ridgeline with 1° of target points

Sightlines (e.g. Figure 3-11) are constructed by connecting the strategic viewing points and the corresponding sets of target points. Each set of sightlines forms a triangular view corridor starting from the strategic viewing points on the Hong Kong Island passing through the Victoria Harbour to the Kowloon mountain ridgeline. All the view corridors are divided into two classes, which are green corridors (not be blocked) and red corridors (be blocked).

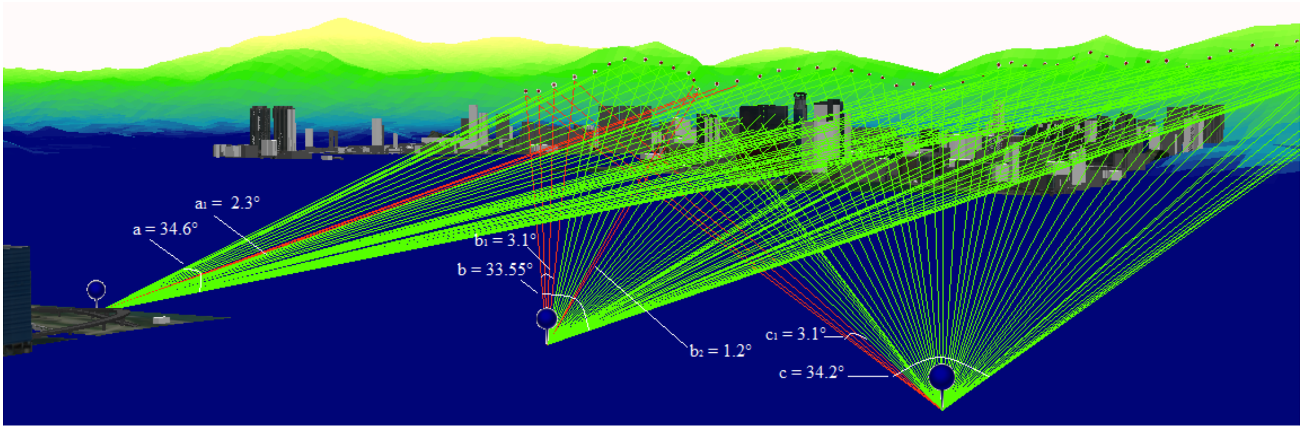

Figure 3-11. Exemplified sightlines and angle of the view corridors

The angle of each view corridor is quantified (see Figure 3-11). The quantification is made by using the following Equation (2):

$$R = \frac{1^\circ \times (n_1 - 1) + 1^\circ \times (n_2 - 1) + \cdots + 1^\circ \times (n_n - 1)}{A^\circ} \qquad (2)$$

Where ‘A°’ is the sum of angle for a view corridor, ‘n_n’ is the number of blocked sightlines in the ‘n^{th}’ sub view corridor, and ‘R’ is the ratio of the blocked angle for the view corridor.

3.5 Simulation Model for Solar Exposure Analysis

The effects of solar exposure in terms of time (hourly) on the direct insolation (excluding the diffused insolation) and the radiation energy of the insolation around the surface (land + build facades) of TSTE are investigated by using a simulation model. The solar exposure for each of the four individual scenarios is simulated. The parameters of the simulation include the date and time of simulation, coordinates of TSTE, and the solar azimuth and altitude (Table 3-5).

Table 3-7. Parameters of simulating the solar exposure in TSTE

Date	Winter Solstice (22-Dec-2013)	Summer Solstice (21-Jun-2013)
Time	8:40 - 16:00	7:15 - 17:32
Coordinates	22.30° for Latitude	114.10° for Longitude
Azimuth	127°SE - 232°SW	72°ENE - 288°WNW
Altitude	20°	20°

Based on these parameters, the simulatoin model is applied in generating the footprint of shadow volume, which is represented by a bundle of sunlight (see Figure 3-12a.) blocked by the buildings (the blockage of sunlight is simular to the blockage of sightline). The generated footprints of building shadow are used as the impact boundaries (Figure 3-12b.) respectively in summer and winter solstices. All the 3D buildings/roads within these boundaries are used as input for the simulation.

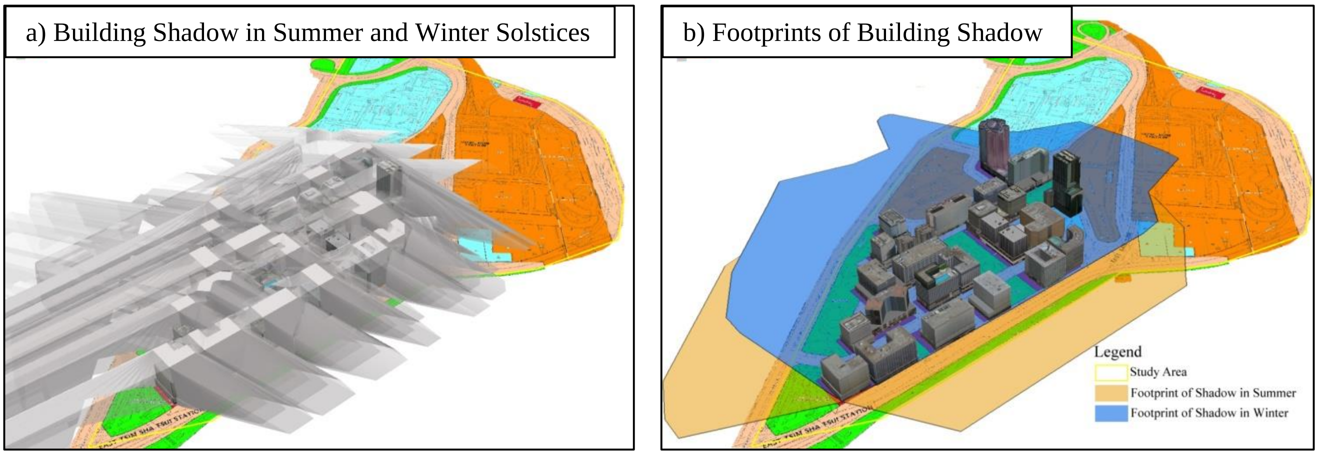

Figure 3-12. Shadow and corresponding footprints of exposure in summer and winter solstices

The simulation is implemented based on Ecotect analysis software (Marsh, 2003), which is an environmental analysis tool widely used in the study of daylighting assessment, thermal performance, and acoustic simulation for building planning and design (Yang et al., 2014; Thuesen, 2010; Wang et al., 2011; Peng, 2016). The results of the simulation include the cumulative exposure time and radiation distributed on the 3D surface within the impact boundaries in summer and winter solstices. The results also include the cumulative exposure radiation distribution on west facing facades.

3.6 Microclimate Model for Analysing Wind Ventilation

Wind flow significantly impacts the living environment and plays an important role in urban climates, development of renewable energy, and crisis management related to outward wind flow. Airflow Analyst® is a software which helps to analyse wind ventilation. It is based on GIS (Geographical Information Systems) and spatial data to simulate complex surrounding airflow movements. It uses a fluid dynamics algorithm, 3D CFD (Computed Fluid Dynamics), which is a core element for a highly accurate airflow analysis and is developed and tested at Kyushu University (Airflow, 2015). It is the first software to integrate CFD with GIS and is available as third party extension software of the ArcGIS (ESRI, 2015). Therefore, terrain and 3D building datasets prepared in ArcGIS can be directly used in Airflow Analyst without any remodelling of spatial data. Airflow technique of wind flow estimation is used and validated in different studies to simulate wind speed (Li, 2011; Uchida et al., 2011a, 2011b, 2011c, Uchida and Ohya, 2011, 2008). Details of the software can be found on the software's homepage: (http://airflowanalyst.com/en/links.html).

Configuration Setting and Simulation:

A Digital Elevation Model (DEM) with a 2-meter spatial resolution and 3D models were used to simulate airflow in the study area using Airflow Analyst. The monthly means of wind direction and wind speed from Star Ferry Automatic Wind Station were acquired from the Hong Kong Observatory (HKO). Three computational grids were generated, corresponding to 3D scenarios (S1, S2, S3, and S4), and then subsequent fluid analysis, visualization and analysis of the results were performed. Lastly, the results were exported as 2D maps of wind speed and 3D animations, and were analysed for the likely effects of increasing building height on wind speed. The output of the airflow analysis was then exported into a point shape file, which then used ArcGIS to extract information by a sequence of processes that included: 're-projection', 'interpolation', and 'subtraction of S1 from S2, S3, and S4'. Maps were ultimately generated and the attribute data were exported for statistical analysis in Microsoft Excel.

3.7 Microclimate Model for Analysing Air Temperature

ENVI-met is a common microclimate model that can simulate the microclimate of a study area, and is widely applied in many applications for studying the relationships between urban designs and microclimates (Toggweiler and Key, 2001; Emmanuel and Fernando, 2007; Fahmy and Sharples, 2009; Ng et al., 2012; Li et al., 2016; Jamei and Rajagopalan, 2017; Morakinyo et al., 2017; Tukiran, 2017). The simulation of ENVI-met considers the interaction among soil, vegetation and atmosphere based on theories of fluid dynamics and thermodynamics, with a few pre-requisites including a steady temperature inside buildings and no heat storage inside the buildings (ENVI-met, 2017). These conditions result in a simulation that focuses only on the physical influence instead of the anthropogenic effect. The capability of ENVI-met in simultaneous calculation of meteorological conditions, soil and vegetation processes, and surface energy fluxes with a broad range of urban configurations can also improve the simulation of an urban micro-climate (B.M, 2011; Jamei and Rajagopalan, 2017). Therefore, in this study, ENVI-met 4.1 was used to simulate the spatial patterns and distribution of air temperature in the TSTE region with different building designs (S1, S2, S3, and S4). The results of this study are expected to provide a foundation for future development that take a climate conscious urban design approach.

This model requires initial weather information, including wind speed (m/s) and direction, air temperature, relative humidity, and special humidity at a specific date and time (Table 3-6). The weather data were acquired from the Hong Kong Observatory (HKO) and shown in Table 3-7 below.

Table 3-8. Configuration setting in ENVI-met

Date	11-Jul-2016 (Summer)	13-Jan-2016 (Winter)
Start Time of Simulation	7:00am	7:00am
Total Simulation Time (Hour)	24	24
Wind Speed in 10m Above Ground (m/s)	2.70	3.42
Wind Direction (degree)	West (260°)	East (100°)
Initial Atmosphere Temperature (°C)	27.50	15.45
Specific Humidity in 2500m (g water/kg air)	10.42	5.24
Relative Humidity in 2m (%)	83	85

Table 3-9. Meteorological elements and climatological database by HKO

Year	2016											
Month	Jan.	Feb.	Mar.	Apr.	May	Jun.	Jul.	Aug.	Sep.	Oct.	Nov.	Dec.
Average Wind Speed (km/h)	29.4	21.3	22.8	17.1	20.2	18.0	19.2	17.1	18.9	26.3	27.0	26.7
Prevailing Wind Direction (degree)	60	20	50	40	70	220	230	60	80	70	70	70
Average Air Temperature (°C)	16.0	15.5	17.5	23.6	26.7	29.4	29.8	28.4	27.9	26.8	22.3	19.6
Date	13-Jan-2016						11-Jul-2016					
Average Wind Speed (m/s)	3.42						2.70					
Prevailing Wind Direction (degree)	100°						260°					

Source: HKO, 2016

Two seasons (summer and winter) were examined based on the meteorological parameters and the climatological database of Star Ferry Automatic Wind Station (Table 3-7) (HKO, 2016). Two typical days 11-July-2016 and 13-Jan-2016, which represent normal weather conditions in summer and winter respectively, are selected to represent the two seasons. The average wind speed in the prevailing directions are 2.7 m/s and west direction (260°) in summer, and 3.42 m/s and east direction (100°) in winter. The average air temperatures were 29.8°C for summer, and 16.0°C for winter (see Table 3-7.). During the comparison of scenarios, S1 acts as a reference, while S2, S3, and S4 act as observations. Comparison values are calculated by deducting the reference values from the observation values.

3.8 Approach for Traffic Impact Analysis

One assumption of the Traffic Impact Analysis (TIA) is the increased hotel/office rooms will generate traffic and distribute to surrounding areas. Therefore, to understand the traffic impact, the following steps are conducted:

Step 1: Basic Scenario
A system of traffic analysis zones and road network will be developed to cover the TSTE study area. If data from an existing travel demand model is available and can be obtained, this will be used. Traffic Analysis Zone will be created; and the zones will be small enough so that each of the new hotels is in its own zone. The speed and capacity of each road link will be based on the data from Hong Kong Transport Department, and the hierarchy of roads described in the most recent Annual Traffic Census of Transport Department.

Step 2: Trip Generation
The growth in travel is forecasted by applying the trip rates used by Transport Department of Hong Kong. For purpose of reference, these rates will be compared to the similar rates shown in the ITE Trip Generation manual for the US.

Step 3: Mode Choice
Mode Choice is one essential part of traffic modelling, since one trip can be completed with different travel modes (e.g., taxi, bus, etc.) In Step 3, the estimated trip generation will be further differentiated into “mode-specific” trip. In Hong Kong, around 80% residents commute by public transportation (e.g. MTR). However, in term of tourists (i.e. hotel guests) taxi might be their first choice. For short-distance, tourists might even choose to walk instead of taking any motorized mode.

Step 4: Future Scenarios
As mentioned, two future scenarios will be considered in this project. Those two future scenarios are different in environmental sense. Thus, different increased hotel room (and people) will be given as the base of future scenarios.

Desire lines are used to illustrate on a map the flows of people or goods from point to point based on the values from a matrix. For both future scenarios, the desire line analysis will be conducted. However, survey is the main tool to achieve above steps. That is, questionnaires are developed for street intercept survey. Respondents are first asked about current travel behaviour. Then, the project detail and pictures of Green Deck will be shown to respondents. Eventually, respondents will share comments on their future travel behaviour.

4. 3D SPATIAL ANALYSES AND RESULTS

4.1 Skyline Analysis and Results

The assessment Area 1 is determined by considering visual acuity for TSTE buildings, and the result of step 1 is highlighted by pink boundary shown in Figure 4-1a. This area is achieved by using a buffer to TSTE by 132m, which is equal to three times of the height of the lowest building - Mirror Tower (BH = 44 m). Figure 4-1b shows Area 2 in horizontal dimensions by excluding commerical land zones with office buildings in TST. Figure 4-1c shows the Area 3, which is obtained by considering a pattern of the visible number of TSTE buildings and by selecting popular places (areas) with relative high value of visual perception to TSTE skylines. It is found by considering the space only for public uses and the identified Area 4 is shown in Figure 4-1d. The intersection of Areas 1, 2, 3, and 4 is shown in Figure 4-2. This intersection is in the southeast side of TSTE (fronted by Victoria Harbour) along with the seaside roads from Hung Hom Bypass to Salisbury Road and the promenades from TST Promenade to Avenue of Stars.

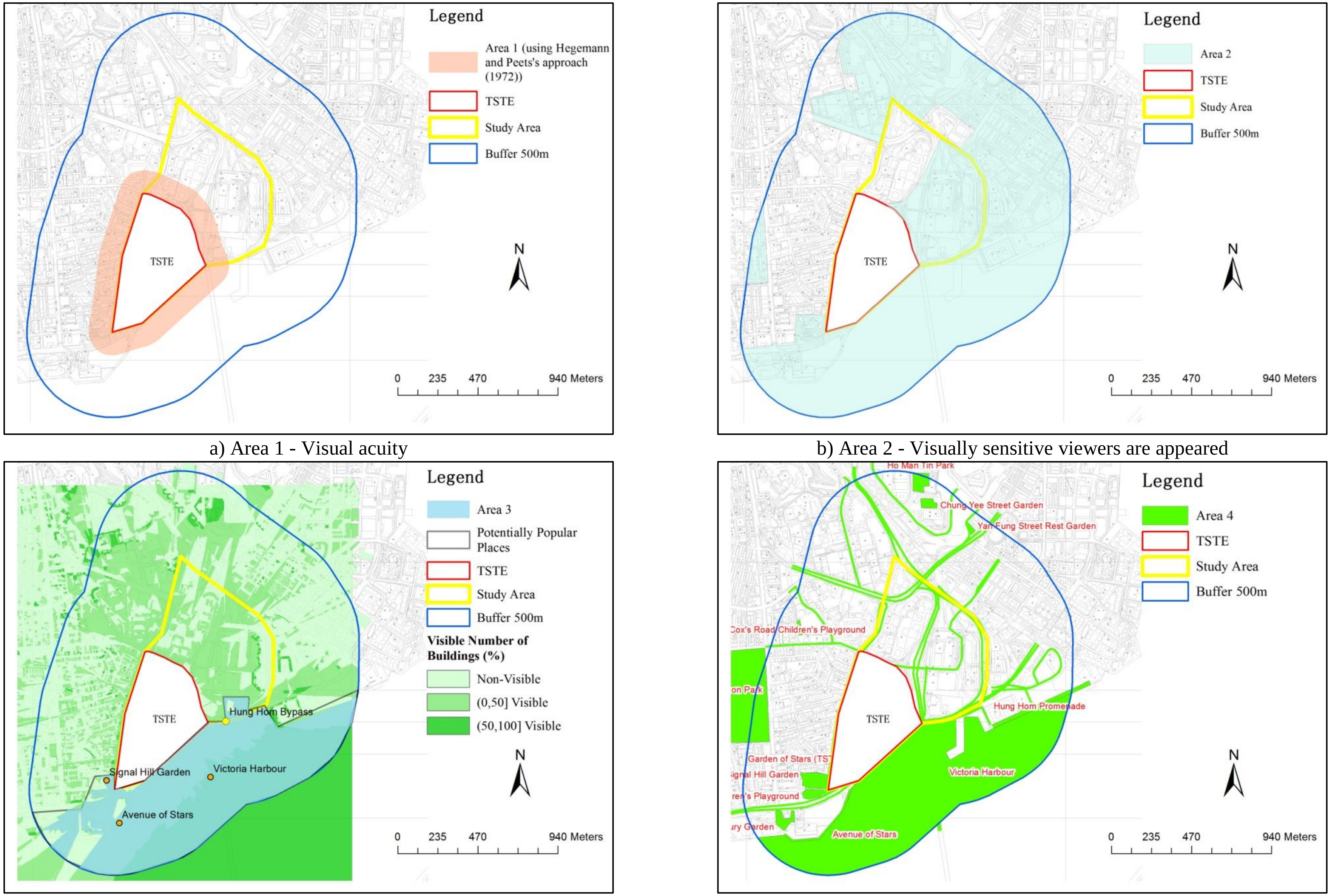

a) Area 1 - Visual acuity

b) Area 2 - Visually sensitive viewers are appeared

c) Areas 3 - Visually sensitive to viewers

d) Area 4 - Only for the public uses

Figure 4-1. Results of Areas 1 to 4 in the process of determining skylines

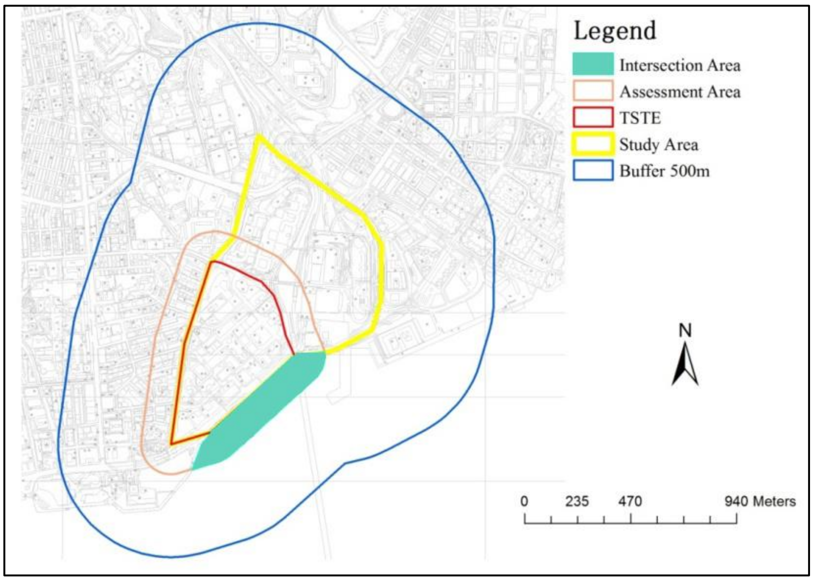

Figure 4-2. Intersection of Areas 1, 2, 3, and 4

Totally three skylines are determined (Figure 4-3) by considering the intersection of Areas 1, 2, 3, and 4. Specifically, Skyline A is viewed from the view corridor from the northeast (80°) to TSTE. Skyline B is viewed from the view corridor from the southeast (141°) to TSTE. Skyline C is viewed from the view corridor from the southwest (215°) to TSTE.

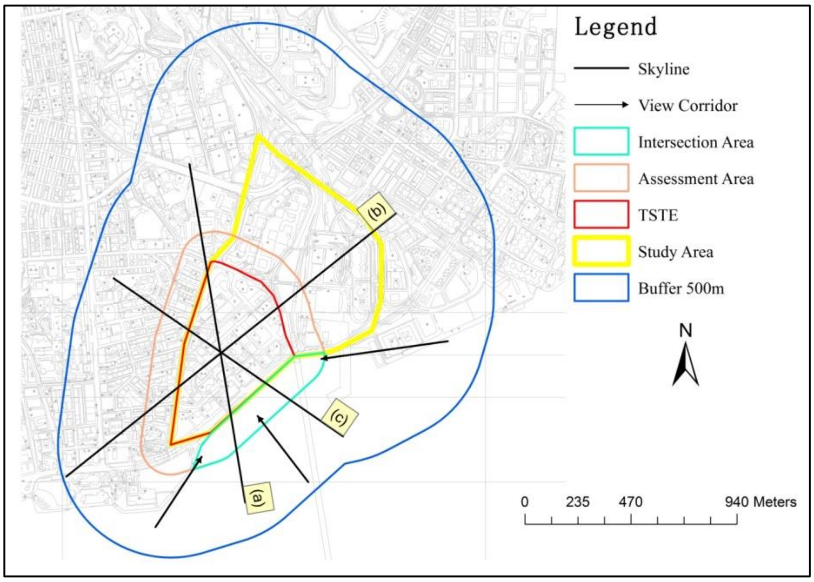

Figure 4-3. Determined skylines a, b, and c

The three skylines are visualized in each of the four scenarios. The terrain, 3D buildings, and roads form these skylines. The skylines in S2, S3, and S4 are compared to the corresponding skylines in S1. The comparison of Skyline A is shown in Figure 4-4, the comparison of

Skyline B is shown in Figure 4-5, and the comparison of Skyline C is shown in Figure 4-6. The results show that the effect of PR/BH relaxation on the skylines is not significant. The impact specifications of each skyline are explained one by one.

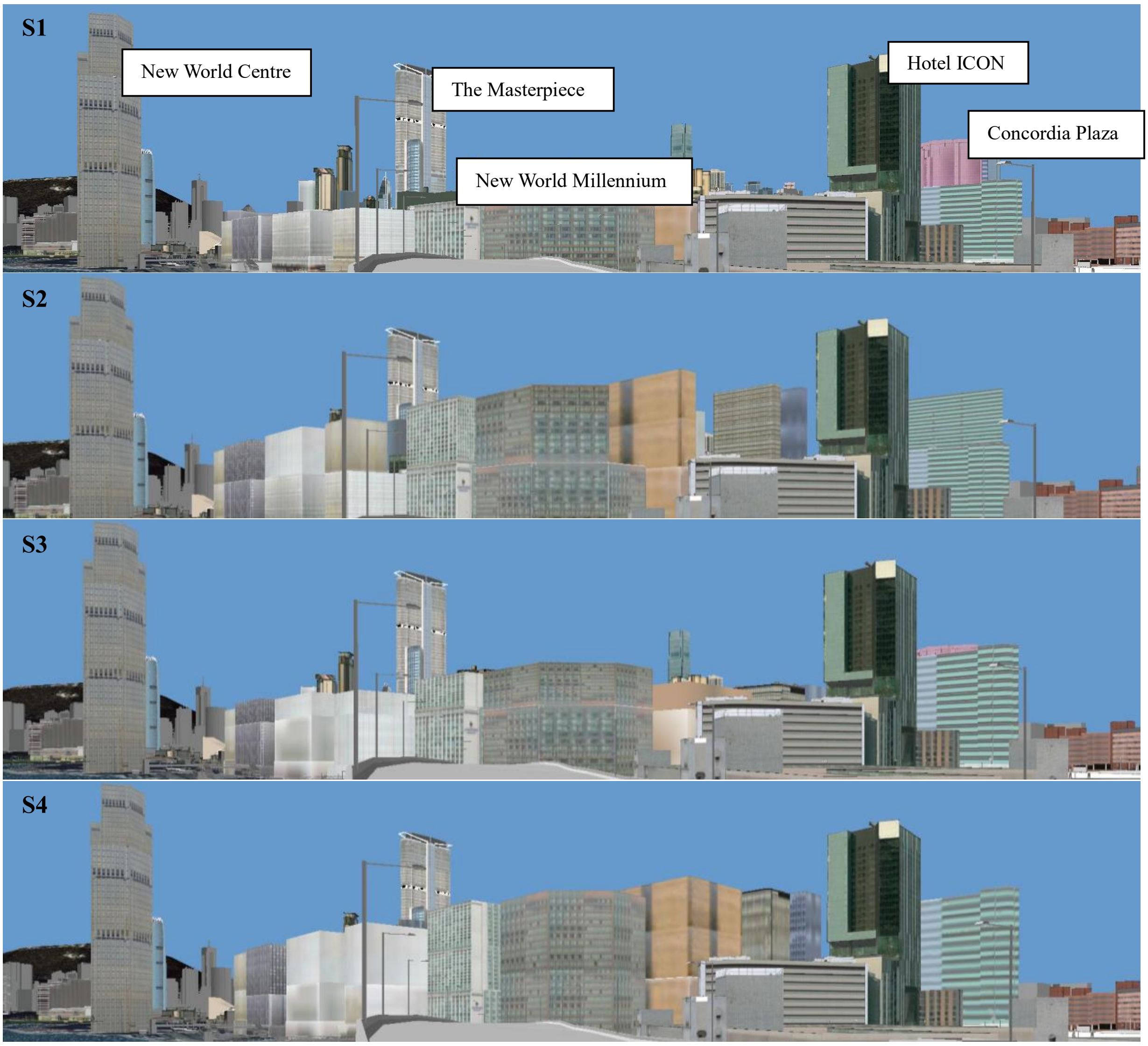

Figure 4-4. Skyline A in the S1, S2, S3, and S4

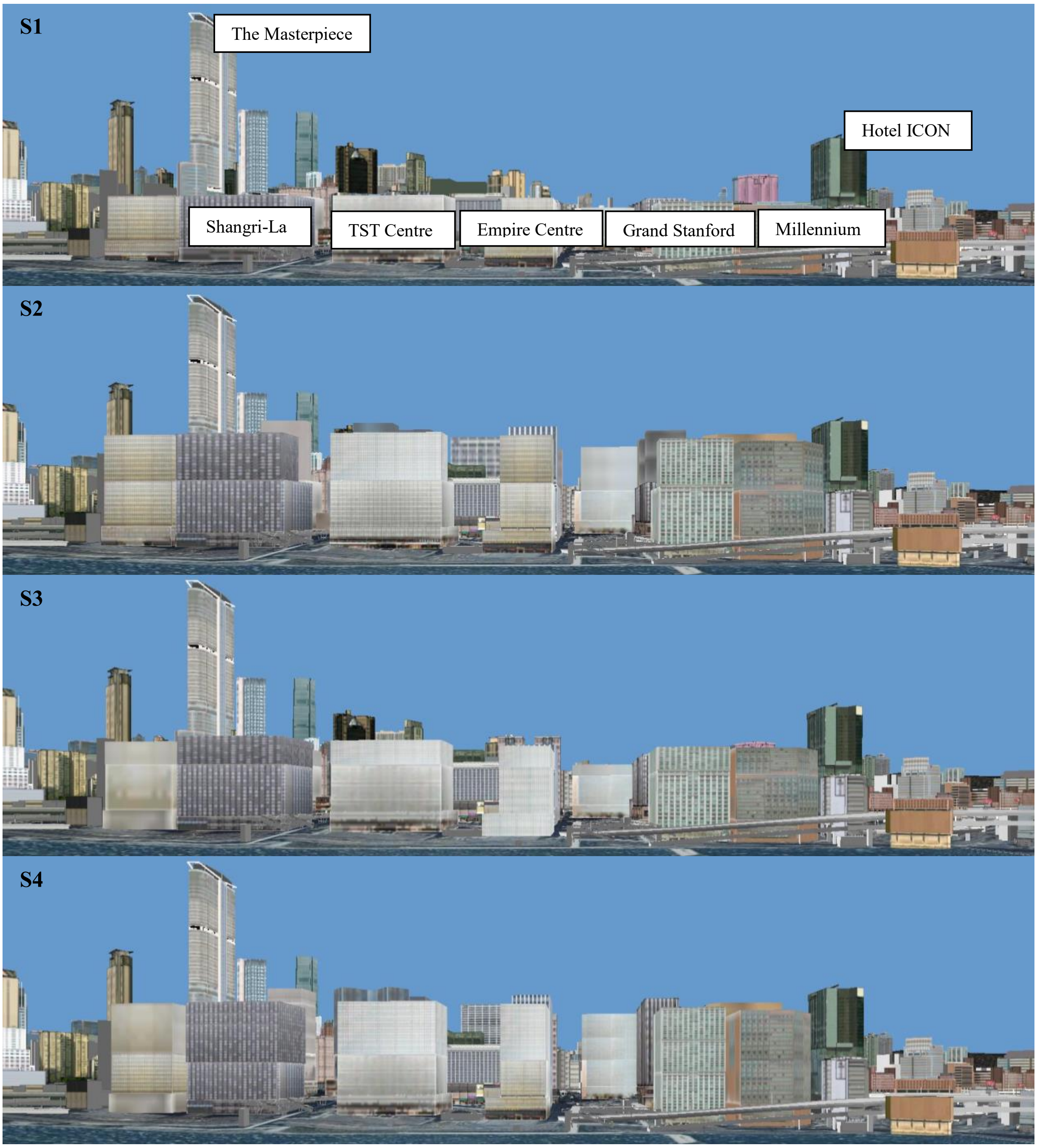

Figure 4-5. Skyline B in the S1, S2, S3, and S4

The skyline in Figure 4-4 is viewed from the northeast (80°) to TSTE. Most of the buildings of S1 in the southeast and northeast of TSTE outmost are visible, which are Hotel ICON, New World Millennium, New East Ocean Centre, Concordia Plaza, Empire Centre, InterContinental Grand Stanford, and TST Centre in the priority of visual acuity. After PR/BH relaxation (S2, S3, and S4), the Concordia Plaza is blocked by the New East Ocean Centre, although some buildings in internal side of TSET are erected out, such as Chinachem

Golden Plaza and Mandarin Plaza. The overall visual feeling of the TSTE image from Skyline A is preserved from S1 to S2, S3, and S4.

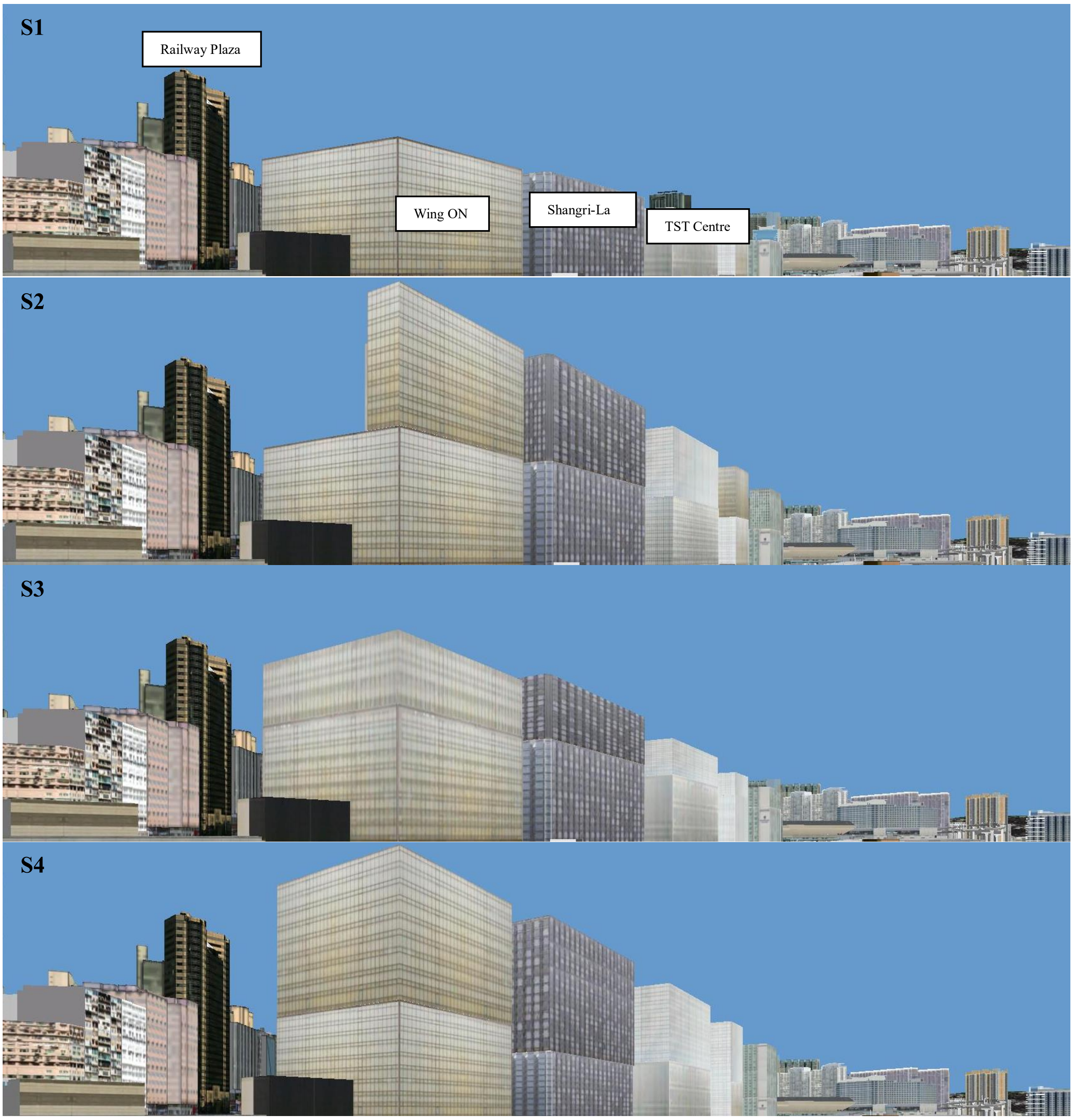

Figure 4-6. Skyline C in the S1, S2, S3, and S4

The skyline in Figure 4-5 mainly comprises the buildings in the southeast side of TSTE. From right to left, one next to the other one they are Hotel ICON, New World Millennium, InterContinental Grand Stanford, Empire Centre, TST Centre, Shangri-La, and Wing On Plaza. The difference between S1 and S2, S3, and S4 is the block of one building (Concordia

Plaza) on internal side of TSTE by the increased PR/BH of the outmost buildings. However, the overall impression of the TSTE in terms of Skyline B is not changed.

Skyline C is viewed from the southwest side of TSTE. The visual perception of the buildings is influenced by visual perspective, which means the visual change of building size and shape with the eye movement from near to far away targets. A few portion of the sky is blocked when changed from S1 to S2, S3, and S4. The overall impact is not significant in terms of the preserved memorable feeling of the TSTE image.

4.2 Mountain Ridgeline Analysis and Results

Site visits to the four strategic viewing points, such as Quarry Bay Park, Hong Kong Convention and Exhibition Centre, Sun Yat Sen Memorial Park, and Central Pier No.7 were conducted for verifying the data’s accuracy (see Figure 4-7).

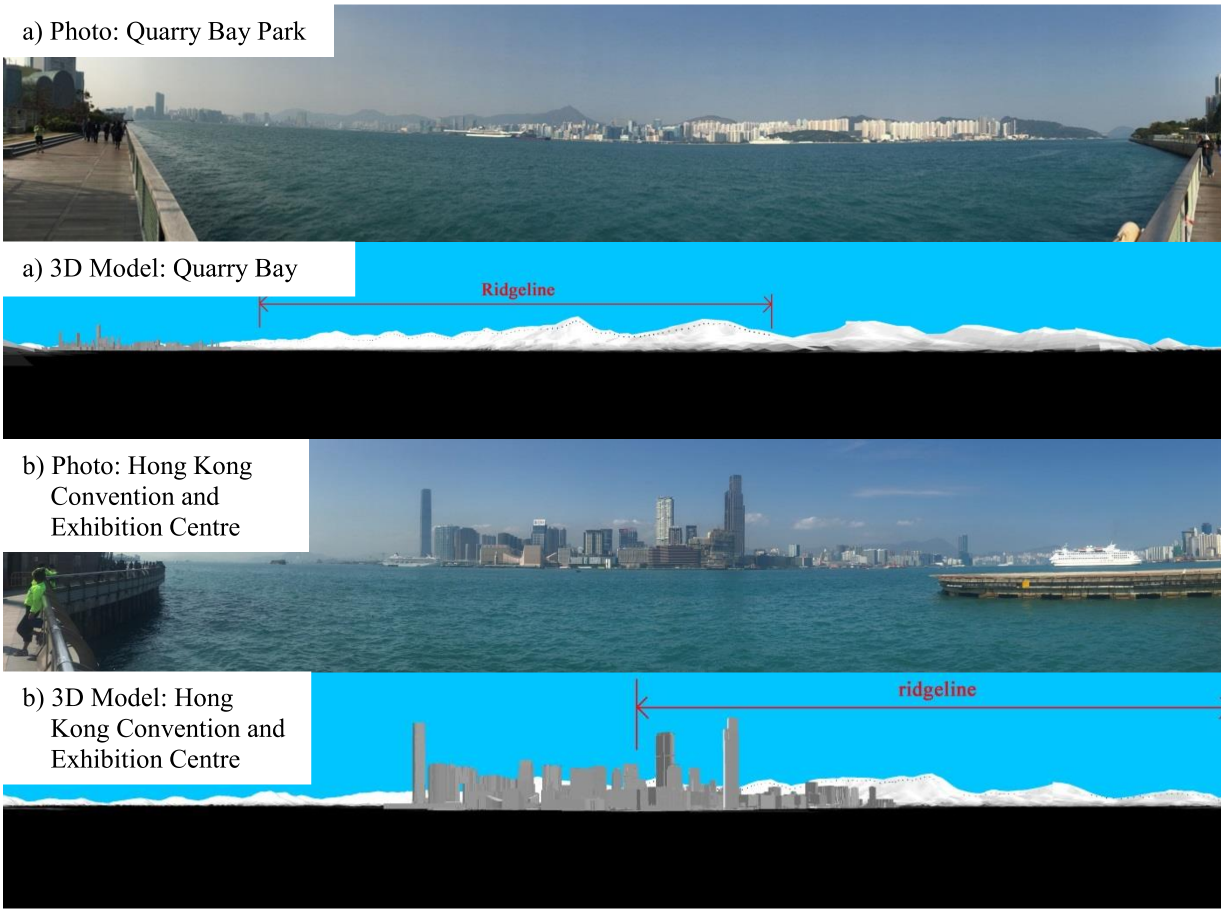

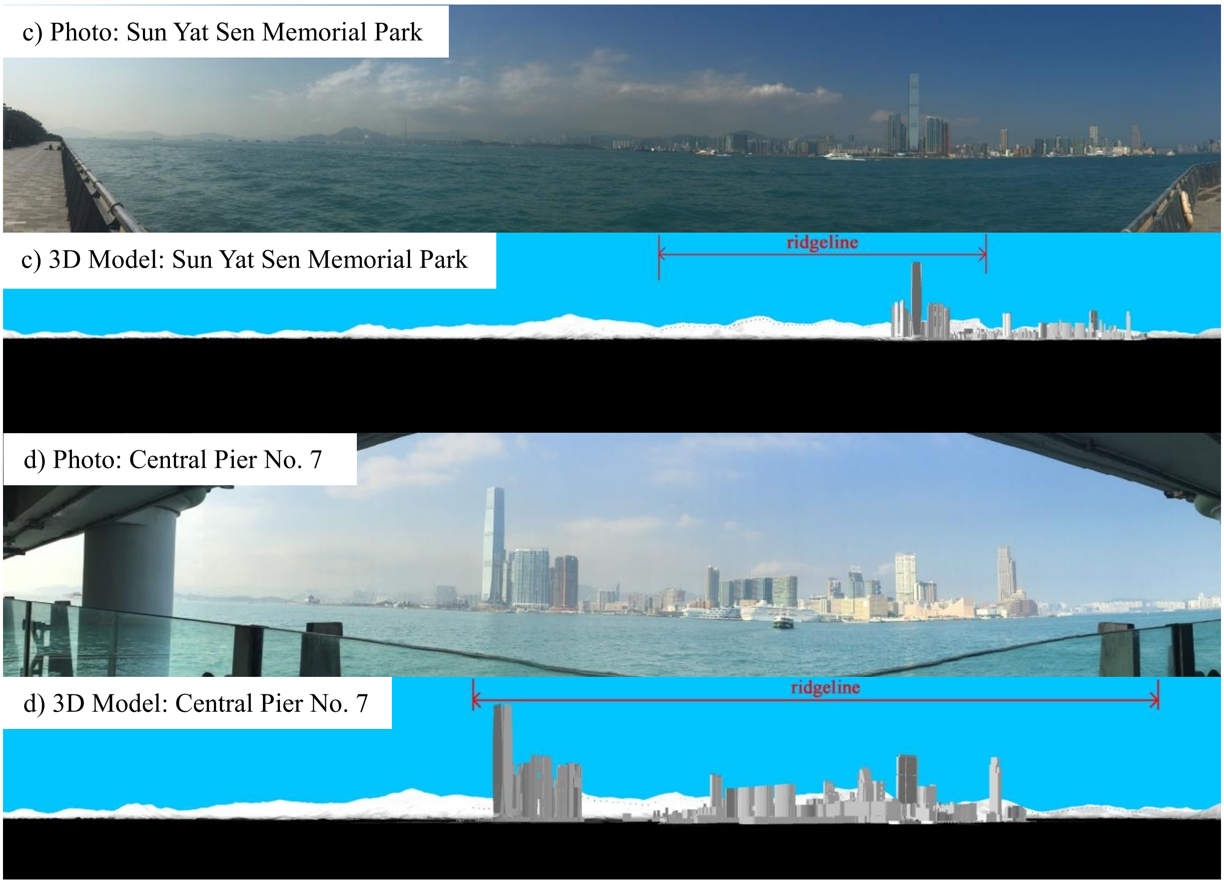

Figure 4-7. View from the four strategic viewing points

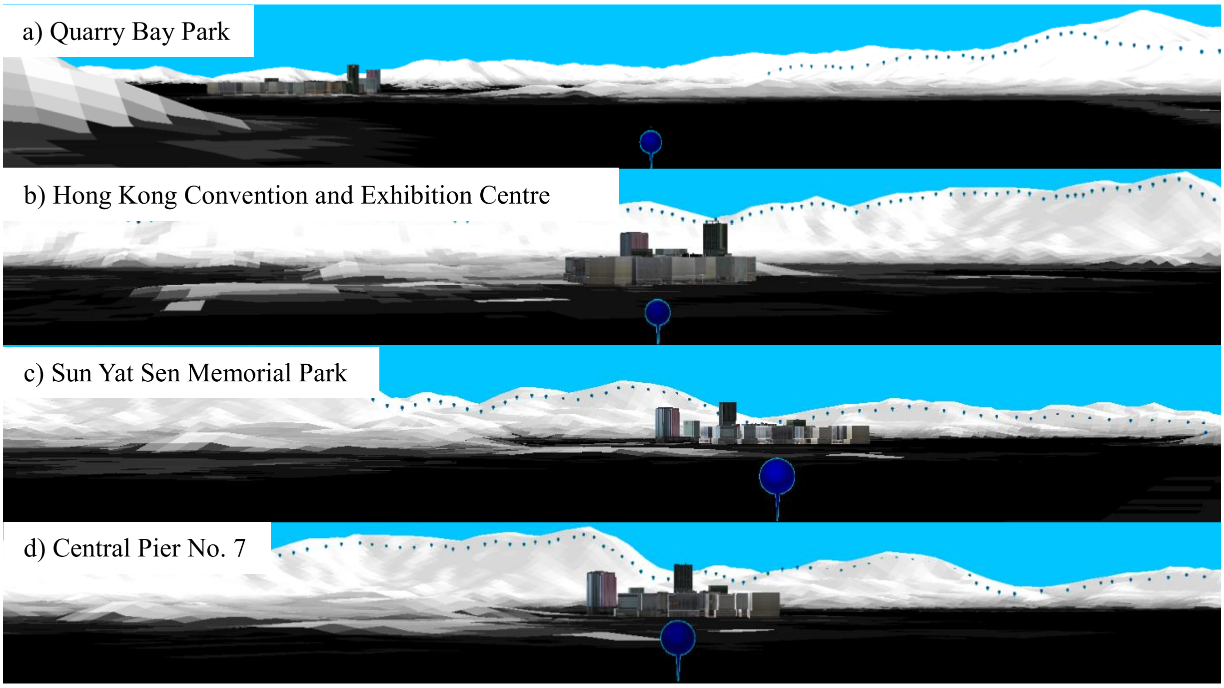

Figure 4-8. Strategic viewing points and corresponding target points

The 1° interval of sampling of the ridgeline running from Beacon Hill through Lion Rock and Tsz Wan Shan to Kowloon Peak is implemented as a result of four sets of target points in total corresponding to the different views from the four strategic viewing points. The strategic viewing points and corresponding sets of target points is shown in Figure 4-8.

The results of constructing sightlines and the quantification of the view blockage are shown in Figure 4-9. Four groups of sightlines are constructed between the viewing/target points, and each group of sightlines is in a fan-shaped structure and forms view corridors. The quantified results are represented by the blocked angle of the view corridors and the ratio to the total view angle.

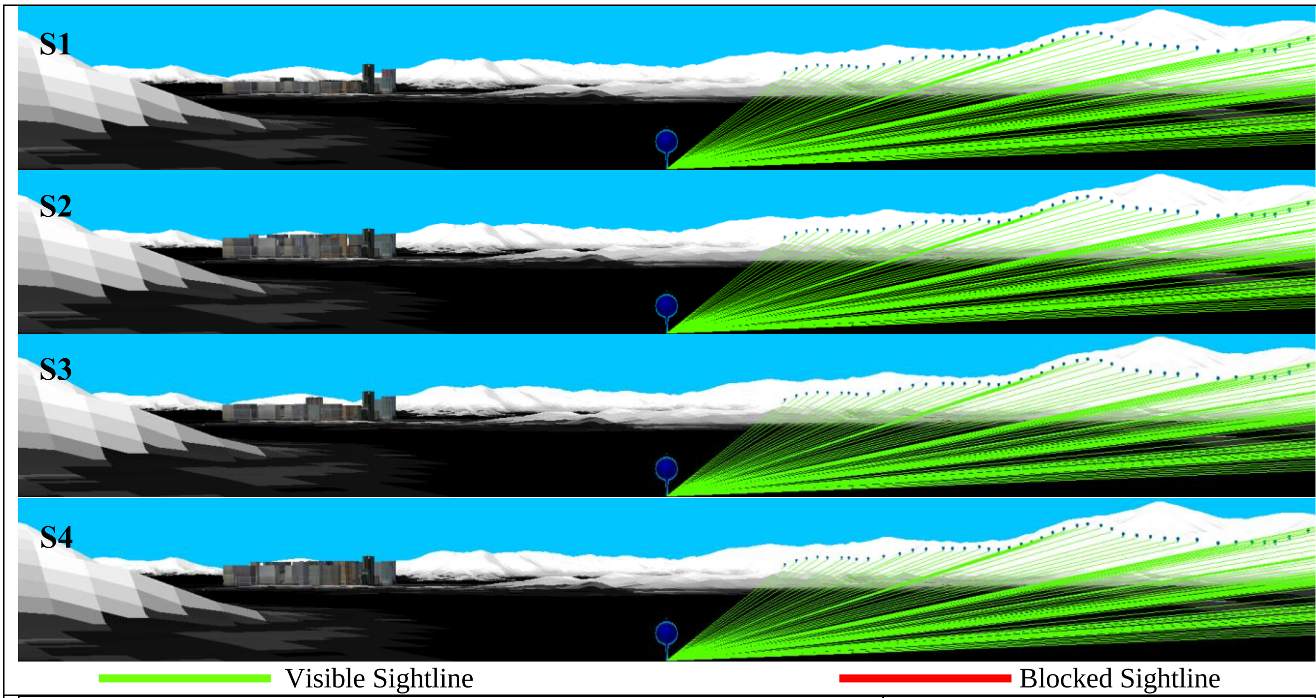

Angle of the View Corridor		130°
Blocked Angle	S1, S2, S3, and S4	0°
Ratio of Blocked Angle		0.00%

Figure 4-9a. Result of effect on ridgeline viewed from Quarry Bay Park

Figure 4.9a shows a quantified result of the effect on mountain ridgeline viewed from Quarry Bay Park. The view corridor from the viewing point to the ridgeline in the four scenarios does not cross over TSTE and all the sightlines of the corridor are not blocked by the buildings in TSTE. The ratio of blocked angle is 0.00%, which implies no impact for this viewing point.

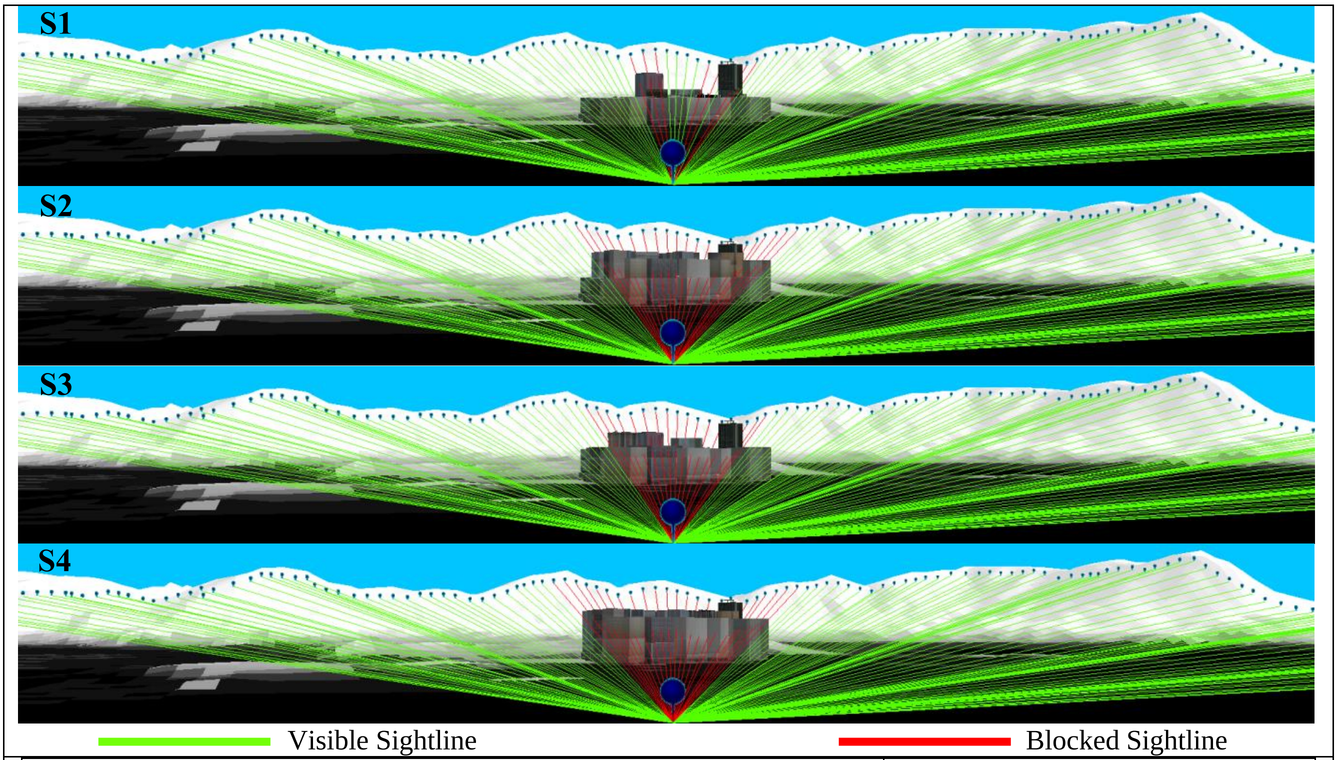

Angle of the View Corridor		168°
Blocked Angle	S1	5°
	S2	20°
	S3	16°
	S4	22°
Ratio of Blocked Angle	S1	2.98%
	S2 / S2-S1	11.90% / 8.92%
	S3 / S3-S1	9.52% / 6.54%
	S4 / S4-S1	13.10% / 10.12%

Figure 4-10b. Result of effect on ridgeline viewed from Hong Kong Convention and Exhibition Centre

Figure 4-9b shows the quantified result of visual impact on mountain ridgeline viewed from Hong Kong Convention and Exhibition Centre. The view corridor in the four scenarios is partially blocked. The ridgeline of S1 is blocked by 5°. The view angle of blocked ridgeline is increased from 5° increased to 20° for S2, increased to 16° for S3, and increased to 22° for S4.

Correspondingly, the ratio of the blocked angle is 2.98% for S1, 11.90% for S2 (8.92% additional block), 9.52% for S3 (6.54% additional block) and 13.10% for S4 (10.12% additional block). The impact is not so significant.

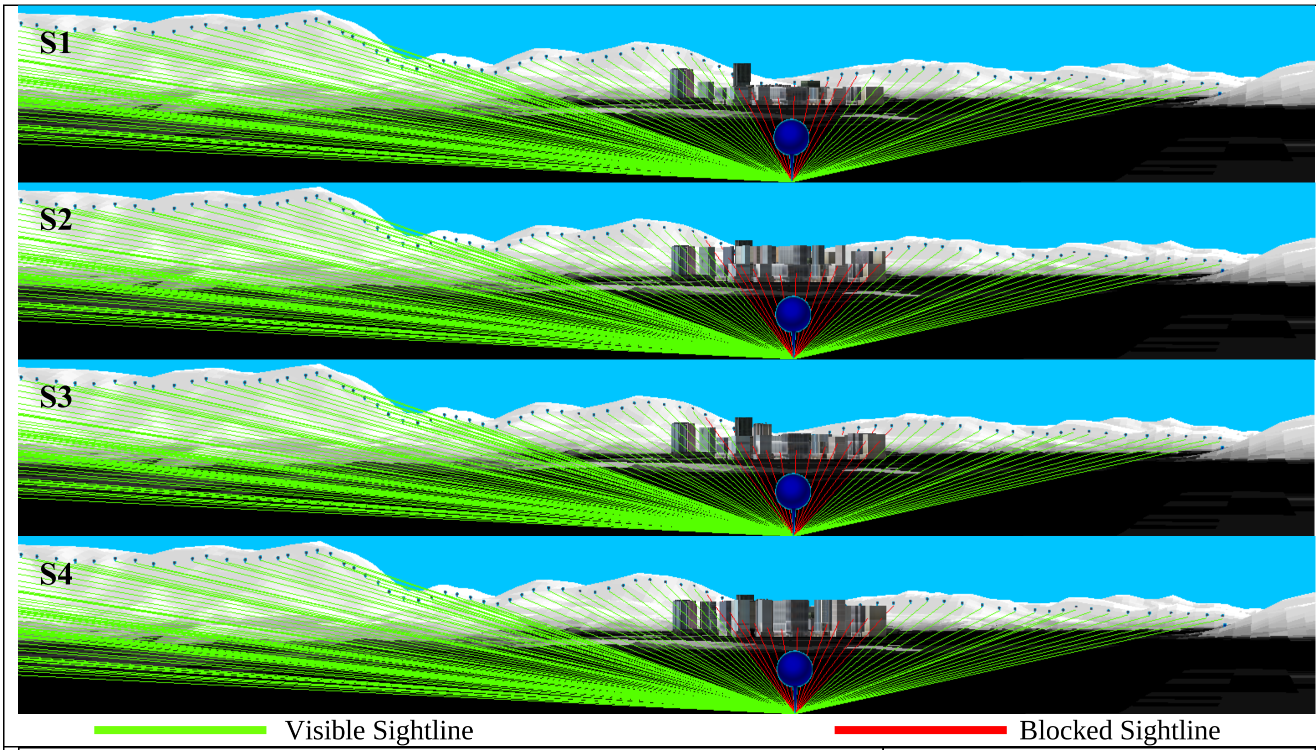

Angle of the View Corridor		140°
Blocked Angle	S1	8°
	S2	12°
	S3	11°
	S4	12°
Ratio of Blocked Angle	S1	5.71%
	S2 / S2-S1	8.57% / 2.86%
	S3 / S3-S1	7.86% / 2.15%
	S4 / S4-S1	8.57% / 2.86%

Figure 4-11c. Result of effect on ridgeline viewed from Sun Yat Sen Memorial Park

Figure 4-9c shows the quantified result of the effect on the mountain ridgeline viewed from Sun Yat Sen Memorial Park. The view corridor in the four scenarios are similarly blocked by the buildings, as part of the ridgeline behind the buildings is relatively lower than the right and left side of this part. The angle of blocked ridgeline is 8° for S1, 12° for S2, 11° for S3, and 12° for S4. Correspondingly, the ratio of the angle is 5.71% for S1, 8.57% for S2 (2.86% additional block), 7.86% for S3 (2.15% additional block) and 8.57% for S4 (2.86% additional block). The quantified results verify the similarity of the four scenarios and indicate the impact is not significant for this viewing point.

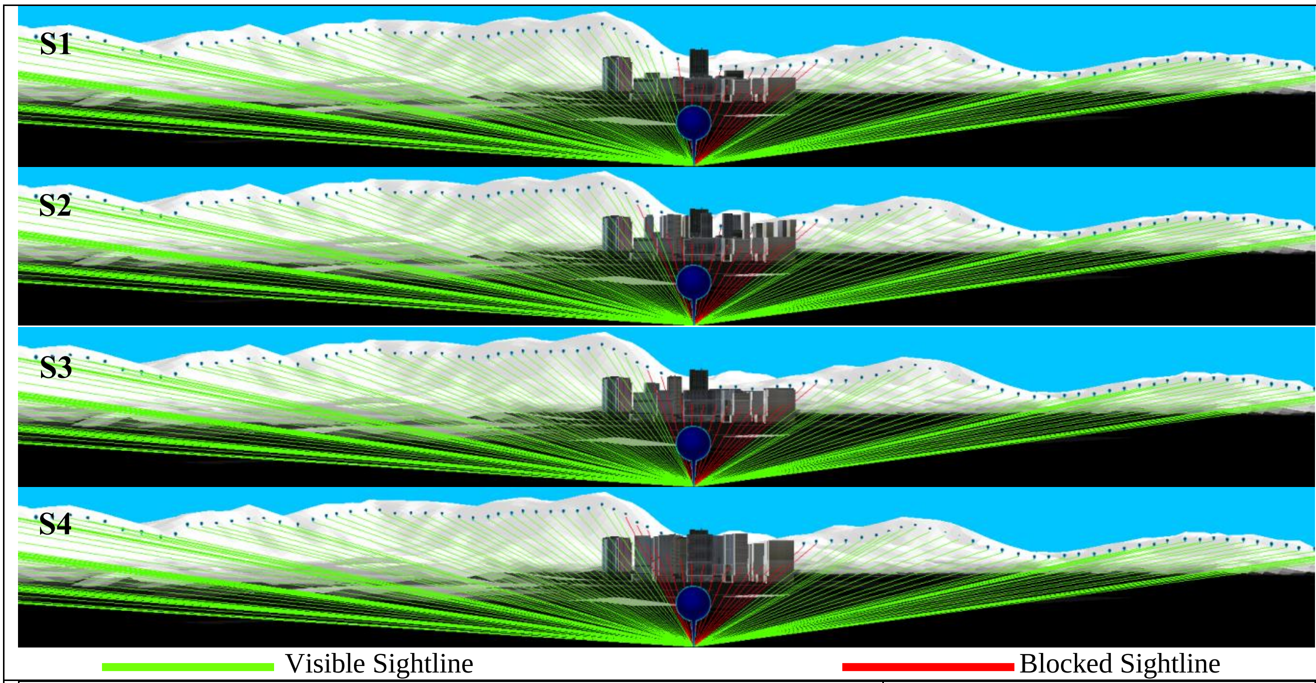

Angle of the View Corridor		132°
Blocked Angle	S1	10°
	S2	12°
	S3	12°
	S4	14°
Ratio of Blocked Angle	S1	7.58%
	S2 / S2-S1	9.09% / 1.51%
	S3 / S3-S1	9.09% / 1.51%
	S4 / S4-S1	10.61% / 3.03%

Figure 4-12d. Results of the effect on mountain ridgeline viewed from Central Pier No.7

Figure 4-9d shows the quantified results of the view from Central Pier No.7. The angle of blocked view is 10° for S1, 12° for S2 and S3, and 14° for S4. Correspondingly, the ratio between these angles and the total angle of the view corridor is 7.58% for S1, 9.09% for S2 and S3 (1.51% additional block) and 10.61% for S4 (3.03% additional block). The results indicate no significant impact on the view from Central PierNo.7 to the ridgeline.

The results show that the block of view angle to the mountain ridgeline is minus for S1 and even for S2, S3, and S4 with increased PR/BH. The detailed explanation is as follows:

1) The view to the mountain ridgeline from Quarry Bay Park is not blocked and this viewing point is in the far right side of Hong Kong Island, which means the view corridor does not cross over TSTE.
2) The view corridor from Hong Kong Convention and Exhibition Centre is partly blocked from 2.98% in S1 to around 11% in S2, S3, and S4 (average 8.52% additional block). TSET is in front of the mountain ridgeline viewed from this viewing point, but the overall ridgeline is not significantly impacted.
3) The view from Sun Yat Sen Memorial Park, which is in the far left side of Hong Kong Island, is slightly blocked. The reason for this is: 1) the southwest side of TSTE (the longest secant across TSTE is located between southwest and northeast sides of TSTE) is facing this viewing point, and 2) the location of TSTE easily blocks this view to the ridgeline. However, the impact is not significant in terms of the additional block at 2.62% on average.
4) The view from Central Pier No.7 is similar to the view from Hong Kong Convention and Exhibition Centre, although the view is a little better than that one in terms of additional block at 2.02% on average. The impact on the view from this point is not significant.

4.3 Solar Exposure Analysis and Results

The results of cumulative time and radiation of solar exposure for summer are shown in Figure 4-10a, Figure 4-10b, Figure 4-11a, Figure 4-11b, and Table 4-1. Specifically, Figure 4-10a shows the patterns (S1, S2, S3 and S4) of summer solar exposure in 3D surface (shadow footprint + building facades) in terms of ten hourly sections from (0, 1], (1, 2] to (9, 10] (from cold to warm colours) of direct insolation. These patterns are similar in terms of the colour distribution. The buildings' roofs are exposed to the sun for a longer time than the ground surfaces are, which is shaded by the surrounding high-rise buildings. Figure 4-10b shows similar phenomenon represented by ten sections from (0, 1200], (1200, 1770], (1770, 2340], (2340, 2910], (2910, 3480], (3480, 4050], (4050, 4620], (4620, 5190], (5190, 5760] to [5760, +∞] of cumulative solar radiation energy in summer.

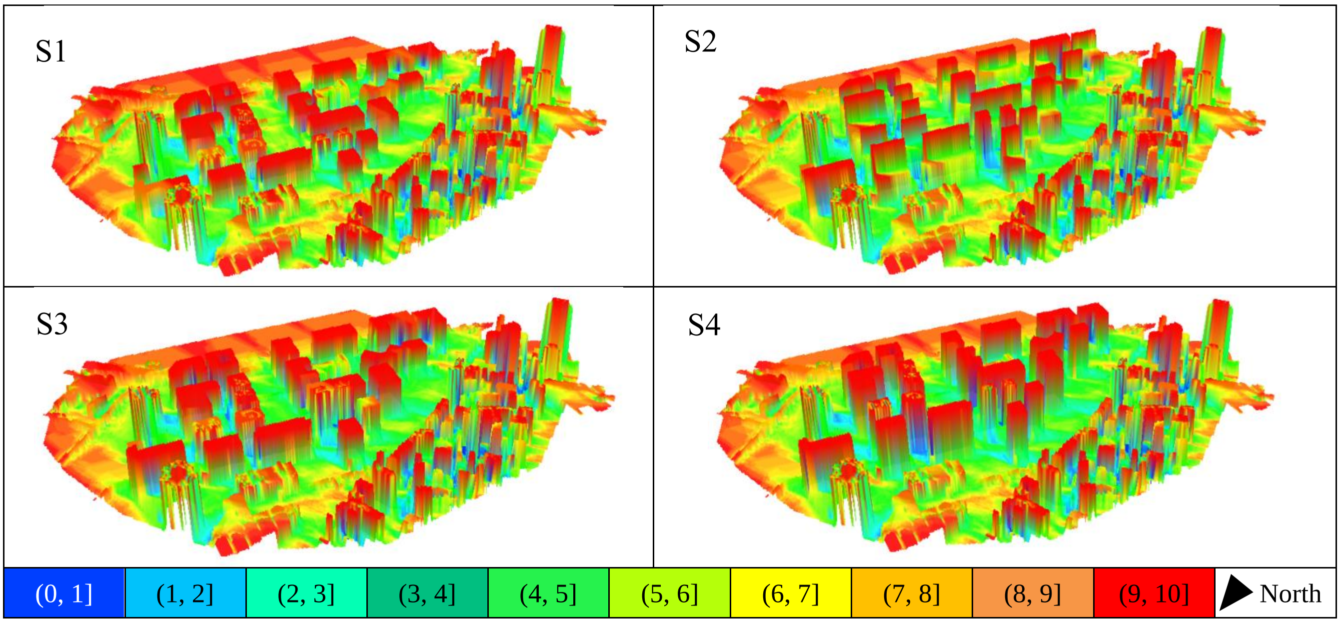

Figure 4-13a. Patterns of summer solar exposure in terms of hourly sections of insolation

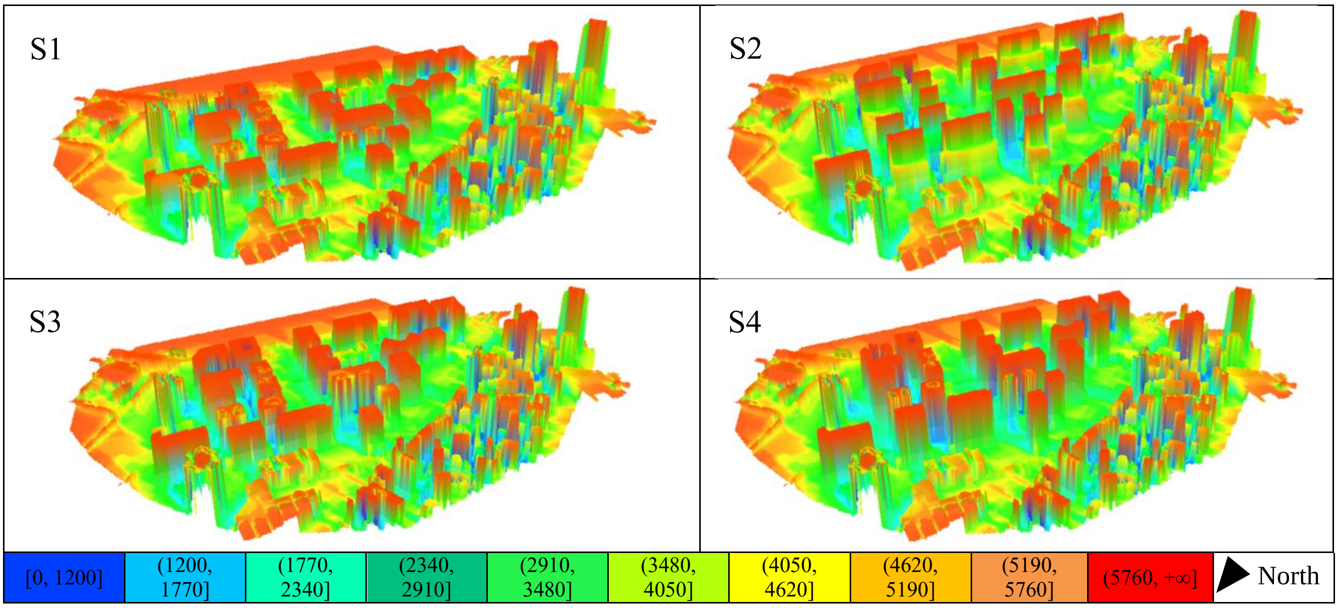

Figure 4-14b. Patterns of summer solar radiation energy (Wh)

Table 4-1. Quantified pattern areas in summer insolation

		Quantified Pattern Areas							
		S1		**S2**		**S3**		**S4**	
Sections of Direct Insolation (Hour)		m^2	%	m^2	%	m^2	%	m^2	%
(9, 10]	red	455516.66	33.06	352967.89	23.23	439642.56	29.93	391220.41	25.69
(8, 9]	dark orange	154546.31	11.22	201322.20	13.25	173291.72	11.80	190921.23	12.54
(7, 8]	orange	141176.67	10.25	170789.92	11.24	142252.18	9.68	146746.21	9.64
(6, 7]	yellow	173972.75	12.63	188149.00	12.38	160494.98	10.93	170993.12	11.23
(5, 6]	yellow green	181397.23	13.17	221051.22	14.55	196355.62	13.37	198664.20	13.05
(4, 5]	light green	116670.32	8.47	165095.90	10.87	156864.28	10.68	178273.36	11.71
(3, 4]	green	71090.74	5.16	100861.16	6.64	89964.09	6.12	119753.79	7.86
(2, 3]	light blue	44016.53	3.19	65527.44	4.31	59847.10	4.07	70797.26	4.65
(1, 2]	blue	30926.01	2.24	42597.45	2.80	38896.15	2.65	42447.51	2.79
(0, 1]	dark blue	8401.38	0.61	10864.81	0.72	11338.51	0.77	12802.12	0.84
Sections of Cumulative Radiation Energy (Wh)									
(5760, +∞]	red	325299.54	23.61	193620.33	12.74	305075.75	20.77	243763.46	16.01
(5190, 5760]	dark orange	196860.24	14.29	248197.25	16.34	223494.03	15.21	235248.25	15.45
(4620, 5190]	orange	134804.04	9.78	171918.85	11.32	133905.93	9.12	145067.18	9.53
(4050, 4620]	yellow	149236.36	10.83	158744.04	10.45	133102.32	9.06	139421.22	9.16
(3480, 4050]	yellow green	179496.78	13.03	223140.50	14.69	191111.36	13.01	201341.65	13.22
(2910, 3480]	light green	167437.28	12.15	212828.45	14.01	197718.85	13.46	213713.39	14.04
(2340, 2910]	green	91981.63	6.68	132209.75	8.70	115303.75	7.85	156328.24	10.27
(1770, 2340]	light blue	71435.81	5.19	91577.18	6.03	88397.56	6.02	99961.22	6.57
(1200, 1770]	blue	41063.73	2.98	62334.05	4.10	56788.74	3.87	62043.83	4.07
[0, 1200]	dark blue	20099.17	1.46	24656.58	1.62	24048.90	1.64	25730.76	1.69
Total		1377714.59	100.00	1519226.98	100.00	1468947.19	100.00	1522619.21	100

Table 4-1 is the quantified pattern areas corresponding to each section (hourly or cumulative radiation energy) of exposure. The sums of pattern areas are increased from S1 to S2, S3, and S4 because of the increased PR/BH of buildings in S2, S3, and S4. The percentage of each section is similar among the four scenarios and this result is identical to the visualized patterns in Figure 4-10a and Figure 4-10b correspondingly.

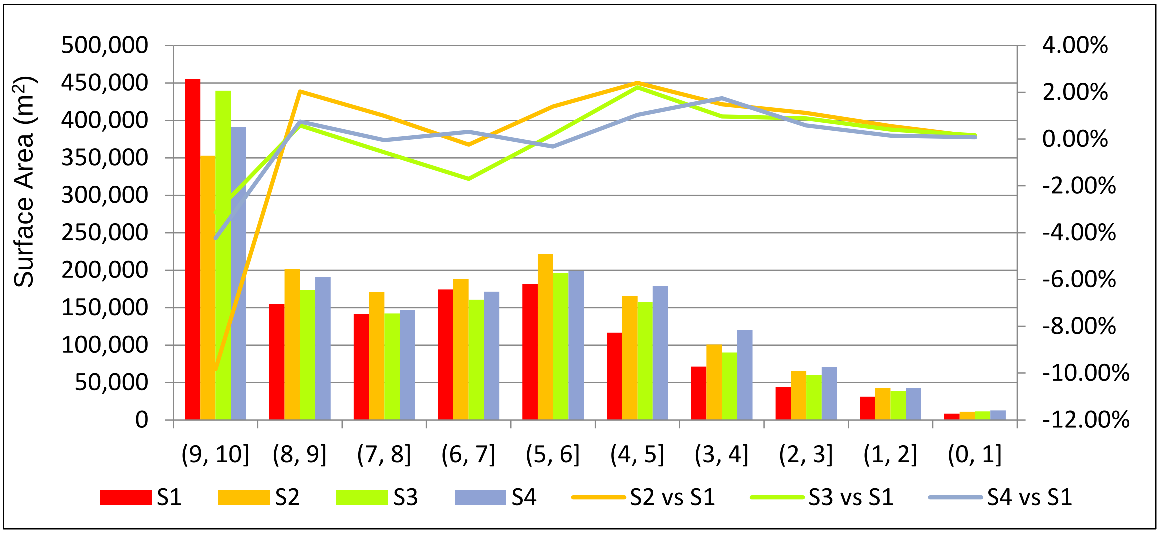

Figure 4-15a. Differences (S1 vs S2, S3, S4) of the corresponding pattern areas in relation to time of exposure (hour) in summer

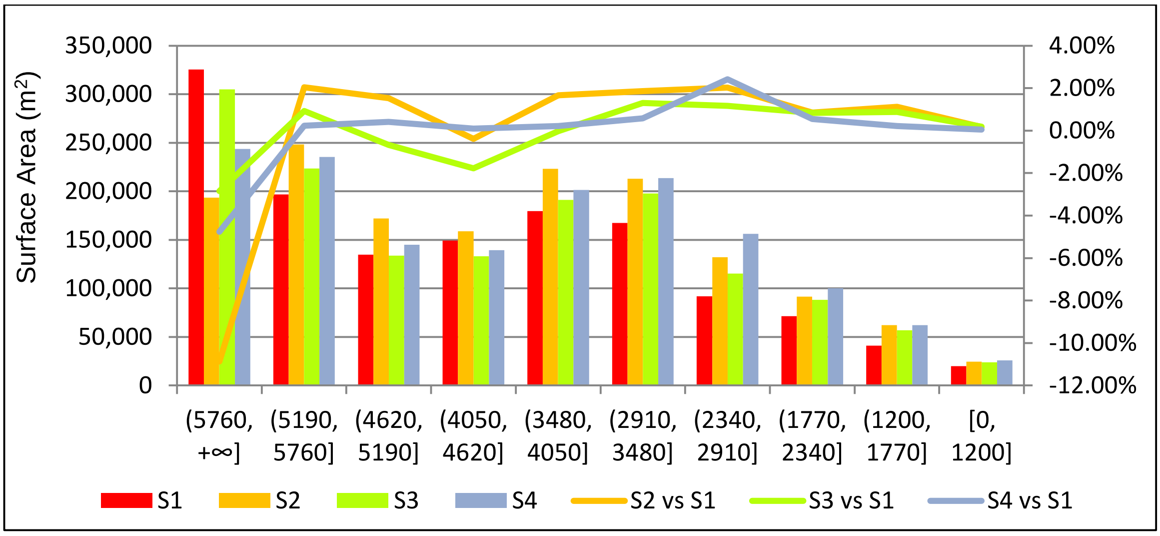

Figure 4-16b. Differences (S1 vs S2, S3, S4) of the corresponding pattern areas in relation to radiation energy (Wh) in summer

Figure 4-11a and Figure 4-11b show the differences (S1 vs S2, S3, and S4) of the corresponding pattern areas and the value of each individual pattern area of the four scenarios. The difference between S1 and S2 (S2 - S1) is in the range of -10% to 2% for the time of exposure and in the range of -11% to 2% for the cumulative radiation energy. The reduced area is mostly in (9, 10] hourly section / (5760, +∞] Wh radiation section. The area exposed by (9, 10] hour / (5760, +∞] Wh insolation in S1 is 10% to 12% decreased with increasing the PR/BH in S2 and the area exposed by (8, 9] hour / (5190, 5760] Wh and (4, 5] hour / (2340, 2910] Wh insolation in S1 is increased by 2%. The difference between S1 and S3 (S3 - S1) is in the range of -3% to 2% for the time of exposure and in the range of -3% to 1% for the cumulative radiation energy and the difference between S1 and S4 (S4 - S1) is in the range of -4% to 1.5% for the time of exposure and in the range of -5% to 2% for the cumulative radiation energy. Both of the differences are similar and they are smaller than the difference between S1 and S2. The trend of change from S1 to S3 / S1 to S4 is also similar to the trend of change from S1 to S2. The change implies that the area, exposed by (9, 10] hour / (5190, 5760] Wh insolation, decreased in S1 is 3% for the time of exposure and 4% to 5% for the radiation energy with increasing the PR/BH in S3 and S4, and the area exposed by (8, 9] and (4, 5] hour / (5190, 5760] Wh and (2340, 2910] Wh insolation in S1 is increased by 1% to 2% with increasing the PR/BH in S3 and S4. All the three differences show no significant impact of the PR/BH relaxation on the summer solar exposure.

The results of winter solar exposure are shown in Figure 4-12a, Figure 4-12b, Figure 4-13a, Figure 4-13b, and Table 4-2. Specifically, Figure 4-12a and Figure 4-12b show the patterns of winter solar exposure in 3D surface (shadow footprint + building roofs and facades) in terms of eight hourly sections from (0, 1], (1, 2] to (7, 8] (presented from cold to warm colour correspondingly) of direct insolation and ten sections from [0, 690], (690, 1020], (1020, 1350], (1350, 1680], (1680, 2010], (2010, 2340], (2340, 2670], (2670, 3000], (3000, 3330] to (3330, +∞] of solar radiation energy. The patterns of the four scenarios are similar in terms of the colour distribution. The buildings' roofs are exposed to the sunlight by (9, 10] hours / (3000, 3330] Wh. By contrast, the area around the buildings' footprint is exposed by (0, 1] hours / (690, 1020] because of the shading effect of the high-rise buildings. The other surfaces such as the ground and podium surfaces are exposed by (2, 3], (3, 4] or (4, 5] hours, which belong to the middle to low hourly sections. The range of time depends on the height of the surrounding buildings, which causes shading effect to the surrounding land/facade surfaces.

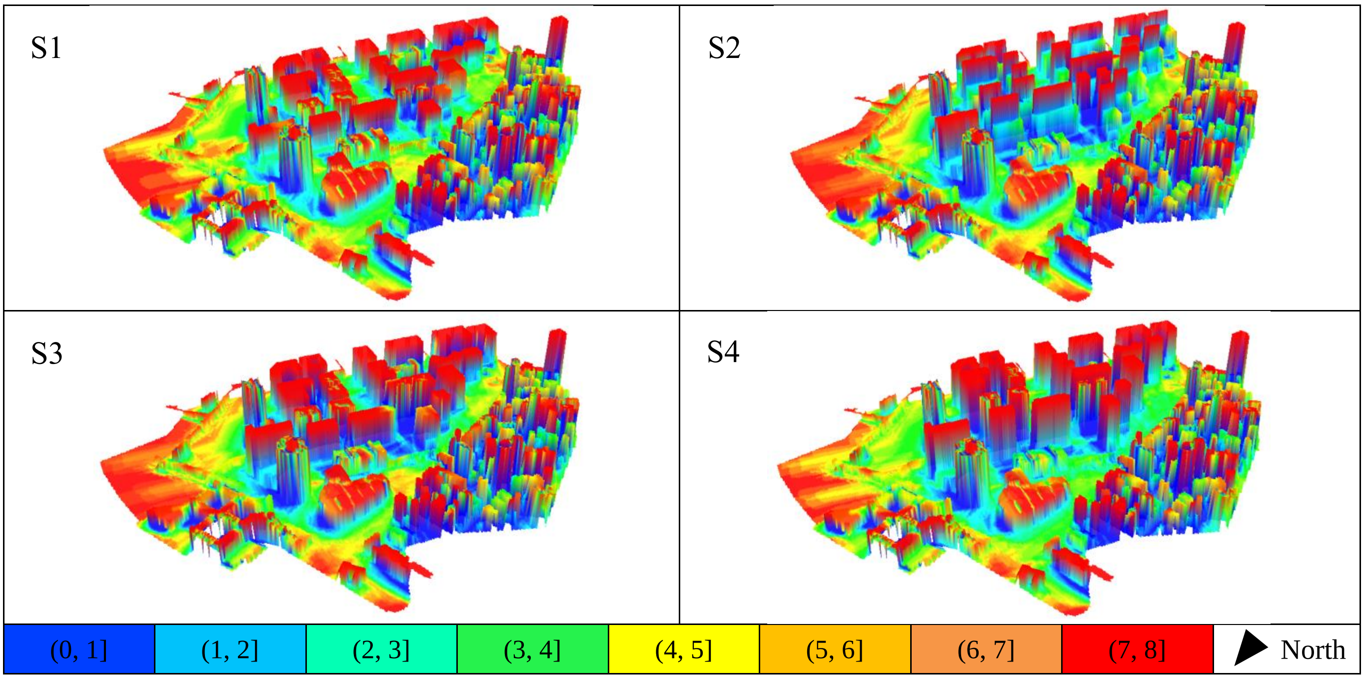

Figure 4-17a. Patterns of winter solar exposure in terms of hourly sections of insolation

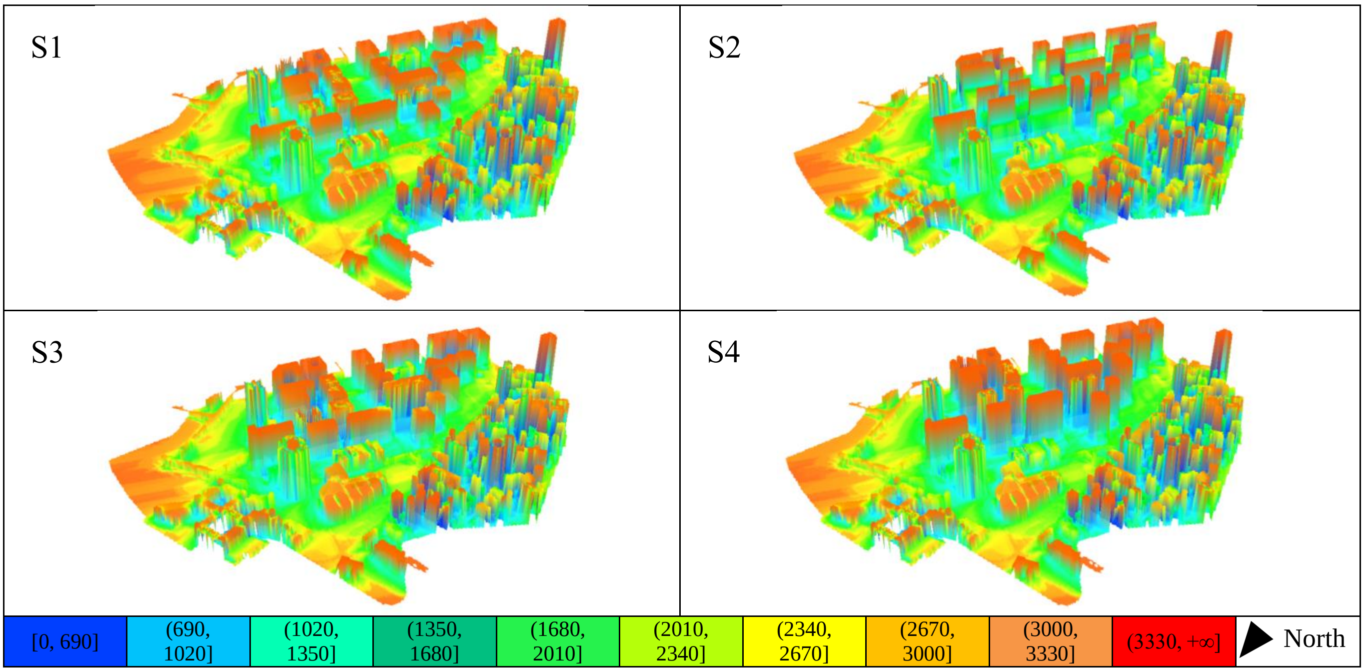

Figure 4-18b. Patterns of winter radiation energy (Wh)

Table 4-2. Quantified pattern areas in each section of winter insolation

Sections of Direct Insolation (Hour)		Quantified Pattern Areas							
		S1		S2		S3		S4	
		m^2	%	m^2	%	m^2	%	m^2	%
(7, 8]	red	390116.28	26.61	359050.22	22.38	440308.13	28.31	339898.24	21.06
(6, 7]	dark orange	130356.75	8.89	137233.38	8.55	148467.27	9.55	136880.87	8.48
(5, 6]	orange	172116.46	11.74	158623.46	9.89	145463.31	9.35	150907.77	9.35
(4, 5]	yellow	193688.71	13.21	172299.64	10.74	143242.99	9.21	200747.31	12.44
(3, 4]	light green	151775.14	10.35	154715.98	9.64	129104.81	8.30	228326.78	14.15
(2, 3]	light blue	124848.29	8.52	169301.66	10.55	135080.07	8.68	162529.09	10.07
(1, 2]	blue	105122.44	7.17	173950.22	10.84	146867.33	9.44	153821.57	9.53
(0, 1]	dark blue	197904.69	13.50	279452.17	17.42	266862.32	17.16	240659.61	14.91
Sections of Cumulative Radiation Energy (Wh)									
(3330, +∞]	red	130429.25	8.90	95572.85	5.96	136106.56	8.75	135805.22	8.42
(3000, 3330]	dark orange	257503.90	17.57	215030.49	13.40	262187.99	16.86	218447.17	13.54
(2670, 3000]	orange	144309.29	9.84	152438.19	9.50	143649.89	9.24	140447.26	8.70
(2340, 2670]	yellow	158743.29	10.83	176794.62	11.02	148842.06	9.57	156135.34	9.68
(2010, 2340]	yellow green	176470.35	12.04	197344.29	12.30	164451.21	10.57	179243.91	11.11
(1680, 2010]	light green	180009.60	12.28	218197.17	13.60	187015.90	12.02	202454.14	12.55
(1350, 1680]	green	134183.94	9.15	187945.34	11.71	166639.10	10.71	203640.06	12.62
(1020, 1350]	light blue	118918.98	8.11	146441.73	9.13	137216.83	8.82	163657.49	10.14
(690, 1020]	blue	109840.02	7.49	146340.67	9.12	144172.37	9.27	146647.95	9.09
[0, 690]	dark blue	55520.14	3.79	68521.39	4.27	65114.32	4.19	67292.71	4.17
Total		1465928.76	100	1604626.74	100	1555396.23	100	1613771.24	100

Table 4-2 shows the quantified pattern areas corresponding to each section (by hour or by radiation energy) of winter insolation. The pattern area is increased from S1 to S2, S3, and S4 as the PR/BH is increased. The percentage of each section is similar for all the scenarios and this finding is identical to the visualized patterns in Figure 4-12a and Figure 4-12b.

Figure 4-13a and Figure 4-13b show the differences (S1 vs S2, S3, and S4) of the corresponding pattern areas in relation to winter exposure. The difference between S1 and S2 (S2 - S1) is in the range of -4% to 4% for the time of exposure and -4% to 2.5% for the radiation, which is similar to the difference between S1 and S4 (S4 - S1) is in the rage of -5% to 4% for the time of exposure and -3.5% to 2% for the radiation. The decrease is in the section from (7, 8] to (3, 4] hours and (3330, +∞] to (3000, 3330]. While the increase is in the section from around (3, 4] to (0, 1] hours and (1680, 2010] to (690, 1020]. It supports the shading effect resulting from the PR/BH relaxation. However, the difference between S1 and S3 (S3 - S1) is in the range of 4% to -4% for the time of exposure and -1.5% to 2% for the radiation, which is different from the trend of change in S1 vs S2 or S1 vs S4. This phenomenon is caused by the different shape of the buildings in S3 when compared with the other buildings in S2 and S4. Overall, the three differences indicate no significant impact of the PR/BH relaxation on the winter solar exposure.

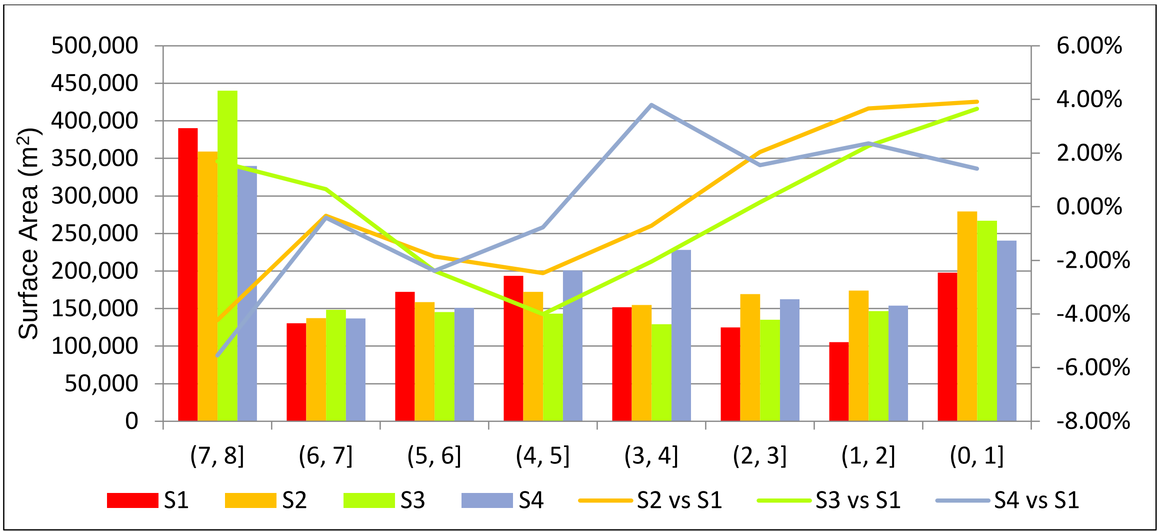

Figure 4-19a. Differences (S1 vs S2, S3, and S4) of the corresponding pattern areas in relation to the time (hour) of winter exposure

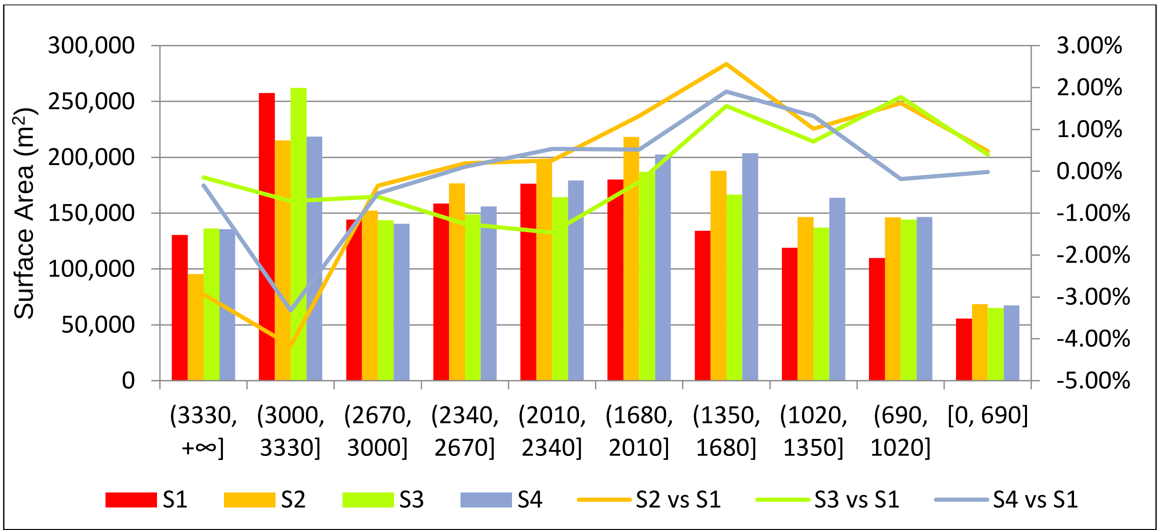

Figure 4-20b. Differences (S1 vs S2, S3, and S4) of the corresponding pattern areas in relation to the winter radiation energy (Wh)

The above result shows the overall situation of insolation in terms of time and radiation. This result implies the phenomenon of the shading effect, which becomes larger after the PR/BH relaxation. The next result (see Figure 4-14 to Figure 4-16, Tables 4-3 and 4-4) shows the quantitative comparisons (S1 vs S2, S3, and S4) of solar radiation on west facing facades to validate the following four hypotheses:

1) The shading effect exists after mid-day and the enhancement of the shading effect from the PR/BH relaxation has a positive impact on the life extension of facade materials.
2) The total energy of radiation on west facing facades is increased after the PR/BH relaxation.
3) The intensity of radiation on west facing facades is relatively higher than the average intensity of TSTE.
4) The PR/BH relaxation reduces the intensity of radiation on west facing facades.

The Figure 4-14a and Figure 4-14b show the difference (S1 vs S2, S3, and S4) of pattern areas in terms of ten classes of cumulative radiation energy on west facing facades for each building in summer and winter solstices respectively. Both seasonal sets of diagrams support the statement that the PR/BH relaxation brings the shading effect on the buildings footprint area and this impact is positive to the life extension of the building facade materials because of the harmonization of insolation to the facades. The harmonization is made through reducing the proportion of relative high radiation energy area and increasing the proportion of relative mid and low radiation energy areas.

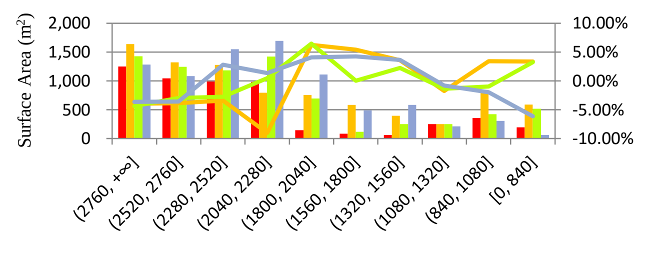

(1) Kowloon Shangri-La

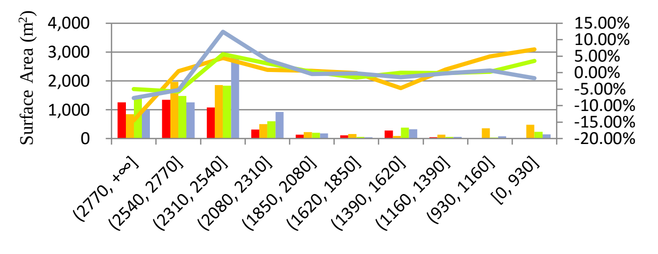

(2) InterContinental Grand Stanford

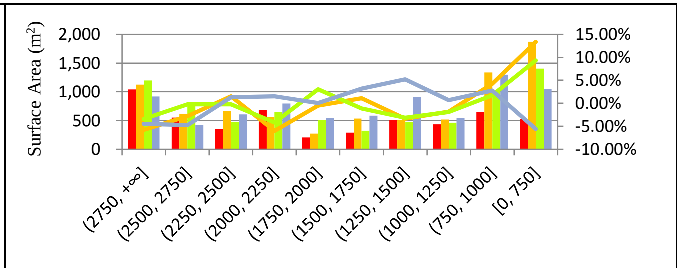

(3) New World Millennium HK Hotel

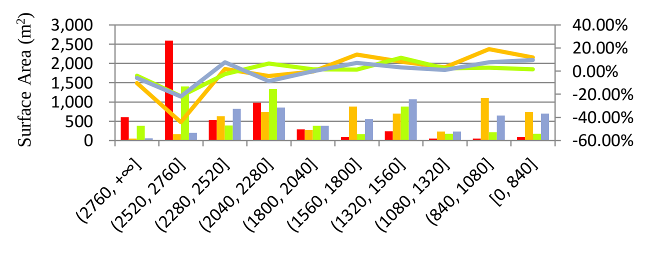

(4) The Royal Garden

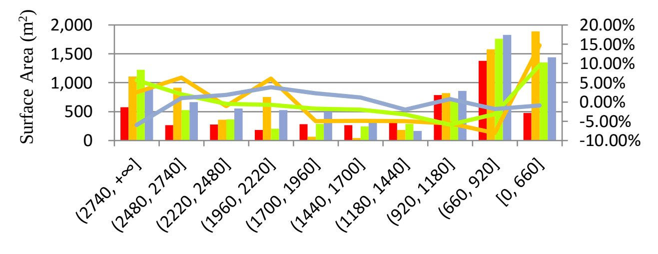

(5) Regal Kowloon Hotel

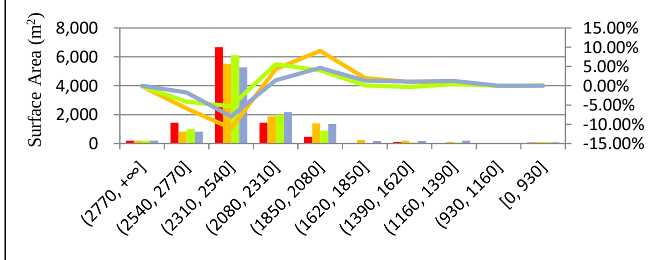

(6) Hotel ICON

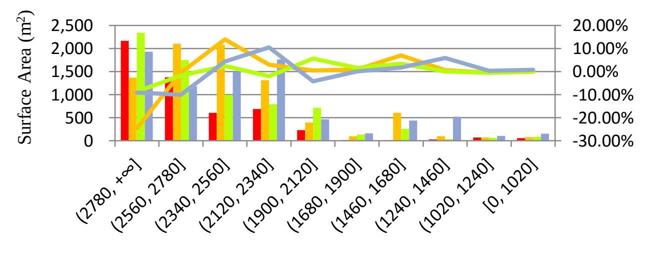

(7) TST Centre

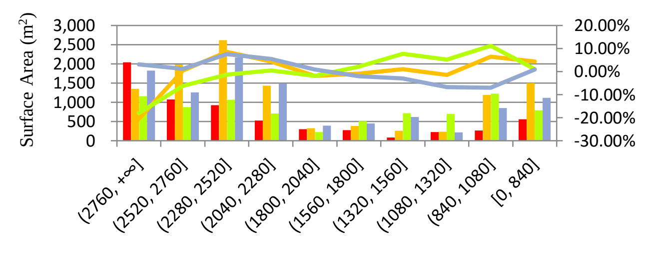

(8) Peninsula Centre

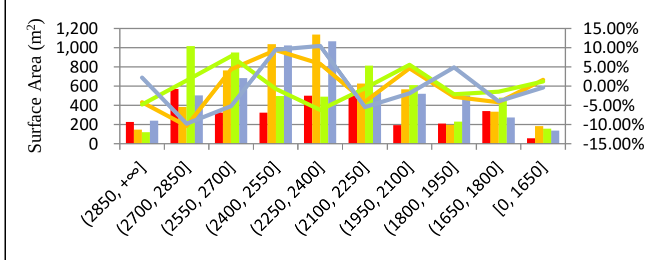

(9) Energy Plaza

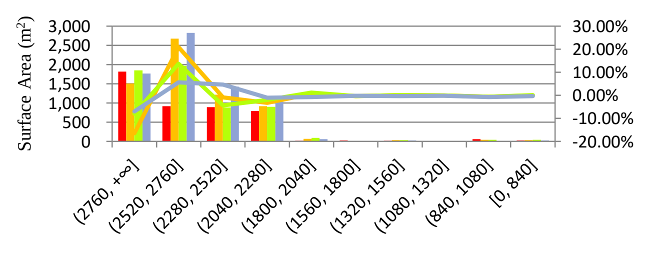

(10) Wing On Plaza

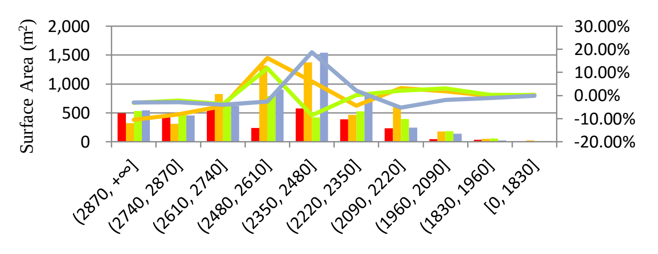

(11) Mirror Tower

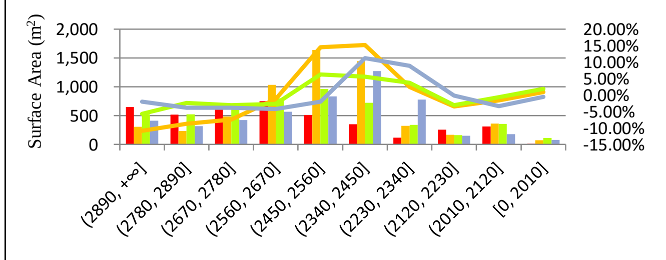

(12) Inter-Continental Plaza

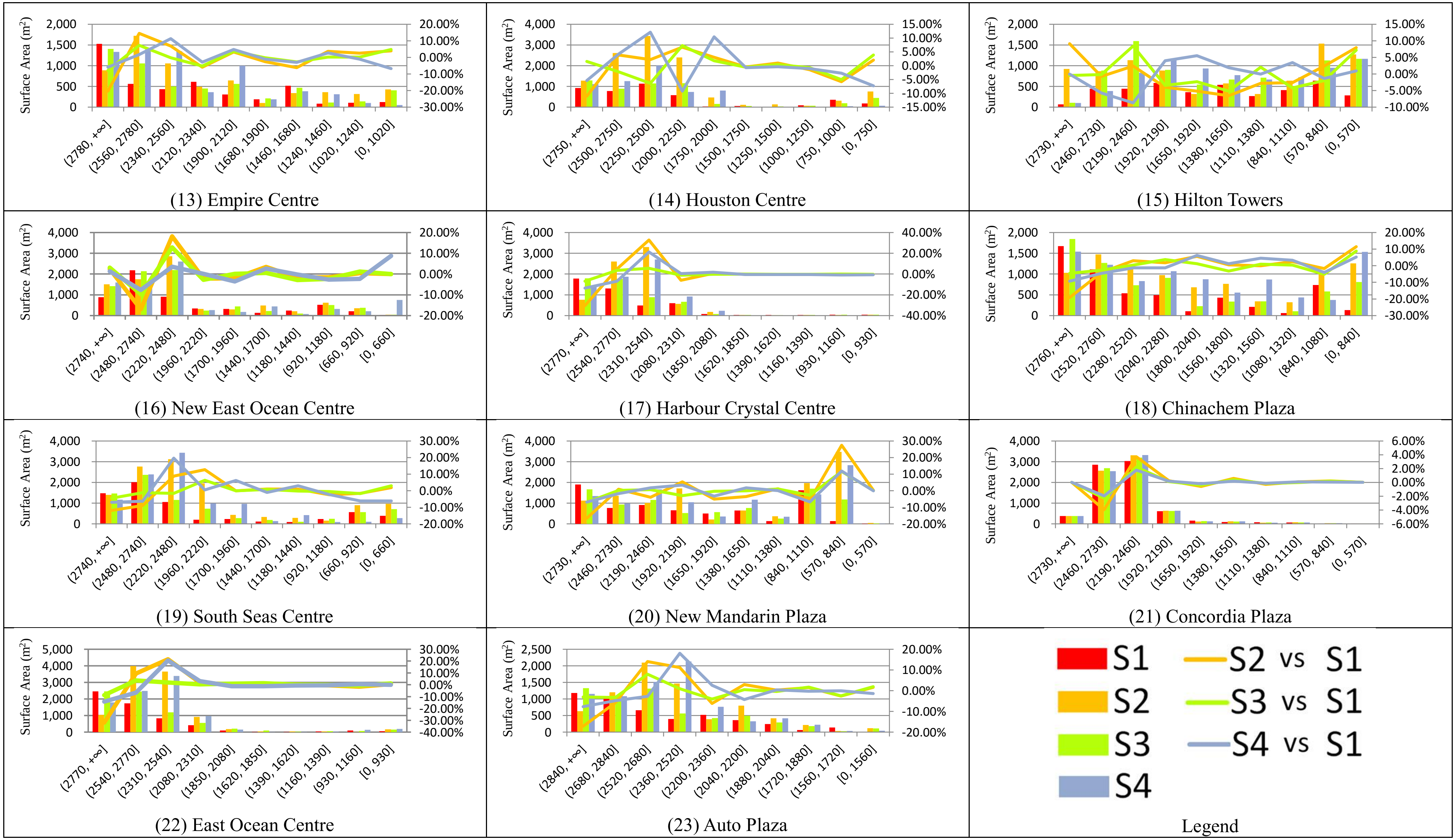

Figure 4-21a. Difference (S1 vs S2, S3, S4) of pattern areas as for cumulative summer radiation energy (Wh) on west facing facades

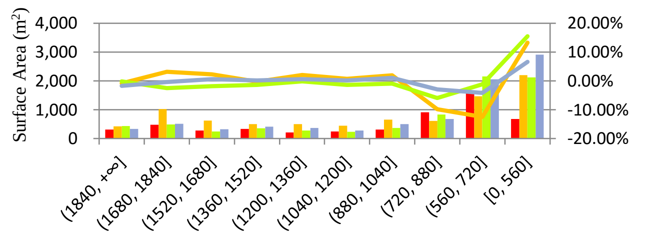

(1) Kowloon Shangri-La

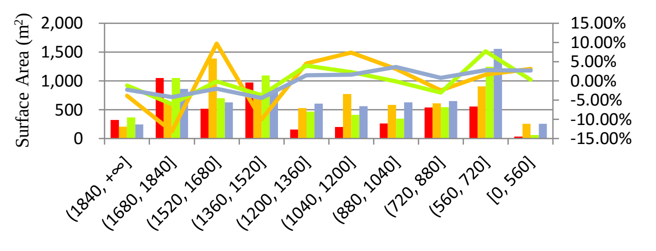

(2) InterContinental Grand Stanford

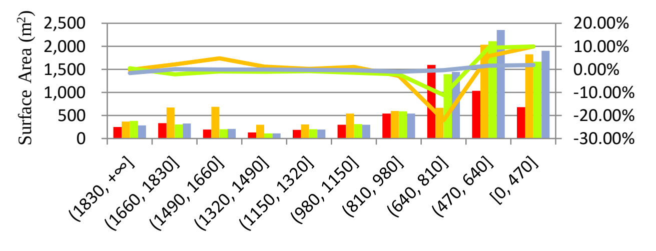

(3) New World Millennium HK Hotel

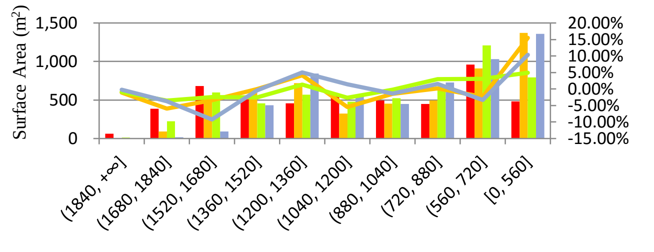

(4) The Royal Garden

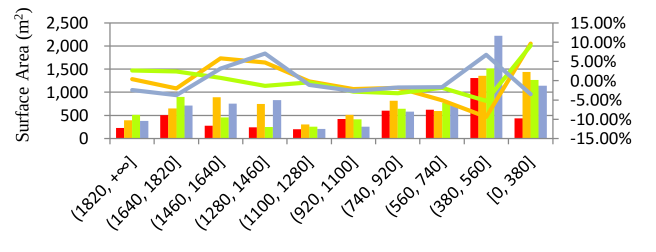

(5) Regal Kowloon Hotel

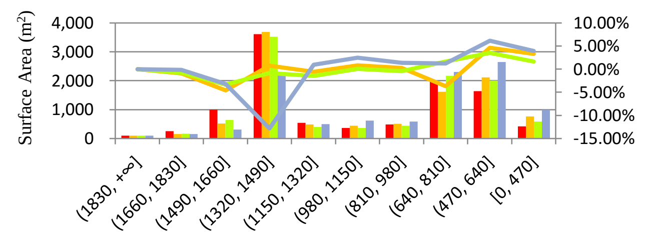

(6) Hotel ICON

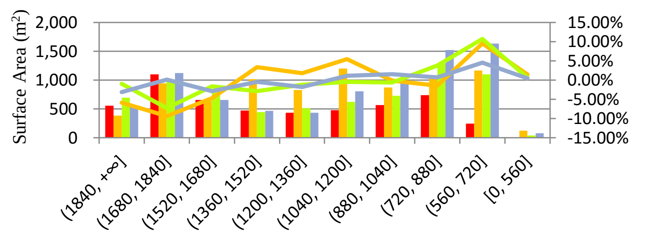

(7) TST Centre

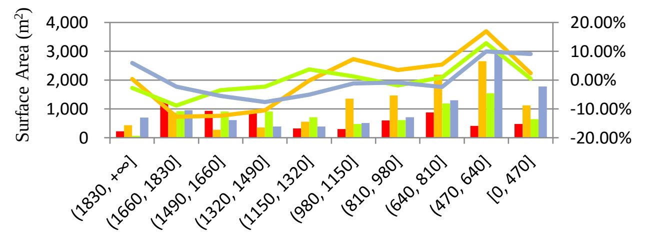

(8) Peninsula Centre

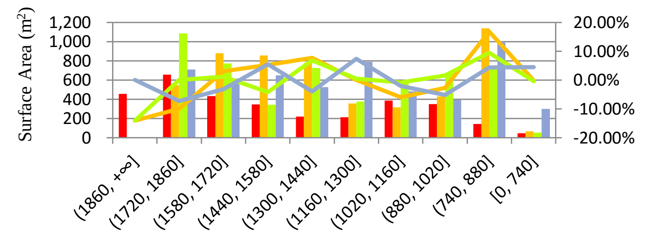

(9) Energy Plaza

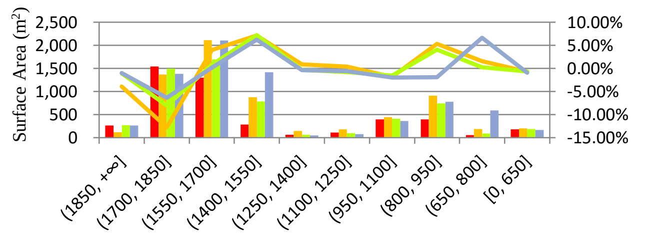

(10) Wing On Plaza

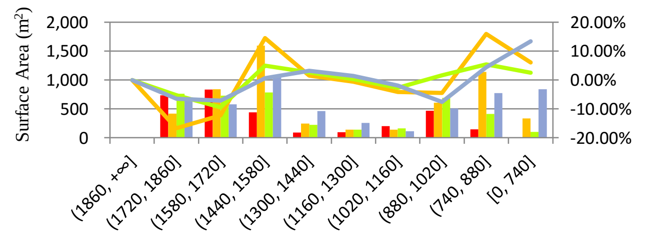

(11) Mirror Tower

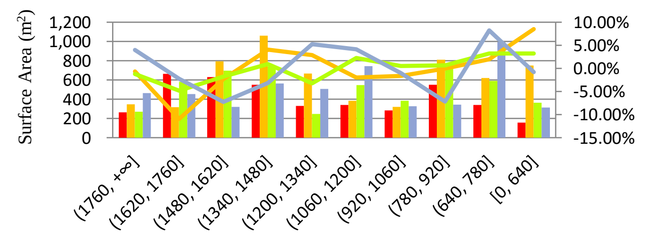

(12) Inter-Continental Plaza

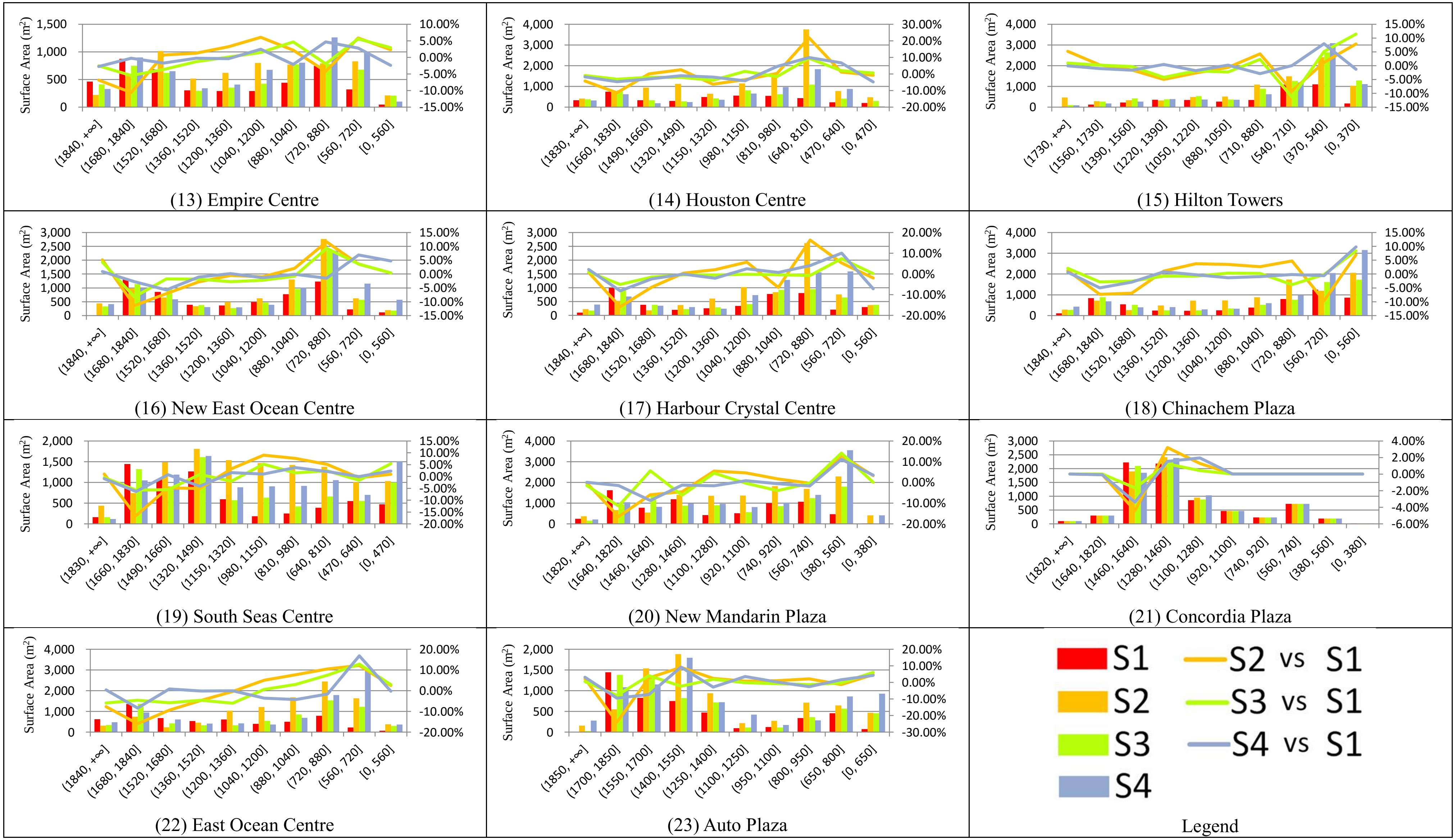

Figure 4-22b. Difference (S1 vs S2, S3, S4) of pattern areas as for cumulative winter radiation energy (Wh) on west facing facades

The Figure 4-15 shows the summer and winter cumulative and intensity solar radiation energy in all area of TSTE. The cumulative energy of radiation is slightly reduced after the PR/BH relaxation and it indicates that the shading effect makes radiation energy reduction. The intensity of radiation energy here also is reduced after the relaxation. The shading effect makes a certain reduction of the intensity.

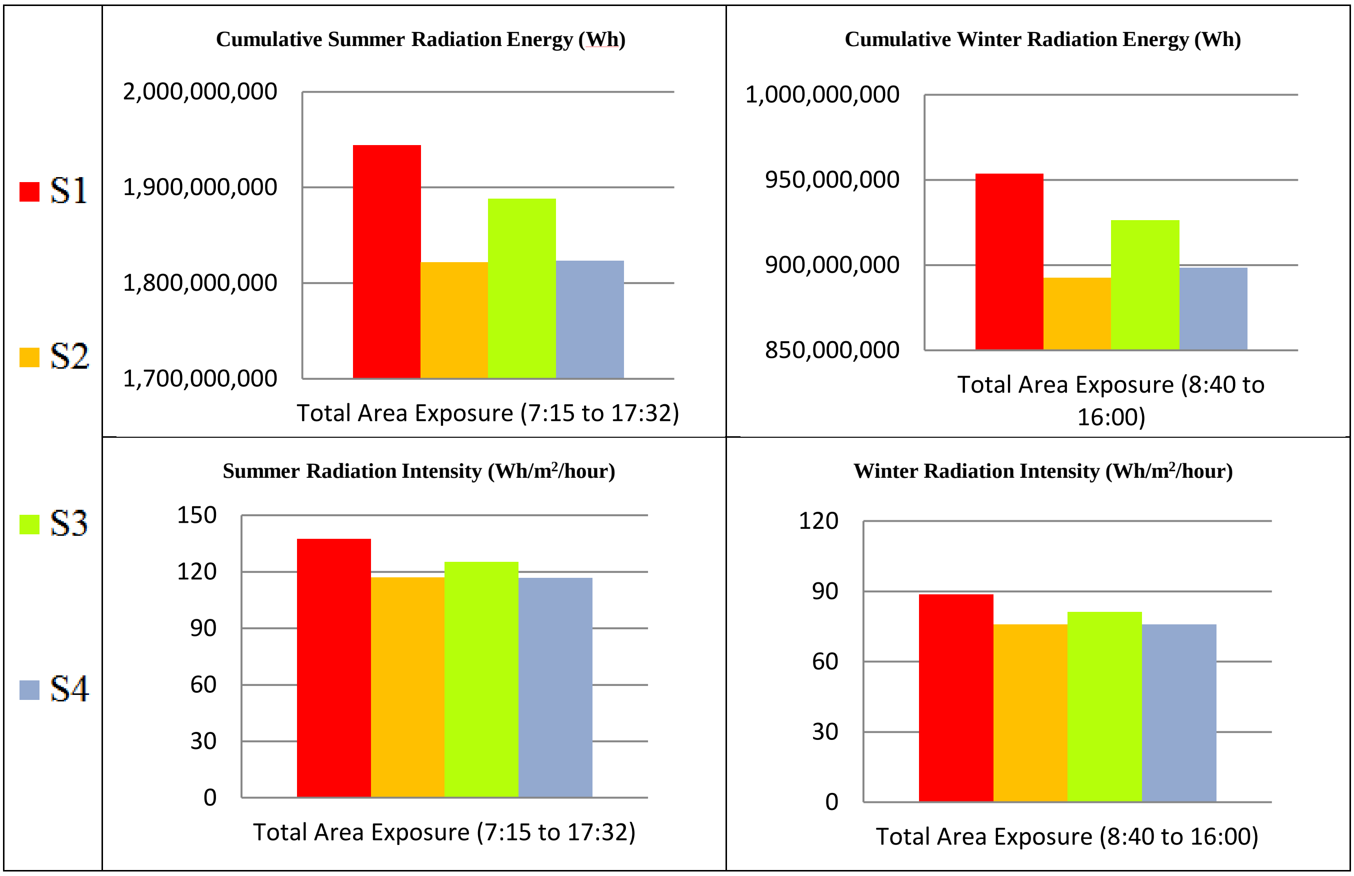

Figure 4-23. Cumulative and intensity of solar radiation energy in all area of TSTE

Figure 4-16 shows the cumulative (see Table 4-3) and intensity (Table 4-4) of solar radiation energy on west facing facades in TSTE. It implies that the cumulative energy of radiation on west facing facades is increased. This result also indicates that the intensity is reduced after the PR/BH relaxation due to the shading effect.

Table 4-3. Difference of cumulative radiation energy (Wh) on west facing facades

Seasons	Summer			Winter		
Buildings	S2 - S1	S3 - S1	S4 - S1	S2 - S1	S3 - S1	S4 - S1
Shangri-La	3823680	3249360	3851280	2341600	1033600	912480
InterContinental Grand Stanford	2434290	2413710	3244525	1316960	1145600	1106720
New World Millennium	2182375	1856250	2014375	1904610	760480	824355
The Royal Garden	-3094320	-1159440	-2811120	-676000	-496000	-963680
Regal Kowloon Hotel	3219000	2168480	3007780	2041750	1300560	1768730
Hotel ICON	-776790	-341820	-797040	-420205	-416205	-1252230
TST Centre	4383720	2973930	3696900	1865760	1091040	1483200
Peninsula Plaza	5510640	316560	4520880	1710480	572690	1067490
Energy Plaza	3260850	1656300	3476775	1421760	589950	1358100
Wing On Plaza	3471420	2428160	3730190	1717050	1249050	1785800
Mirror Tower	3972255	1575160	3673265	1732970	702520	1390870
Inter-Continental Plaza	3256365	1784935	3468435	1393740	736440	1519060
Empire Centre	2383700	1806570	3565180	1161440	692320	1206880
Houston Centre	4187500	2147000	4445000	1254530	682545	1205310
Hilton Towers	4602345	4400910	3323880	2158295	1792615	1344775
New East Ocean Centre	4445330	3496640	3402720	1630560	1332800	764320
Harbour Crystal Centre	5062155	1700965	4779145	1746720	604160	1750720
Chinachem Plaza	3096480	1901040	3677040	1857280	879680	1223360
South Seas Centre	4957360	1583490	5516790	1989945	496585	1649190
New Mandarin Plaza	2860110	846315	2690475	1761480	304150	956940
Concordia Plaza	-91800	-50055	-96390	-60220	-23580	-79300
East Ocean Centre	6583770	2022935	4469775	1660640	160960	852480
Auto Plaza	4555160	3189480	5425280	2191275	1552375	2473875
Sum	**74,285,595**	**41,966,875**	**72,275,140**	**33,702,420**	**16,744,335**	**24,349,445**
Ratio of Change	**38.43%**	**21.71%**	**37.39%**	**32.85%**	**16.32%**	**23.73%**

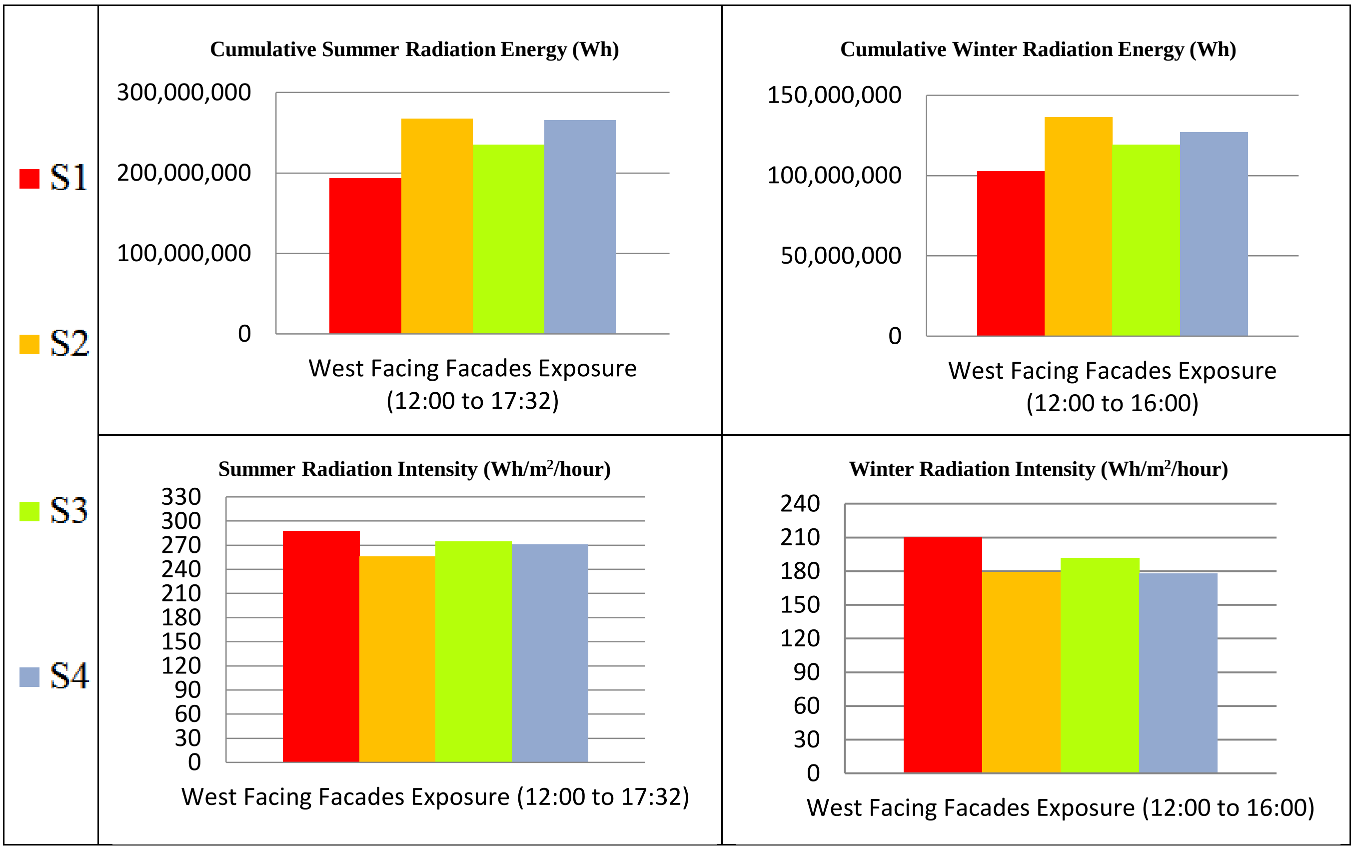

Figure 4-24. Cumulative and intensity of solar radiation energy on west facing facades

Table 4-4. Difference of radiation intensity (Wh/m^2/hour) on west facing facades

Seasons	Summer			Winter		
Buildings	S2 - S1	S3 - S1	S4 - S1	S2 - S1	S3 - S1	S4 - S1
Shangri-La	-28	-9	-25	3	-18	-38
InterContinental Grand Stanford	-35	-21	-25	-26	-21	-42
New World Millennium	-32	-19	-27	6	-17	-22
The Royal Garden	-102	-38	-93	-46	-38	-59
Regal Kowloon Hotel	11	3	3	9	0	-1
Hotel ICON	-14	-6	-14	-10	-10	-30
TST Centre	-28	-18	-44	-33	-29	-45
Peninsula Plaza	-40	-55	-36	-58	-28	-60
Energy Plaza	-13	-67	-12	-40	-78	-47
Wing On Plaza	10	14	-10	-4	4	-22
Mirror Tower	-19	-12	-17	-39	-21	-46
Inter-Continental Plaza	21	16	82	6	4	46
Empire Centre	-24	13	4	-26	-5	-28
Houston Centre	-116	5	43	-113	-20	-20
Hilton Towers	-3	-1	-14	-6	-13	-20
New East Ocean Centre	0	8	-10	-26	-14	-43
Harbour Crystal Centre	20	14	28	-7	1	2
Chinachem Plaza	-53	-19	-48	-21	-12	-42
South Seas Centre	-71	-18	-7	-76	-28	-46
New Mandarin Plaza	-53	-25	-44	-44	-26	-51
Concordia Plaza	-2	-1	-2	-2	-1	-3
East Ocean Centre	-7	-9	-20	-50	-38	-55
Auto Plaza	-16	26	-8	-24	10	-24
Sum	**-32**	**-13**	**-17**	**-31**	**-18**	**-32**
Ratio of Change	**-11.02%**	**-4.44%**	**-5.83%**	**-14.61%**	**-8.67%**	**-15.20%**
Buildings with Intensity Reduction	**18/23**	**15/23**	**18/23**	**19/23**	**18/23**	**21/23**

4.4 Wind Ventilation Analysis and Results

The results of wind ventilation in summer are shown in Figure 4-17, Figure 4-18, and Figure 4-19. Specifically, Figure 4-17 shows the average wind speed patterns in S1, S2, S3, and S4 in terms of twelve ranges of wind speed from > 0 m/s to 12 m/s. Fig.4-18 shows the quantified pattern areas corresponding to the twelve wind speed ranges. Figure 4-19 shows the differences (S1 vs S2, S3, and S4) of summer wind speed at the corresponding locations. The differences are mainly in the range of -1 m/s to 1 m/s for S1 vs S2, S3, and S4 and only a small portion of areas of S1 vs S4 are in the range of 1m/s to 3m/s. All the differences indicate that there is no significant impact of the PR/BH relaxation on the summer wind ventilation.

The results of wind ventilation in winter are shown in Figure 4-20, Figure 4-21, and Figure 4-22. Specifically, Figure 4-20 shows the average winter wind speed patterns in S1, S2, S3, and S4 in terms of twelve speed ranges. Figure 4-21 shows the quantified pattern areas corresponding to the twelve speed ranges. Figure 4-22 shows the differences (S1 vs S2, S3, and S4) of winter wind speed at the corresponding locations. The differences are mainly in the range of -1 m/s to 1 m/s for S1 vs S2, S3, and S4 and only a small portion falls within the range of -5 m/s to -4 m/s or 4 m/s to 6 m/s. All the differences indicate that no significant impact of the PR/BH relaxation on the winter wind ventilation.

Interestingly, as indicated by shades of blue in the Figures 4-19 and 4-22, wind speed is slightly increased in S4 in the TSTE area in both summer and winter season. This shows that widening of distance between buildings in S4 permits more air flow in TSTE, which increases the wind ventilation in the area. Although these patterns are similar in both seasons, increases of wind speed are more prominent during winter season when the wind is entering TSTE.

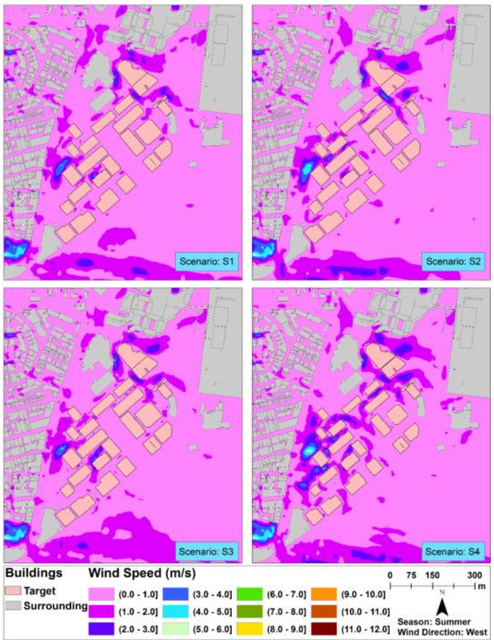

Wind Speed (m/s)	Percentage Area			
	S1	S2	S3	S4
(0.0 - 1.0]	80.82	80.67	80.77	79.68
(1.0 - 2.0]	15.68	15.09	16.03	16.04
(2.0 - 3.0]	3.04	3.62	2.72	3.73
(3.0 - 4.0]	0.36	0.45	0.36	0.38
(4.0 - 5.0]	0.09	0.15	0.10	0.15
(5.0 - 6.0]	0.01	0.02	0.02	0.02
(6.0 - 7.0]	0.00	0.00	0.00	0.00
(7.0 - 8.0]	0.00	0.00	0.00	0.00
(8.0 - 9.0]	0.00	0.00	0.00	0.00
(9.0 - 10.0]	0.00	0.00	0.00	0.00
(10.0 - 11.0]	0.00	0.00	0.00	0.00
(11.0 -12.0]	0.00	0.00	0.00	0.00

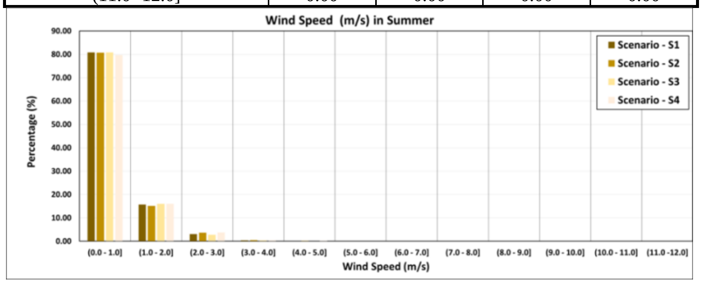

Figure 4-25. Average summer wind speed patterns in S1, S2, S3, and S4

Figure 4-26. Quantified pattern areas (%) in each summer wind speed sections

Generally, wind speed in summer is relatively slower than in wind speed in winter. Spatial patterns of wind speed in summer do not indicate significant spatial variations and most of the areas show very slow (≤ 1 m/s) (Figure 4-17 and Figure 4-18) and these observations are similar in all scenarios (S1, S2, S3, and S4). It is evident that the S4 indicate relatively higher proportion (19.77%) of wind speed ranging from > 1 m/s to ≤ 3 m/s as compared to S1 (18.72%), S2 (18.71%), and S3 (18.75%). Comparisons of difference in scenarios S2, S3, and S4 with respect of S1 also indicate that wind ventilation inside the TSTE area is better in S4.

There are significant observable patches of increased wind speed in S4, indicate tones of light blue colour in the maps which positive shows change of > 1 m/s to ≤ 3 m/s in S4 as compared to S1 (see Figure 4-19).

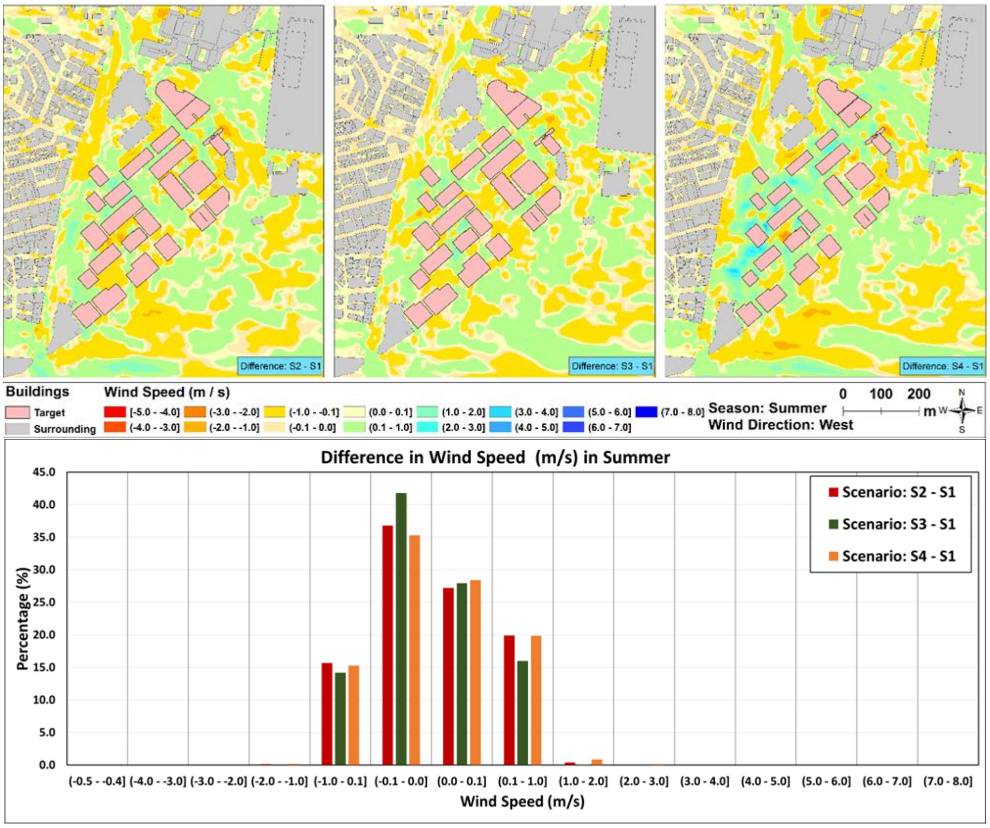

Figure 4-27. Differences of summer wind speed at corresponding locations

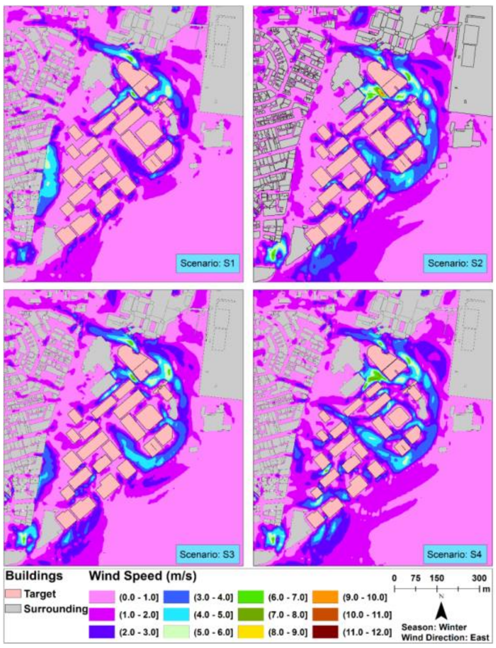

Figure 4-28. Average winter wind speed patterns in S1, S2, S3, and S4

Wind Speed (m/s)	Percentage Area			
	S1	S2	S3	S4
(0.0 - 1.0]	68.55	65.09	66.63	64.05
(1.0 - 2.0]	22.87	24.11	23.47	24.34
(2.0 - 3.0]	6.24	7.30	6.91	7.81
(3.0 - 4.0]	1.46	2.26	1.97	2.48
(4.0 - 5.0]	0.66	0.79	0.74	0.90
(5.0 - 6.0]	0.17	0.30	0.21	0.29
(6.0 - 7.0]	0.05	0.12	0.06	0.11
(7.0 - 8.0]	0.00	0.02	0.01	0.02
(8.0 - 9.0]	0.00	0.01	0.00	0.00
(9.0 - 10.0]	0.00	0.00	0.00	0.00
(10.0 - 11.0]	0.00	0.00	0.00	0.00
(11.0 -12.0]	0.00	0.00	0.00	0.00

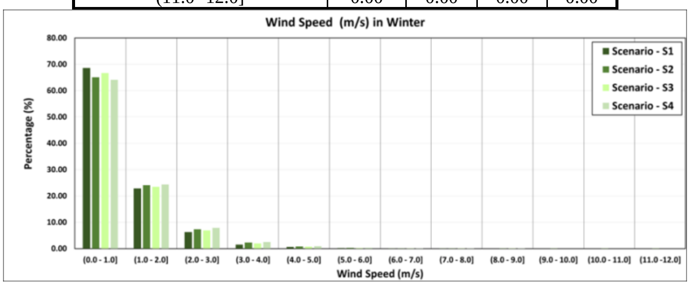

Figure 4-29. Quantified pattern areas (%) in each winter wind speed sections

The average wind speed in winter is higher than the wind speed in summer. Higher wind speed and prevailing wind direction from the East direction creates strong wind patches in the TSTE area which are shown in tones of blue and green colour (see Figure 4-20). As compared to summer season a considerable proportion of the area in each scenario of S1(29.11%), S2 (31.41%), S3 (30.38%), and S4 (32.15%) lies in wind speed ranging from > 1 m/s and ≤ 3 m/s. Additionally, each scenario of S1 (2.34%), S2 (3.47%), S3 (2.98%), and S4 (3.78%) indicates a small, but significant, proportion of high wind speed patches which ranges from >3 m/s and ≤ 7m/s (see Figure 4-21). Notably, the proportion of high wind speed is greater in S4 in both the cases and it is also evident in comparison maps (see Figure 4-18) which shoe difference in wind speed in each scenario (S2, S3, and S4) when compared to S1. These observations suggest that the wind ventilation is better in S4 as compared to S1, S2, and S3, especially in summer as wind coming from the eastern direction will have better flow into the TSTE through the widened distances between the buildings (see Figure 4-22).

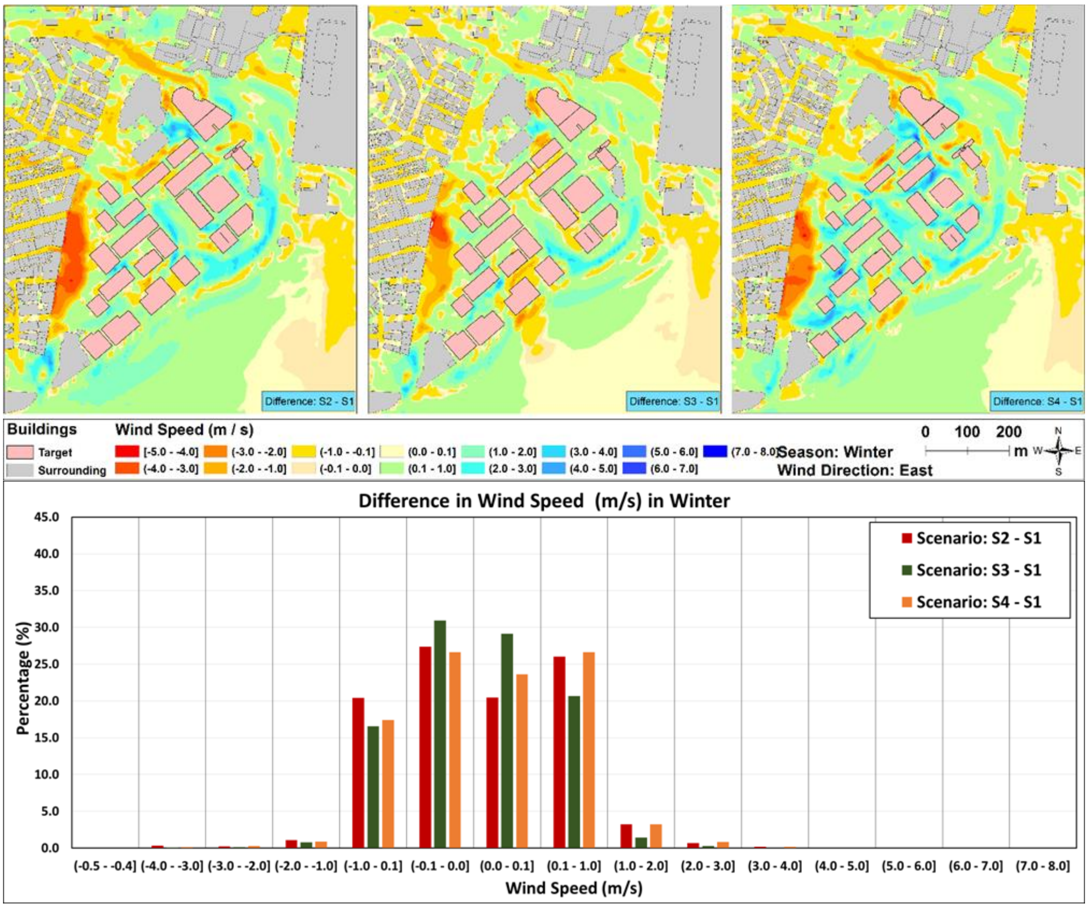

Figure 4-30. Differences of winter wind speed at corresponding locations

Distributions of wind flow direction during the winter season are shown in Figure 4-23. As shown in the figure, wind comes from the west and enters the TSTE area from gaps between the buildings and circulates into the northern TSTE area (ellipse A in the figures), which is primarily the Urban Council Centenary Garden. This garden provides a significantly important corridor of wind inflow to TSTE regions during winter. However, the area highlighted with the ellipse B indicates that wind could not enter the TSTE area through the narrow gaps and would bounce back from the buildings to become wind flow along the harbour rather than flowing into the area; and this phenomenon is enhanced in S2, S3, and S4. On the other hand, wind circulations inside the TSTE area creates a strong outward wind flow from west to north east and south east, highlighted with ellipse C, which seems to be reflected by the closely spaced building on the western side of Nathan road. It is evident that wind circulation is improved in S4 as compared to S1, S2, and S3. However, wind prevalence during the summer season (see Figure 4-23) is relatively simple, as wind that is already slowed down by the dense buildings in the west of TSTE, enters the TSTE area and slowly circulates to primarily ventilate TSTE from the corridor formed by the Urban Council Centenary Garden. It is notable that ventilation is relatively better in S4 as compared to S1, S2, and S3 during the summer season.

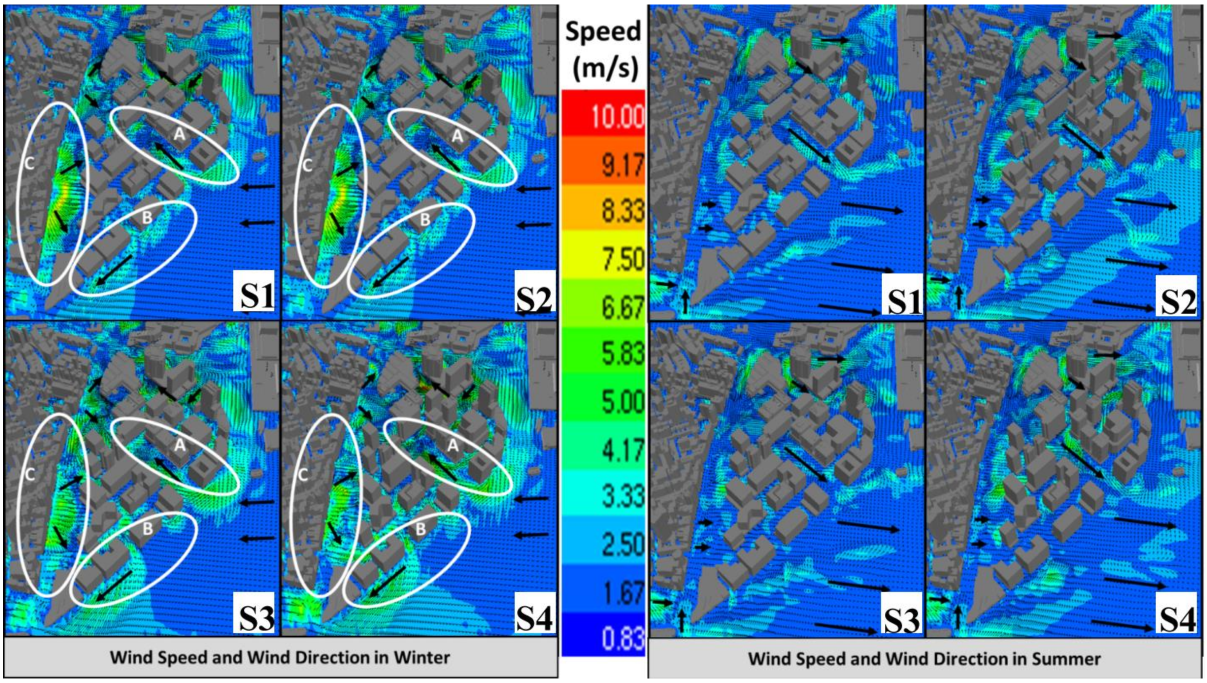

Figure 4-31. Wind speed and prevailing wind direction in each scenario (S1, S2, S3, and S4) a during winter and summer season in the study are arrows indicate prevailing wind direction

4.5 Air Temperature Analysis and Results

The simulation results of air temperature for each scenario (S1, S2, S3, and S4) were extracted at 1:00 am and 1:00 pm on the representative day of winter and summer seasons. Spatial patterns of air temperature and changes in air temperature are given in Figure 4-24 to Figure 4-39. A colour legend is designed to present changes in air temperature due to the changes in building dimension corresponding to the different scenarios. The temperature range (-0.20 °C to 0.20 °C) is considered as insignificant, while changes in air temperature beyond this range, i.e., below -0.20 °C or above 0.20 °C, are deemed as significant changes in air temperature.

Spatial patterns and distribution of changes in air temperature (Figure 4-26, Figure 4-27, Figure 4-30, and Figure 4-31) indicate that most of the areas lies within an insignificant range (-0.20 °C to 0.20 °C) when comparing S2, S3, and S4 with S1 on a winter afternoon and night. However, a very small area in the northeast of the study area shows a relatively significant change in temperature and it is interesting to note that S3 more resembles S1 while S2 and S4 indicate a decline of temperature on winter afternoons while a similar but opposite trend is observed in winter night. In particular, 7.1% of the area (summation of the area for the change of air temperature ranging from -0.20 °C to above -0.40 °C) exhibits significant decreases in air temperature in S4 on winter afternoon, whereas there is no significant change in air temperature. This pattern is also similar with S2. On the other hand, S3 does not show any significant change in temperature patterns. This observed decreases in air temperature in S2 and S4 on winter afternoons could be attributed to elongated shades due to the increased building heights and relatively lower solar elevation on winter afternoons.

In the summer season, spatial patterns and distribution of changes in air temperature (Figure 4-34, Figure 4-35, Figure 4-38, and Figure 4-39) do not show any significant change at night. However, a very significant increase in air temperature in S4 is observed, as compared with S1, on summer afternoons. This might be due to the fact that the prevailing wind direction in summer is from the west and the increased height in building increases and expands the air temperature regime as indicated in Figure 4-32. However, most of the regions with increased temperature lie over the coastal region, away from the core study area.

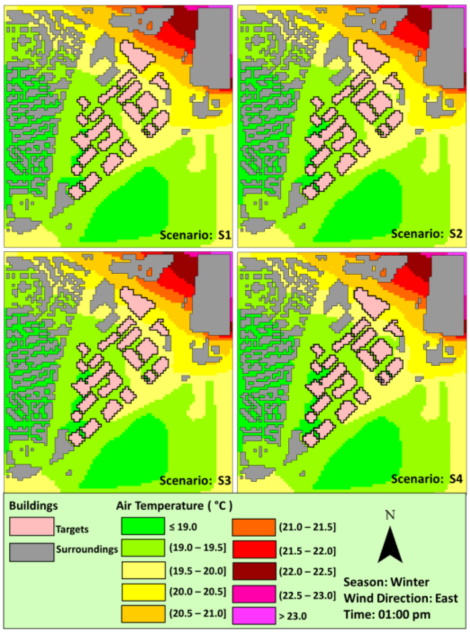

Figure 4-32. Spatial patterns of winter (1:00 pm) air temperature in each scenario

Air Temperature (°C)	Percentage Area			
	S1	S2	S3	S4
≤ 19.0	22.3	26.1	26.2	26.2
(19.0 - 19.5]	36.3	36.2	33.8	36.2
(19.5 - 20.0]	19.2	16.4	18.4	16.2
(20.0 - 20.5]	11.0	10.7	10.7	10.7
(20.5 - 21.0]	6.1	6.2	6.2	6.4
(21.0 - 21.5]	1.8	1.5	1.6	1.4
(21.5 - 22.0]	1.3	1.3	1.3	1.3
(22.0 - 22.5]	1.3	1.1	1.3	1.1
(22.5 - 23.0]	0.3	0.3	0.3	0.3
>23.0	0.3	0.3	0.3	0.3

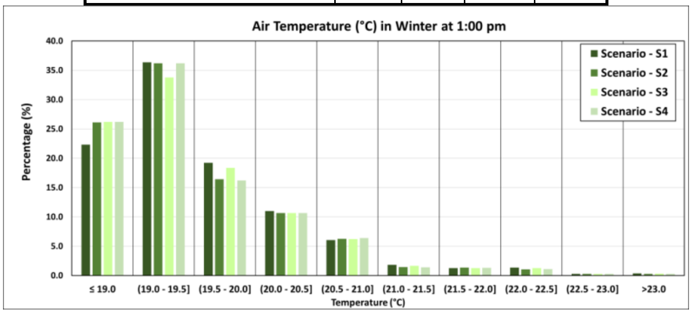

Figure 4-33. Quantified distribution of area (%) in each range of winter (1:00 pm) air temperature in each scenario

Air temperature on winter afternoons ranges of ≤19.0 °C to >23.0 °C and the spatial patterns of the air temperatures (Figure 4-24) indicate that the TSTE area is relatively cooler (ranging of ≤ 19.0 °C to 20.5 °C) than the area nearby Hung Hom MTR Station and The Hong Kong Polytechnic University in the north and northeast of the study area (ranging of > 20.5 °C to 23.0 °C). And the distribution graph (Figure 4-32) shows that most of the study areas (~88%) lie in the temperature range of ≤ 19.0 °C to 20.5 °C. Spatial patterns and distribution of air temperatures on winter afternoons do not show significance changes as compared S2, S3, and S4 to S1 (Figure 4-26 and Figure 4-27). However, some of the areas indicate a decrease in temperature in S2 and S4 as compared to S1**.**

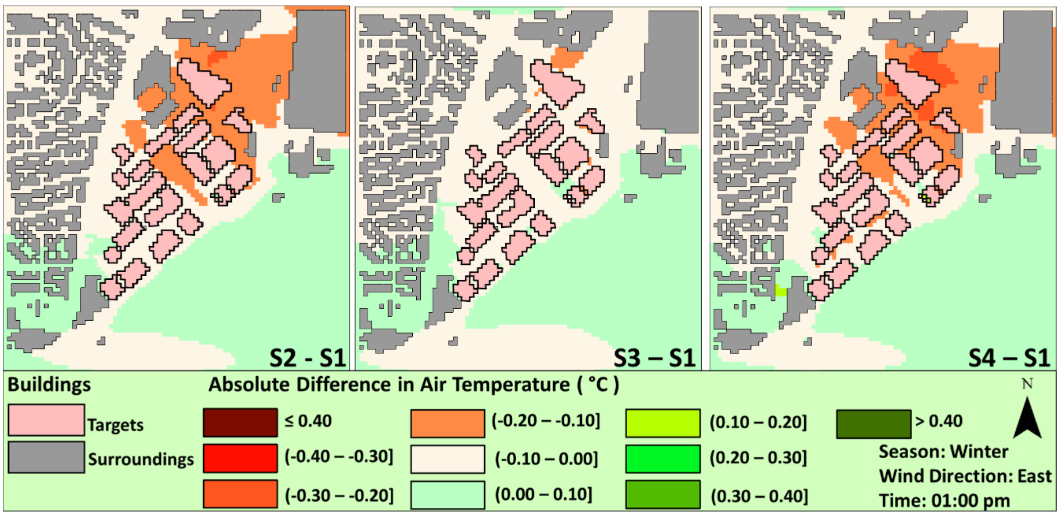

Figure 4-34. Spatial patterns of differences in winter (1:00 pm) air temperature

Difference in Air Temperature (°C)	Percentage Area		
	Scenario: S2 - S1	Scenario: S3 - S1	Scenario: S4 - S1
≤ -0.40	4.2	0.2	3.2
(-0.40 - -0.30]	0.1	0.8	1.0
(-0.30 - -0.20]	3.2	2.5	2.9
(-0.20 - -0.10]	11.6	3.7	12.7
(-0.10 - 0.00]	48.6	61.2	45.3
(0.00 - 0.10]	32.2	31.6	34.9
(0.10 - 0.20]	0.0	0.0	0.1
(0.20 - 0.30]	0.0	0.0	0.0
(0.30 - 0.40]	0.0	0.0	0.0
> 0.40	0.0	0.0	0.0

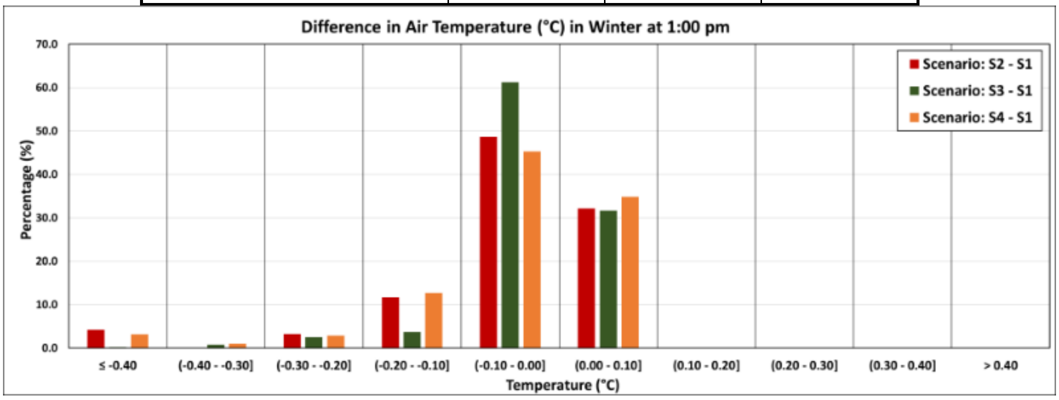

Figure 4-35. Quantified distribution of differences in winter (1:00 pm) air temperature

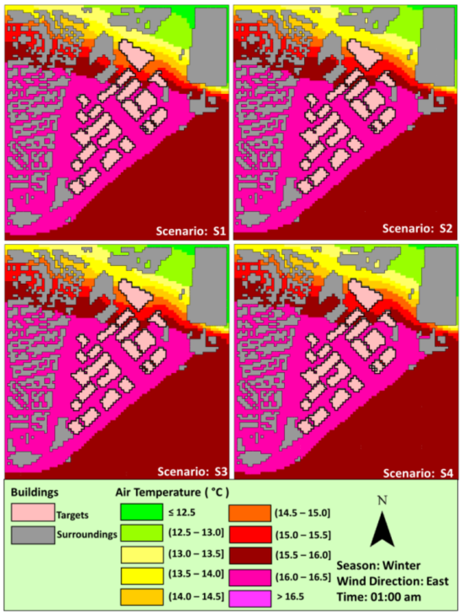

Figure 4-36. Spatial patterns of winter (1:00 am) air temperature in each scenario

Air Temperature (°C)	Percentage Area			
	S1	S2	S3	S4
≤ 12.5	1.4	0.6	1.0	0.5
(12.5 - 13.0]	2.5	2.6	2.6	2.3
(13.0 - 13.5]	2.5	1.5	1.9	1.6
(13.5 - 14.0]	2.0	3.0	2.6	2.9
(14.0 - 14.5]	1.6	1.6	1.6	1.7
(14.5 - 15.0]	2.0	1.6	1.8	1.6
(15.0 - 15.5]	2.9	3.3	3.2	3.2
(15.5 - 16.0]	30.2	31.6	31.4	30.8
(16.0 - 16.5]	25.2	24.4	24.2	25.5
> 16.5	29.7	29.8	29.8	29.8

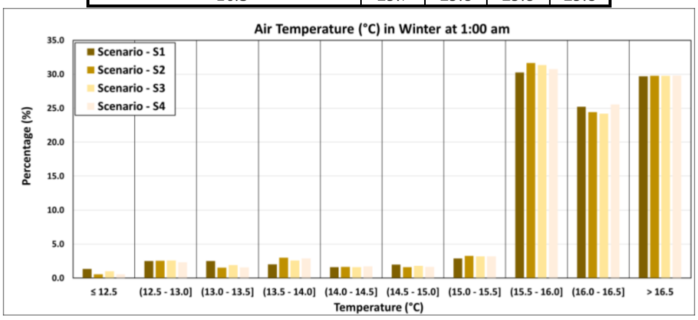

Figure 4-37. Quantified distribution of area (%) in each range of winter (1:00 am) air temperature in each scenario

In contrary to spatial patterns of afternoon air temperature in winter, night-time temperature shows relatively warm temperatures in the TSTE area (Figure 4-28). Night time air temperatures in winter range from ≤ 12.5 °C to > 16.5 °C and the spatial patterns of the air temperature (Figure 4-28 and Figure 4-29) indicate that the TSTE area is relatively warmer (> 16.0 °C) than the area around Hung Hom MTR Station and The Hong Kong Polytechnic

University in the north and northeast of the study area (ranges from ≤ 12.5 °C to 16.0 °C). And the distribution graph (Figure 4-29) shows that most of the study area (~85%) lies in temperature range of ≤ 19.0 °C to 15.5 °C in all scenarios. Spatial patterns and distribution (Figure 4-30 and Figure 4-31) analysis of air temperature on winter mid-nights shows that S3 indicates very less 0.70% significant increase (> 0.20 °C) in temperature while S2 and S4 shows 6.80% and 8.42% significant increase in air temperature. However, majority of area did not indicate notable change (< -0.20 °C or > 0.20 °C), but a cold island is also observed in northeast of the study area.

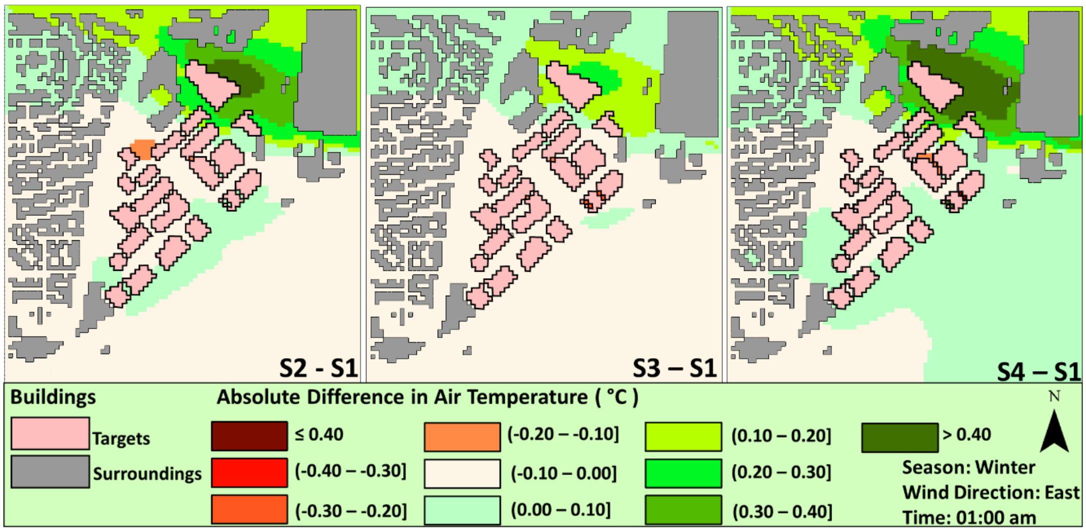

Figure 4-38. Spatial patterns of differences in winter (1:00 am) air temperature

Difference in Air Temperature (°C)	Percentage Area		
	Scenario: S2 - S1	Scenario: S3 - S1	Scenario: S4 - S1
≤ -0.40	4.2	1.5	8.00
(-0.40 - -0.30]	0.7	1.7	1.99
(-0.30 - -0.20]	1.7	3.3	6.17
(-0.20 - -0.10]	7.7	1.4	6.95
(-0.10 - 0.00]	62.7	73.9	26.63
(0.00 - 0.10]	10.4	13.2	36.22
(0.10 - 0.20]	5.9	4.3	5.78
(0.20 - 0.30]	3.2	0.7	2.77
(0.30 - 0.40]	2.7	0.0	2.25
> 0.40	0.9	0.0	3.24

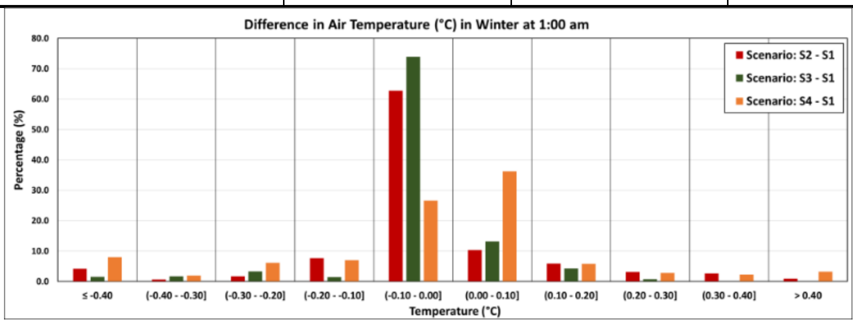

Figure 4-39. Quantified distribution of differences in winter (1:00 am) air temperature

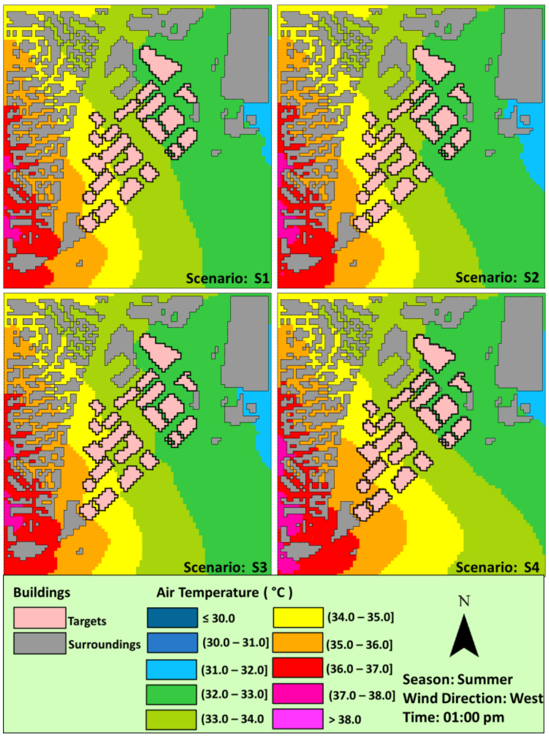

Figure 4-40. Spatial patterns of summer (1:00 pm) air temperature in each scenario

Air Temperature (°C)	Percentage Area			
	S1	S2	S3	S4
≤ 30.0	0.0	0.0	0.0	0.1
(30.0 - 31.0]	0.0	0.0	0.0	0.0
(31.0 - 32.0]	2.1	4.0	3.0	1.6
(32.0 - 33.0]	37.7	36.9	37.7	25.6
(33.0 - 34.0]	25.3	24.0	24.4	29.1
(34.0 - 35.0]	15.4	14.8	14.6	18.7
(35.0 - 36.0]	11.8	11.6	12.0	14.1
(36.0 - 37.0]	6.9	7.4	7.3	8.5
(37.0 - 38.0]	0.7	1.3	0.9	2.4
> 38.0	0.0	0.0	0.0	0.0

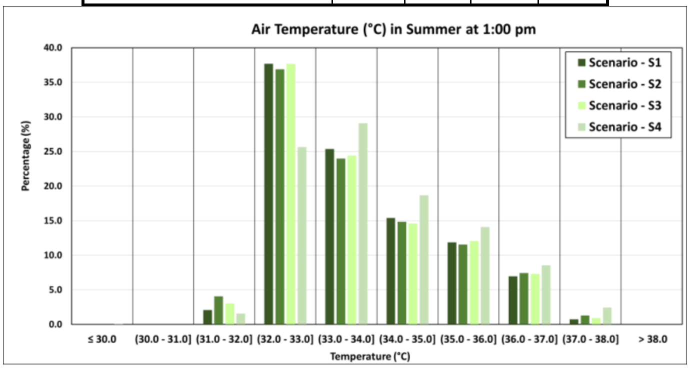

Figure 4-41. Quantified distribution of area (%) in each range of summer (1:00 pm) air temperature in each scenario

In summer, the prevailing wind direction is from the west. Afternoon air temperatures in the summer range from ≤ 30.0 °C to > 38.0 °C and the spatial patterns of the air temperature (Figure 4-32) indicate warm to cold fringes from the southwest to northeast and temperatures in the TSTE area ranging from > 32.0 °C to ≤ 36.0 °C. And the distribution graph (Figure 4-33) shows that most of the study areas (~95%) lie in the temperature range of > 32.0 °C to ≤ 36.0 °C in all scenarios.

Spatial patterns and distribution analysis of air temperature on summer afternoons are shown in Figure 4-34 and Figure 4-35. There is no notable change in S2 and S3 midnight temperatures when compared to S1, as 98.53% and 99.9% of the area lie within an insignificant range of temperature change (-0.20 °C to 0.20 °C), respectively. However, there is an uncharacteristic pattern of change in air temperature in S4 as a relatively higher temperature is observed in the southeast of the study area where most of the areas lie by the sea.

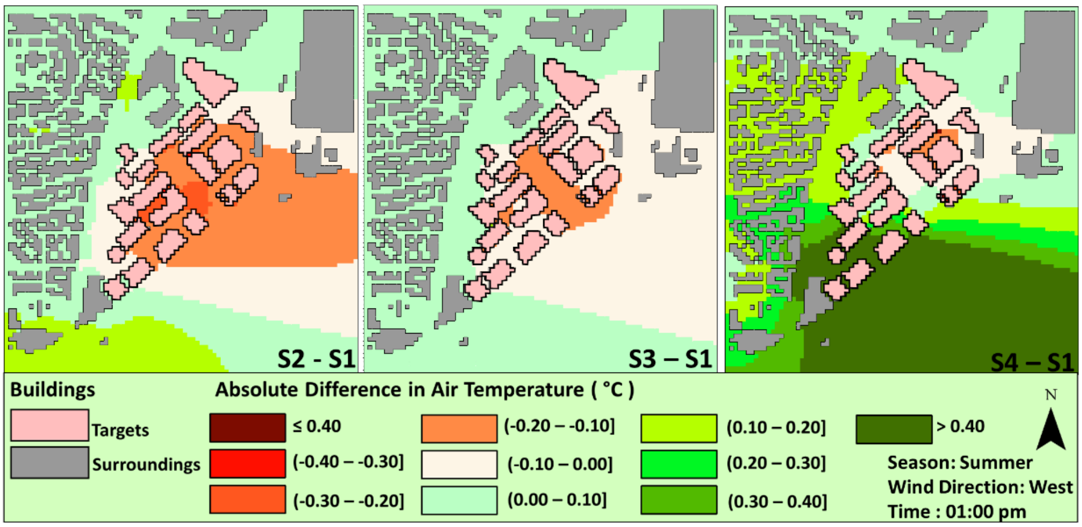

Figure 4-42. Spatial patterns of differences in summer (1:00 pm) air temperature

Difference in Air Temperature (°C)	Percentage Area		
	Scenario: S2 - S1	Scenario: S3 - S1	Scenario: S4 - S1
≤ -0.40	0.00	0.00	0.06
(-0.40 - -0.30]	0.04	0.00	0.00
(-0.30 - -0.20]	1.43	0.07	0.04
(-0.20 - -0.10]	20.89	4.26	0.80
(-0.10 - 0.00]	20.54	38.26	7.11
(0.00 - 0.10]	46.08	57.38	24.13
(0.10 - 0.20]	11.02	0.02	17.78
(0.20 - 0.30]	0.00	0.00	6.83
(0.30 - 0.40]	0.00	0.00	6.85
> 0.40	0.00	0.00	36.40

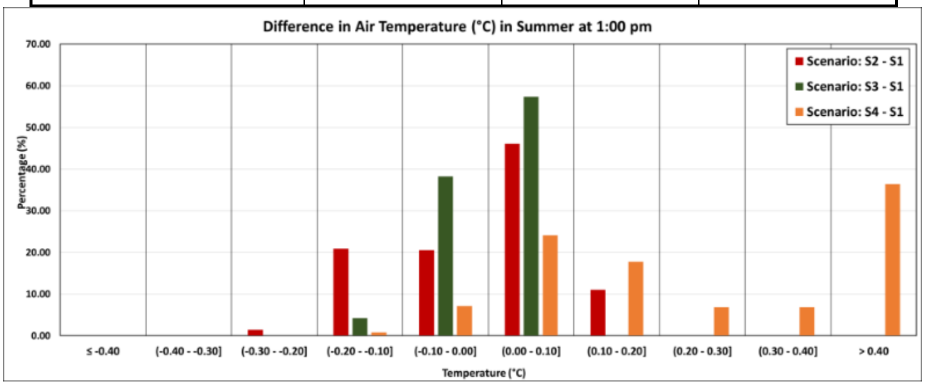

Figure 4-43. Quantified distribution of differences in summer (1:00 pm) air temperature

Summer midnight temperatures show homogenous temperature patterns and most of the areas, 96.7%, 96.3%, 96.5% and 97.3% in S1, S2, S3, and S4, lie within a narrow temperature range of 22.6 °C to 23.2 °C (Figure 4-36 and Figure 4-37).

Comparisons of air temperature in S2, S3, and S4 with S1 do not indicate notable changes in air temperatures in summer mid-nights (Figure 4-38 and Figure 4-39), although S2 and S4 are relatively warmer but lie in an insignificant range of -0.10 °C to 0.10 °C.

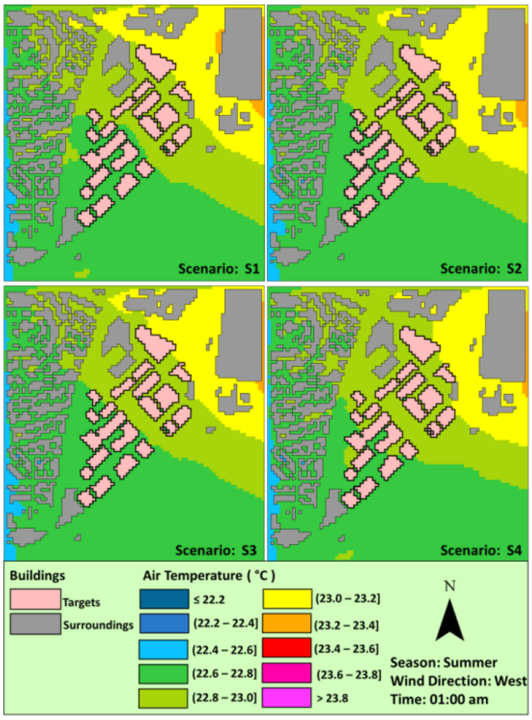

Figure 4-44. Spatial patterns of summer (1:00 am) air temperature in each scenario

Air Temperature (°C)	Percentage Area			
	S1	S2	S3	S4
≤ 22.2	0.0	0.0	0.0	0.0
(22.2 - 22.4]	0.0	0.0	0.0	0.0
(22.4 - 22.6]	2.2	2.7	2.8	2.0
(22.6 - 22.8]	52.3	53.8	55.5	53.0
(22.8 - 23.0]	28.5	27.3	27.0	30.2
(23.0 - 23.2]	15.9	15.2	14.0	14.1
(23.2 - 23.4]	1.1	1.0	0.6	0.6
(23.4 - 23.6]	0.0	0.0	0.0	0.0
(23.6 - 23.8]	0.0	0.0	0.0	0.0
> 23.8	0.0	0.0	0.0	0.1

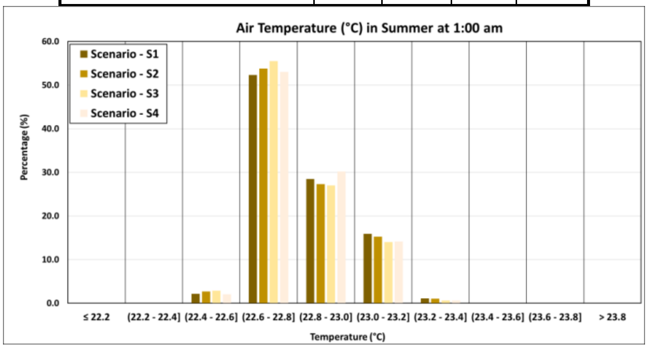

Figure 4-45. Quantified distribution of area (%) in each range of summer (1:00 am) air temperature in each scenario

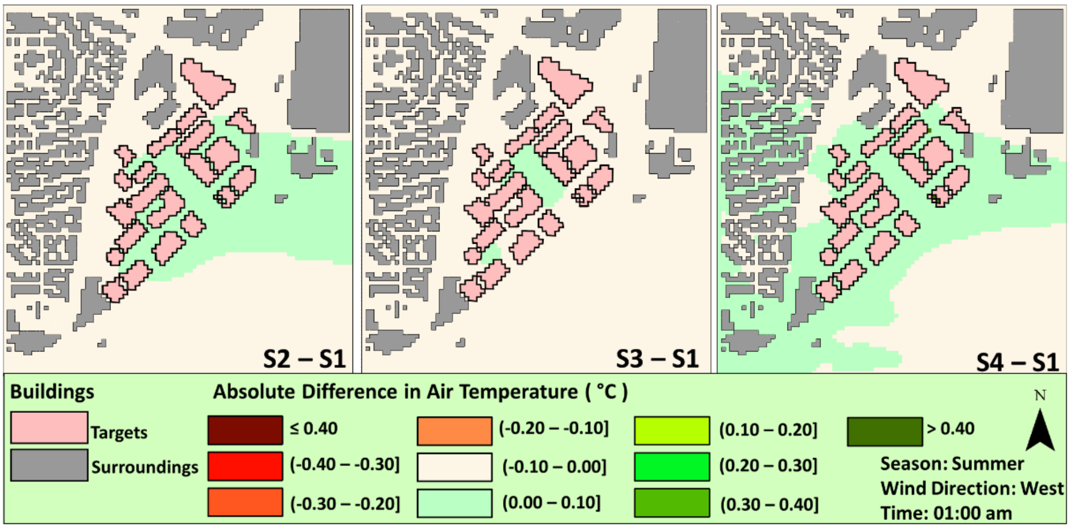

Figure 4-46. Spatial patterns of differences in summer (1:00 am) air temperature

Difference in Air Temperature (°C)	Percentage Area		
	Scenario: S2 - S1	Scenario: S3 - S1	Scenario: S4 - S1
≤ -0.40	0.00	0.00	0.00
(-0.40 - -0.30]	0.00	0.00	0.00
(-0.30 - -0.20]	0.00	0.00	0.00
(-0.20 - -0.10]	0.00	0.00	0.00
(-0.10 - 0.00]	76.52	97.65	56.69
(0.00 - 0.10]	23.48	2.35	43.25
(0.10 - 0.20]	0.00	0.00	0.00
(0.20 - 0.30]	0.00	0.00	0.00
(0.30 - 0.40]	0.00	0.00	0.00
> 0.40	0.00	0.00	0.06

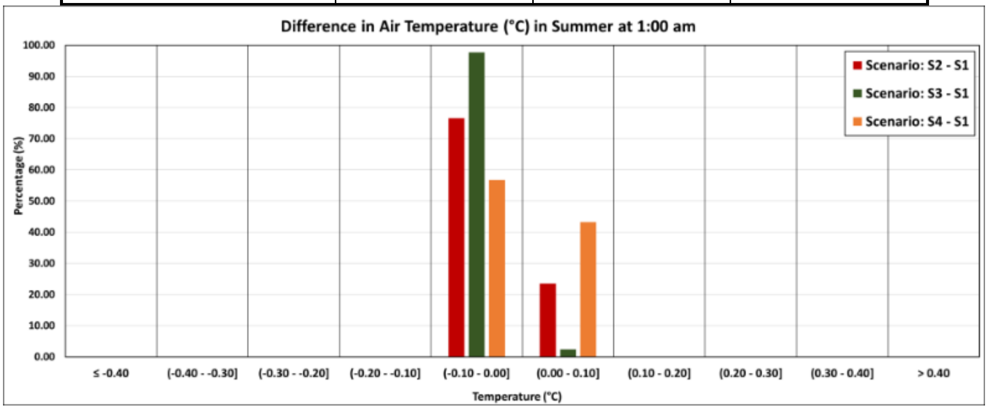

Figure 4-47. Quantified distribution of differences in summer (1:00 am) air temperature

4.6 Traffic Analysis and Results

There are two ways to understand the impact brought by increased hotel room. First, it can be shown by future trip generated due to the increased hotel capacity. Second, it can be explained by the change of local people's travel behaviour. The following two tables are from "*West Kowloon Reclamation Development Traffic Study* (Transport Department, 2009)". Due to the low trip generation rate, the impact brought by the Green Deck development is very limited.

Based on Table 4-5, the trip generation rate (for hotels) is 1.7 pedestrian/hr/room; which means daily trip (all mode) total will be -24 (hr) x 1.7 pedestrian/hr/room x 896 (increased hotel rooms) = 36557 trips. However, assuming 90% of people will take public transportation; only 10% people take private cars. Thus, the "passenger car trip" is only 36557 x 10% = 3656 trips/day. This 3656 trips/day (daily average) is considered as low impact, compared to the original traffic in TSTE.

Table 4-5. Trip Generation Rates in Hong Kong

Land-use	Assumed/Adopted Trip Generation/ Attraction Rate (Two-way)
Residential (apartment)	0.60 ped/hr/flat
Service Apartment	0.40 ped/hr/flat
Hotel	1.70 ped/hr/room
Office	2.88 ped/hr/100m^2 GFA
Retail	7.89 ped/hr/100m^2 GFA

Besides, Table 4-6 is focused directly on the hotel in TSTE. The impact is generally low. Taking the Intercontinental Hotel (Tsim Sha Tsui) as an example, its AM Peak Trip Generation Rate is 0.095; and PM Peak Trip Generation Rate is 0.154. That is to say, for the increased 896 hotel room, its increased trip (passenger car) is 896 x 0.095 = **85 trips/AM Peak hr**; and 896 x 0.154 = **138 trips/PM Peak hr**. Both numbers are low, which indicate the low impact after the Green Deck development and its' associated hotel increased.

Table 4-6. Trip Generation Rates for Hotel (pcu*/hr/room) in Hong Kong

Source	Data Source	Development Sites	Location	No. Rooms (nos.)	AM Peak		PM Peak	
					Gen.	Att.	Gen.	Att.
Survey of this Study	By Survey	InterContinental HK	Tsim Sha Tsui	495	0.095	0.097	0.154	0.214
		Conrad Hotel Hong Kong	Admiralty	513	0.113	0.113	0.172	0.168
		Grand Hyatt Hong Kong	Wan Chai	549	0.158	0.169	0.217	0.209
TGS 2006	By Survey	Excelsior Hotel Hong Kong	Causeway Bay	884	0.163	0.146	0.146	0.084
		Hong Kong Peninsula Hotel	Tsim Sha Tsui	300	0.217	0.247	0.280	0.327
WKCD TIA	By DR 439	Central Reclamation Phase III – Land Traffic Impact Assessment (September 1995)	N/A	N/A	0.055	0.055	0.065	0.067
Site A TIA	By Survey	Two International Finance Centre	Central	910 (Hotel with Service Apartment)	0.091	0.100	0.188	0.204
	Adopted Rate	N/A	N/A	N/A	0.182	0.197	0.210	0.234

pcu: Passenger Car Unit

In addition to re-confirm the trip generation rate and its impact, another aspect to investigate is the change of people's travel behaviour. The following are current vs. future (after Green Deck Project) travel behaviour. People are asked on what's your frequently used road in the

TSTE area.

Figure 4-48. Frequently used road weekday (current)

Figure 4-49. Frequently used road weekend (current)

Figure 4-50. Frequently used road weekday (future)

Figure 4-51. Frequently used road weekday (future)

Numbers achieved from above lines (above Figures 4-40 to 4-43) are number of cases out of a total of 93 respondents in the final survey. By comparing the “current vs. future” most used road, it can be noticed that popular roads did not changed much, such as Moody Road, Nathan Road, etc. However, after the Green Deck project, people tend to change to roads a little bit away from the TSTE area.

The following Figures 4-44 and 4-45 are the O-D (origin-destination) desire line showing people to visit other paces in Hong Kong. Most people (surveyed) in TSTE didn’t go Hong Kong Island or New Territory. In the survey, people were asked directly on what behaviour change (e.g. travel routes, and modes) they might have, due to the Green Deck project. Most people mentioned about the mode change (i.e. walk or taking MTR more instead of driving). However, there are fewer people mentioned about the route (e.g. O-D desire line) change.

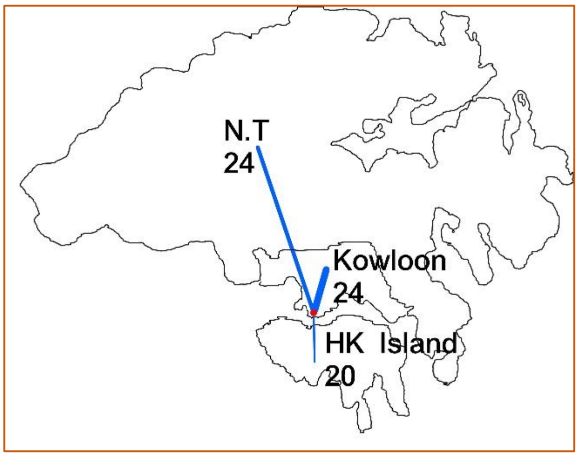

Figure 4-52. O-D pattern Weekday (current)

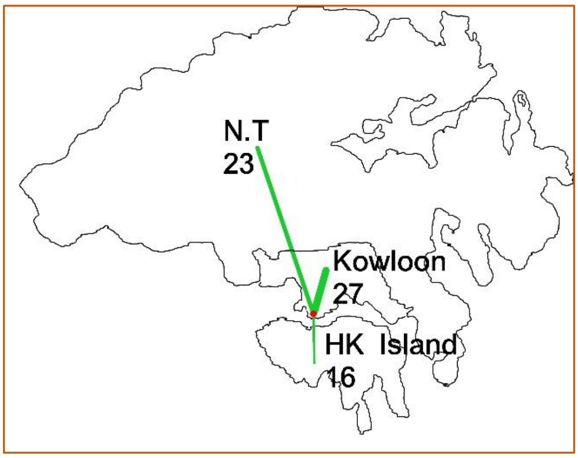

Figure 4-53. O-D pattern Weekend (current)

5. DISCUSSION AND CONCLUSIONS

5.1 Discussion

The analyses of this project included urban skyline, mountain ridgeline, solar exposure, wind ventilation, air temperature, and traffic impact. Three parts of analyses is similar to the analyses in the pilot study of PR/BH relaxation for residential/mixed use buildings in Kai Tak (Guo et al., 2017). However, the results represent the development potential in TSTE where most buildings are densely built in commercial zones rather than PR/BH relaxation in residential zones in the Kai Tak study. Therefore, the findings of this study are more representative of the issues in the compact development of a high-density city and also supportive of maintaining social-economic development in a suitable manner. The findings show that the potential of GFA increases in TSTE is 208,493.297 m^2 (Table 5-1).

Table 5-1. GFA before and after the PR/BH relaxation

No.	Hotels	Gross Floor Area (m^2)			Number of Rooms			Capacity for Guests		
		Original	After Relaxation	Increase (%)	Original	After Relaxation	Increase (%)	Original	After Relaxation	Increase (%)
1	Shangri-La	46383.644	65900.000	42.08%	688	977	42.08%	1376	1955	42.15%
2	InterContinental Grand Stanford	26128.660	37185.000	42.31%	570	811	42.31%	1140	1622	42.28%
3	New World Millennium	33718.948	46010.400	36.45%	464	633	36.45%	928	1266	36.50%
4	The Royal Garden	33278.630	33278.630	0.00%	450	450	0.00%	900	900	0.00%
5	Regal Kowloon Hotel	31746.004	41922.560	32.06%	600	792	32.06%	1200	1585	32.00%
6	Hotel ICON	35964.050	35964.050	0.00%	262	262	0.00%	524	524	0.00%
	Total	207219.936	260260.64	**25.60%**	3034	3926	**29.41%**	6068	7852	**29.41%**
	Increase	**53040.704**			**892**			**1784**		

No.	Other Buildings (Planned for Commercial Use)	Gross Floor Area (m^2)		
		Original	After Relaxation	Increase (%)
7	TST Centre	47753.070	59692.500	25.00%
8	Peninsula Centre	52797.950	66000.000	25.00%
9	Energy Plaza	17999.945	22500.000	25.00%
10	Wing On Plaza	34703.923	43498.800	25.34%
11	Mirror Tower	18585.491	23250.000	25.10%
12	Inter-Continental Plaza	16550.158	20700.000	25.07%
13	Empire Centre	30533.856	39000.000	27.73%
14	Houston Centre	38203.503	47995.980	25.63%
15	Hilton Towers	19311.737	32250.000	67.00%
16	New East Ocean Centre	34265.340	46740.000	36.41%
17	Harbour Crystal Centre	28190.304	35250.000	25.04%
18	Chinachem Plaza	60734.869	76005.000	25.14%
19	South Seas Centre	41413.253	51870.000	25.25%
20	New Mandarin Plaza	53954.740	67500.000	25.10%
21	Concordia Plaza	66419.730	66419.730	0.00%
22	East Ocean Centre	34797.903	43500.000	25.01%
23	Auto Plaza	39149.397	48645.752	24.26%
	Total	635, 365.169	790, 817.762	**24.47%**
	Increase	**155, 452.593**		
	Increase of All (hotels + others)	**208, 493.297**		

Based on this increased GFA, a statistical assessment of the corresponding land premium was implemented to investigate the economic benefit of the PR/BH relaxation in TSTE. The outcome is shown in Figure 5-1 with a 15,192,909,632 HKD land premium for alternation of 23 buildings.

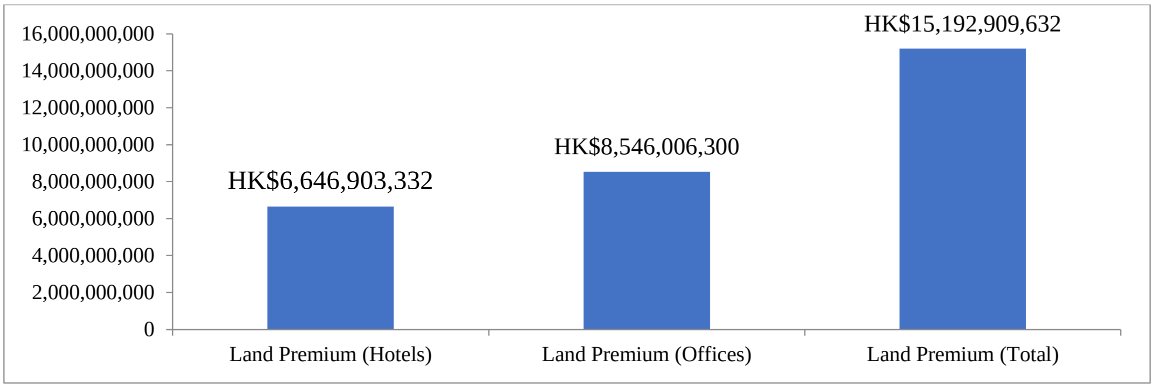

Figure 5-1. Total assessed land premium

5.2 Conclusions

This study was carried out against the background of the Green Deck plan. It investigated the development potential of TSTE in terms of the PR/BH relaxation of buildings for increasing the capacity of living and working spaces to meet the increased population flow whilst preserving the environment. The impacts of the PR/BH relaxation on the environment of the study area were assessed in respect of urban skyline, mountain ridgeline, solar exposure, wind ventilation and air temperature. The six analyses and the corresponding results are as follows:

(1) Three skylines were determined with proper consideration of visual acuity of TSTE buildings, the area of possible viewers, the area visually sensitive to TSTE, and the area only for public uses. The three skylines were comparatively analysed among S1, S2, S3, and S4. The effect of PR/BH relaxation on the three skylines is not significant and all three skylines are preserved as reasonable and acceptable from S1 to S2, S3, and S4.

(2) The ridgeline running from Beacon Hill through Lion Rock and Tsz Wan Shan to Kowloon Peak is preserved when viewed from the strategic viewing points of Quarry Bay Park, Hong Kong Exhibition and Convention Centre, Sun Yat Sen Memorial Park, and Centre Pier No.7. The impact of the PR/BH relaxation on the ridgeline is not significant in terms of the blocked angle of the view corridor between the viewing points and the ridgeline.

(3) The effect of the PR/BH relaxation on solar exposure was analysed in summer (21-Jun-2013) and winter (22-Dec-2013) solstices, both of which have extreme duration of solar exposure within the whole year. The patterns of solar exposure in

terms of sections of time (hour) and cumulative radiation energy (Wh) were generated for S1, S2, S3, and S4. The differences (S1 vs S2, S3, and S4) of the corresponding pattern areas indicate the enhancement of shading near the building footprint areas and this effect is positive for the life extension of facade materials. The radiation energy on the west facing facades is increased after the PR/BH relaxation and this is a reasonable phenomenon. The intensity of radiation on west facing facades is higher than the intensity of radiation in TSTE and this intensity is effectively decreased by the PR/BH relaxation.

(4) Wind ventilation was simulated in S1, S2, S3, and S4 respectively in summer (11-Jul-2016) and winter (13-Jan-2016) seasons. The comparison (S1 vs S2, S3, and S4) shows a small range of wind speed change from -1 m/s to 1 m/s for both seasons and the S4 is more ventilated (higher wind speed) for the wind as the SC of the buildings is narrowed. The wind direction is not significantly changed after the relaxation.

(5) Air temperature was analysed in S1, S2, S3, and S4 respectively in both day (1:00 pm) and night (1:00 am) and in both summer (11-Jul-2016) and winter (13-Jan-2016) seasons. The differences (S1 vs S2, S3, and S4) imply a minus range of air temperature change [-0.2, 0.2] °C, which is a not insignificant zone of change, for both time and seasons from S1 to S2, and S3. The southwest area has a change by more than 0.4 °C from S1 to S4 in summer as the speed of the west wind carrying heat to TSTE is improved by the widened spacing between buildings.

(6) For the traffic impact aspect, the Green Deck development will not bring significant impact on the surrounding road. Especially when considering 90% Hong Kong people using public transportation. The “traffic impact” due to the increased hotel room is not so significant, either.

REFFERENCES

Airflow (2015). ©Airflow Analyst All Rights Reserved.

Arakawa, A. and Lamb, V. R. (1977). Computational design of the basic dynamical processes of the UCLA general circulation model, *Methods of Computational Physics*, 17, pp. 173-265.

BD (2012). Cap. 123F building (planning) regulations. https://www.elegislation.gov.hk/hk/cap123F!en@2015-02-06T00:00:00?xpid=ID_1438402647394_002

BD (2017). Building records access and viewing on-line (BRAVO). http://www.bd.gov.hk/english/services/index_bravo.html

B.M (2011). ENVI-met, About ENVI-met; General idea.

Cervero, R. (2002). Built environments and mode choice: Toward a normative framework, *Transportation Research Part D*, (7), pp. 265–284.

Cervero, R. and Kockelman, K. (1997). Travel demand and 3Ds: Density, diversity, and design, *Transportation Research Part D*, 2(3), pp. 199-291.

Cervero, R., Sarmiento, O. L., Jacoby, E, Gomez, L .F. and Neiman. A. (2009). Influences of built environments on walking and cycling: lessons from Bogota, *International Journal of Sustainable Transportation*, 3, pp. 203–226.

Emmanuel, R. and Fernando, H. J. S. (2007). Urban heat islands in humid and arid climates: Role of urban form and thermal properties in Colombo, *Sri Lanka and Phoenix*, USA. Clim. Res., 34, pp. 241–251.

ENVI-met (2017). ENVI-met simulation model. http://www.envi-met.com/innovation#simulation_model

EPD (2010). Preparation of landscape and visual impact assessment under the environmental impact assessment ordinance. http://www.epd.gov.hk/eia/hb/materials/GN8.pdf

ESRI (2015). ArcGIS Desktop: Release 10, Redlands, CA: Environmental Systems Research Institute.

Fahmy, M. and Sharples, S. (2009). On the development of an urban passive thermal comfort system in Cairo, *Egypt. Build. Environ.*, 44, pp. 1907–1916.

Fisher, P. F. (1992). 1st experiments in viewshed uncertainty-simulating fuzzy viewsheds, *Photogrammetric Engineering & Remote Sensing*, 58(3), pp. 345-352.

Fisher, P. F. (1993). Algorithm and implementation uncertainty in viewshed analysis, *International Journal of Geographic Information Science*, 7(4), pp. 331-347.

Fisher, P. F. (1994). Probable and fuzzy models of the viewshed operation, In: Worboys M. (ed.), *Innovations in GIS 1*, Taylor & Fancis, London, pp. 161-175.

Fisher, P. F. (1996). Extending the applicability of viewsheds in landscape planning, *Photogrammetric Engineering & Remote Sensing*, 62(11), pp. 1297-1302.

Foth, M., Bajracharya, B., Brown, R. and Hearn, G. (2009). The second life of urban planning? Using NeoGeography tools for community engagement, *Journal of Location Based Services*, 3(2), pp. 97-117.

GE (2017). Google earth. https://www.google.com/earth/

Guo, J., Sun, B., Qin, Z., Wong, S. W., Wong, M. S., Yeung, C. W. and Shen, Q. (2017). A study of plot ratio/building height restrictions in high density cities using 3D spatial analysis technology: A case in Hong Kong, *Habitat International*, 65(2017), pp. 13-31.

He, Q., Tan, R., Gao, Y., Zhang, M., Xie, P. and Liu, Y. (2016). Modeling urban growth boundary based on the evaluation of the extension potential: A case study of Wuhan city in China, *Habitat International*, In Press.

Hegemann, W. and Peets, E. (1972). The American vitruvius: An architects' handbook of civic art, New York.

HKO (2016). Climatological information services. http://www.hko.gov.hk/cis/climat_e.htm

HKPU (2015). Green Deck – An Innovative solution to enhance the environment. https://www.polyu.edu.hk/cpa/greendeck/

HKTB (2017). Top 10 attractions. Highlight Attractions. http://www.discoverhongkong.com/eng/see-do/highlight-attractions/top-10/index.jsp

Isaacs, J. P., Gilmour, D. J., Blackwood, D. J. and Falconer, R. E. (2011). Immersive and non immersive 3D virtual city: Decision support tool for urban sustainability, *Journal of Information Technology in Construction*, 16(2011), pp. 149-159.

Jamei, E. and Rajagopalan, P. (2017). Urban development and pedestrian thermal comfort in Melbourne, *Sol. Energy*, 144, pp. 681–698.

Jason, M. C. Ni, Loo, B. P. Y. (2013). Vehicle use and the built environment: Case study of Shanghai, China

Lands Department (2016). Maps and services. http://www.Landsd.gov.hk/mapping/en/digital_map/mapprod.htm

Leszek, K. (2015). Environmental and urban spatial analysis based on a 3D city model, *Computational Science and Its Applications*, 9157, pp. 633-645.

Li, G. (2011). Proposal of designed wind speed evaluation technique in WTG installation point by using the meteorological model and CFD model, 141, pp. 1–12.

Li, J., Wang, J. and Wong, N. H. (2016). Urban Micro-climate Research in High Density Cities: Case Study in Nanjing, *Procedia Eng.*, 169, pp. 88–99.

Li, W., Putra, S. Y. and Yang, P. P.-J. (2004). GIS analysis for the climatic evaluation of 3D urban geometry - The development of GIS analytical tools for sky view factor, *Proceedings of GISDECO*.

LR (2017). Integrated registration information system online services. https://www2.iris.gov.hk/eservices/welcome.jsp?language=en

Mak, A. S.-H., Yip, E. K.-M., and Lai, P.-C. (2005). Developing a city skyline for Hong Kong using GIS and urban design guidelines, *URISA Journal*, 17(1), pp. 33-42.

Marsh, A. (2003). Ecotect and energyplus, *From the Building Energy Simulation User News*, 24(6).

Md. Tukiran, J. (2017). A study on the cooling effects of greening for improving the outdoor thermal environment in Penang, Malaysia, *Int. J. GEOMATE*.

Morakinyo, T. E., Dahanayake, K. W. D. K. C., Ng, E. and Chow, C. L. (2017). Temperature and cooling demand reduction by green-roof types in different climates and urban densities: A co-simulation parametric study, *Energy Build.*, 145, pp. 226–237.

Moudon, A. V., Lee, C., Cheadle, A. D., Collier, C. W., Johnson, D., Schmid, T. L. and Weather, R. D. (2005). Cycling and the built environment, a US perspective.

Ng, E., Chen, L., Wang, Y. and Yuan, C. (2012). A study on the cooling effects of greening in a high-density city: An experience from Hong Kong. *Build. Environ.*, 47, pp. 256–271.

Peng, C. (2016). Calculation of a building's life cycle carbon emissions based on Ecotect and building information modeling, *Journal of Cleaner Production*, 112, pp. 453-465.

PlanD (2003). Planning study on the harbor and its waterfront areas final report. Planning Studies. http://www.pland.gov.hk/pland_en/p_study/comp_s/harbour/harbour_finalreport/contents.htm

PlanD (2008). Hung Hom district study final report. Planning Studies. http://www.pland.gov.hk/pland_en/p_study/prog_s/hungHomSite/site/EN/studyreport.html

PlanD (2010). Strategic viewing points. http://www.pland.gov.hk/pland_en/info_serv/via/web/vp_intro.htm

PlanD (2016). Urban design guidelines. Chapter 11 of Hong Kong Planning Standards and Guidelines. http://www.pland.gov.hk/pland_en/tech_doc/hkpsg/full/ch11/ch11_text.htm

Pullar, D. V. and Tidey, M. E. (2001). Coupling 3D visualization to qualitative assessment of built environment designs, *Landscape and Urban Planning*, 55, pp. 29-40.

Ranzinger, M. and Gleixner, G. (1997). GIS Datasets for 3D urban planning, *Comput., Environ. And Urban Systems*, 21(2), pp. 159-173.

Stevens, D., Dragicevic, S. and Rothley, K. (2007). iCity: A GIS - CA modelling tool for urban planning and decision making, *Environmental Modelling & Software*, 22, pp. 761-773.

Tayyebi, A., Pijanowski, B. C. and Tayyebi, A. H. (2011). An urban growth boundary model using neural networks, GIS and radial parameterization: An application to Tehran, Iran, *Landscape and Urban Planning*, 100(2011), pp. 35-44.

Terzi, F. and Bölen, F. (2012). The potential effects of spatial strategies on urban sprawl in Istanbul, *Urban Studies*, 49(6), pp. 1229-1250.

Thill, J.-C., Dao, T. H. D. and Zhou, Y. (2011). Traveling in the three-dimensional city: Applications in route planning, accessibility assessment, location analysis and beyond, *Journal of Transport Geography*, 19(2011), pp. 405-421.

Thuesen, N. (2010). Evaluation of BIM and Ecotect for conceptual architectural design analysis, *Proceedings of the International Conference on Computing in Civil and Building Engineering*.

Toggweiler, J. and Key, R. (2001). Ocean circulation: Thermohaline circulation, *Encycl. Atmos. Sci.*, 4, pp. 1549–1555.

TPB (2010). TPB guidelines on submission of visual impact assessment for planning applications to the town planning board. http://www.info.gov.hk/tpb/en/forms/Guidelines/TPB_PG_41.pdf and http://www.pland.gov.hk/pland_en/info_serv/via/web/vp_intro.html

TPB (2016). Statutory planning portal 2. http://www1.ozp.tpb.gov.hk/gos/default.aspx

Uchida, T. and Ohya, Y. (2008). Verification of the prediction accuracy of annual energy output at Noma Wind Park by the non-stationary and non-linear wind synopsis simulator, *RIAM-COMPACT. J. Fluid Sci. Technol.*, 3, pp. 344–358.

Uchida, T. and Ohya, Y. (2011). Latest developments in numerical wind synopsis prediction using the RIAM-COMPACT CFD model-design wind speed evaluation and wind risk (terrain-induced turbulence) diagnostics in Japan, *Energies*, 4, pp. 458–474.

Uchida, T., Maruyama, T., Ishikawa, H. and Zako, M. (2011a). Investigation of the causes of wind turbine blade damage at Shiratakiyama wind farm in Japan: A computer simulation based approach, 141, pp. 2–3.

Uchida, T., Maruyama, T. and Ohya, Y. (2011b). New evaluation technique for WTG design wind speed using a CFD-model-based unsteady flow simulation with wind direction changes, *Model. Simul. Eng.*

Uchida, T., Ohya, Y. and Sugitani, K. (2011c). Comparisons between the wake of a wind turbine generator operated at optimal tip speed ratio and the wake of a stationary disk, *Model. Simul. Eng.*, pp. 3–9.

Wang, E., Shen, Z. and Barryman, C. (2011). A building LCA study using Autodesk Ecotect and BIM model, *47th ASC Annual International Conference Proceedings*.

Wong, M. S., Nichol. J. and Ng, E. (2011). A study of the “wall effect” caused by proliferation of high-rise buildings using GIS techniques, *Landscape and Urban Planning*, 102(2011), pp. 245-253.

Xia, F., Shen, Y., Yan, J. and Bao, X. H. (2016). On the potential of urban three-dimensional space development: The case of Liuzhou, China, *Habitat International*, 51(2016), pp. 48-58.

Xu, Z. and Coors, V. (2012). Combining system dynamics model, GIS and 3D visualization in sustainability assessment of urban residential development, *Building and Environment*, 47, pp. 272-287.

Yang, L., He, B.-J. and Ye, M. (2014). Application research of ECOTECT in residential estate planning, *Energy and buildings*, 72, pp. 195-202.

Zhang, X., Zhu, Q. and Wang, J. W. (2004). 3D city models based spatial analysis to urban design, *Geographic Information Sciences*, 10(1), pp. 82-86.